Université des Sciences et Technologies de Lille
Laboratoire de Génie Civil et géo- Environnement

Année 2015 **N°**

THESE

Pour obtenir le grade de

Docteur de l'Université Lille1 - Sciences et Technologies et de l'Université de Wuhan

Discipline: Génie Civil

Présentée et soutenue publiquement par

HE Ting

Analysis of the impact of corrosion on the durability of blot-reinforced structures

Soutenue le 22 septembre à l'Université de WUHAN

Devant le Jury Composé de :

CHEN Shenhong, professeur, Wuhan Université, Directeur de thèse

SHAHROUR Isam, Professeur, Université Lille 1, Directeur de Thèse

HAGE CHEHADE Fadi, Professeur, Université Libanaise, Rapporteur

WU Aiging, Wuhan Université, Rapporteur

Abstract

Bolts are largely used in rock and concrete engineering practices. The corrosive medium of bolts results in a fast aging and significant damage of bolt, which leads to a reduction of the life-service of plots, particularly when these plots face deficiency in self-protective system. Many anchor projects have suffered from this issue and its catastrophic consequences.

According to the statistical data, corrosion is a leading factor in decreasing blot durability. It has an effete on the capacity of bolts: Firstly it leads to the cracking of the mortar cover due to the expansion of corrosion products; secondly it results in the imperfect bonding between bolts and mortar. In the dissertation, theoretical analyses, experiments and numerical analyses are conducted on the mechanical properties of corroded anchorage system. A method to evaluate durability of corroded anchorage system is also proposed. The principle achievements in the dissertation are as follows.

Firstly, the corrosion mechanism of bolt in concrete is summarized; the prediction model of bolt corrosion rate has been conducted. In the meantime, theoretical formulas of corroded expansion force changes over time are established, and applied to numerical simulation experiments.

Secondly, a spatially analytical model of bolt rust has been established to study the three-dimensional stress field of the bolt under the joint action of pull-out force and rust expansion force, to find the analytical solutions of each stress components in the bolt issues. Numerical analysis gives the following stress distribution pattern in rusting bolt: (i) the axial stress of the bolt is distributed in the form of exponential decay function; (ii) on the plane perpendicular to the bolt, radial stress within the mortar protective layer is in transition from tensile stress to compressive stress, tensile stress peaks at the radial edge of the mortar; (iii) along the length of bolt, compressive stress within the mortar peaks at the end of the bolt, but on the plane perpendicular to the bolt, hoop stress peaks near the edge of the bolt in the mortar; (iv) shear stress between the bolt and mortar matches linear distribution. Most values of shear stress on bolt surface are negative and peaks at the bolt end, vectors of shear stress are in the opposite direction to that of pull-out force. In the transition from negative values to positive values, the shear stress will go through a ‘neutral point’, at this point, the value of the shear stress is zero.

The use of the elastic-viscoplastic theory allows us to follow the mechanical process in time. The finite element program for corroded bolt of elastic-viscoplastic potential theory is used in this work for the first time. In the cases considered in the study, the distribution of axial tensile stress along the bolt under the action of Expansion Force increases linearly. The Expansion Force induces displacement in the concrete, which increases with time. Under the joint action of Expansion Force and a pull-out force, the axial stress decreases exponentially along the length of the bolt. The displacement peaks at the bolt decreases when approaching to the free end.

The composite element method has been developed to deal with the issue of blot durability: sub-units of bolt, mortar, concrete, joints, and various contact surfaces are defined in bolted jointed concrete. Virtual nodes are added on the node of composite unit to map displacement vector of bolt, mortar and rock sub-units, as well as to interpolate displacement of sub-unit domain. The contact surface treatment has been employed, using the displacement difference of adjacent sub-units between mortar and bolt to interpolate displacement of interface. The results of the composite element method match well with the finite element modeling.

The numerical model is validated on reinforced concrete experiments.

Keywords: bolt, mortar, corrosion, analytical model, FEM analysis, CEM analysis

Table of Contents

Chapter 1: Introduction

1.1 Issues raised

Bolt is buried tension member in reinforced rock and concrete, through the interaction of bolt and rock or concrete to bear external load. It transfers load from the blocs, to the confined (and much stronger) interior of the concrete. It prevents displacement in the surrounding rock mass and provides stabilizing forces to resist the movement of rock blocks. Rock bolts were first used in mining in the 1890s, with systematic use documented at the St Joseph Lead Mine in the US in the 1920s. Rock bolts were first applied to civil tunneling support in the US and in Australia in the late 40s. Rock bolts were used and further developed in 1947, by Australian engineers who began experimenting with four meters long expanding bolted rock while working on the Snowy Mountains Scheme. Geotechnical pre-stressed anchorage technology was produced in the early 20th century first and used in mining, with successful use documented at the Al Scotia dam in Algeria in the 1930s. Pre-stressed anchorage technology was applied to reinforced dam and foundation in the American Milton Lake Dam, Morocco Tektronix Hout Talal Dam and in France De Nute dam, starting in the 1940s. A large number of bolts were used in the Xiaowan Hydropower Project for stability of the slope (Fig 1.1). Practical engineering applications show that Bolt Technology have many advantages such as significant reinforcing effect, low cost, high reliability and durability. Besides, they have been successfully applied in civil engineering, water conservancy, and transportation, municipal, mining and other projects. Under western development and the construction of infrastructure background, bolt technology has broad application prospects.

(a)Bolt

(b) Right bank slope

(c)Right bank of the inlet façade

(d) Left Bank bolt age wall

Fig 1.1 Bolts in Xiao wan Project

Although the bolt technology has been applied for nearly a century, however, it is obvious that the status of its theoretical research lags far behind the level of construction, especially for the research of the bolt durability. Bolt is often applied to engineering projects which require a higher level of safety, some of which even belong to the state lifeline engineering, such as dam foundation and abutment reinforcement, large span tunnel underground caverns and mines supporting, high slope stability and traffic tunnel rock support and so on. Durability is an important indicator of the safety evaluation, and therefore the durability of bolt has a crucial impact on the safety of the anchor project.

Geotechnical pre-stressed bolts, mainly through high-intensity tendons, put some pre-rock stress on the rock foundation, so the geotechnical stability and strength meet basic application requirements. Bolts are mostly embedded in rock and soil, which may be surrounded by corrosive media and stray currents. The service environment is relatively complex, and working long-term in such environment will cause gradually aging, damage or even destruction. Coupled with the internal factors, the imperfect self-protection system resulted in a shortage of durability. Bolt once destroyed, its pre-compressive stress on rock structure will drop, which could lead to the destruction of rock reinforcement structure. So the corrosive environment imposes particular requirements for the durability of geotechnical pre-stressed bolts.

Around the world we have observed bolt failure due to bolts degradation: Ternational Working Group of Fédération Internationale de la Précontrainte (FIP) collected 35 cases of

pre-stressed bolt instances of corrosion damage: Switzerland, a pipeline bridge reinforced by bolt collapsed after five years, due to the fact that the groundwater in the bolt segment layer contained corrosive substances and the bolt segment did not fill with grout caused by low-quality construction, strand exposed to corrosive permeable formations and serious corrosion damage is caused. In Algeria, a dam linoleum protective layer near the head of the reinforcement bolt was broken, resulting in a number of bolt failures near the anchorage due to localized corrosion and damage. In Germany, the pre-stressed concrete roof of the parliament building in Berlin was surrounded by poor cement paste, resulting in hydrogen evolution of stress corrosion damage, and ultimately led to collapse of concrete roof. In Mumbai, a tensioned concrete bridge on the Shsneriver had to be replaced earlier due to the corrosion of the tendons steel. In United Kingdom, a single-span post-tensioned concrete bridge (Ynys-y-Gwas) suffered from salt infiltration, which caused severe erosion and the collapse of the entire bridge. According to some reports, Acoyne designed thirty four pre-stressed bolts of 10,1000kN with anti-corrosion technology to reinforce the dam Sher in 1933-1934. But in 1965 the dam inspection observed around 9% of pre-stressing losses, due to bolt head relaxation and corrosion [1]. Romnaoff in 1962 observed the corrosion of steel columns buried in the soil medium, which occurred mainly in backfill part, which due to the osteoporosis of the backfill soil for the soil contained a large amount of oxygen.

International Working Group of Fédération International de la Précontrainte (FIP) conducted a statistical analysis of 35 cases of bolts corrosion damage (Table1.1)[2]. Analysis showed: (i) 24 cases of permanent bolt, some of which had protective measures, some of which were unprotected. 11 cases of unprotected are temporary bolt that anchorage segment have grout package and free section have isolation units; (ii) In terms of destroyed parts, in 19 cases damage occurred in the bolt head or less than 1 meter away from the bolt head, 21 cases in the free section, 2 cases in the anchorage section; (iii) Corrosion was localized within bolt length; (iv) In terms of service life, 9 cases occurred within six months, 10 cases between six months and two years, and the remaining within 2 to 31 years; (v) Short-term damage of bolt is caused by stress corrosion or hydrogen embrittlement, the reason is that the bolt stayed in a corrosive environment without protective layer or inadequate protection.

European scholars assessed 242 instances of pre-stressed corrosive damage in the period 1951

- 1979 all around the world; Figure1.2 shows the bolt work environment is almost concerned by corrosion.

Table1.1 The statistical analyses of 35 instances of damage of bolts [2]

Statistical Classification		Number
Bolt type	Permanent bolt	24
	Temporary bolt	11
Stretch varieties	Pre-stressing steel wire	19
	Pre-stressing steel	9
	Pre-stressing strand	7
Bolt Working Hours	6 months	9
	6 months to 2 years	10
	More than 2 years	18
	31 years	1
Destroy parts	Near the bolt head	19
	Free end	21
	Bolt end	2

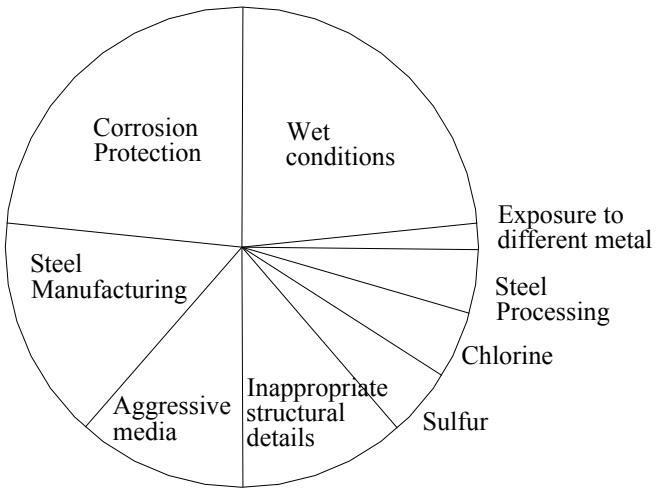

Fig 1.2 The cartogram of factors causing corrosion [2]

Although the application of the bolt technology in China is late, with the popular use of New Austrian Tunneling Method (NATM) in the world, the number of the anchorage structure

engineering is quite large in the country. After 1980 the railway tunnels built according to the principles of NATM accounted for 10% of the total number and the length of railway tunnel in China [3]. Survey showed that most of the failures were due to bolt durability. Pre-stressed bolts of Anhui Meishan reservoir were damaged after using 6 to 8 years due to stress corrosion of some wires. Guangzhou Haiyin Bridge suffered from pre-stressed cables broken, due to stress corrosion [2]. Third research Institute of general Staff Corps of Engineers investigated bolt durability in domestic situation: the bolt of Jiaodong in Mine Jiaozuo City, the installation is in poor quality and the thinnest bond layer was only 1 ~ 2mm, the depth of neutral surface of 12a is about 0.5mm, at the surface of the rod existed rust, but if the bond layer thickness has greater than 3mm then there was no rust; The wedge joints bolt of fourth Hebi coal mine , 28a depth of pitting corrosion were respectively 0.4 ~ l.5mm (2 # and 5 # bolt, water leakage) and 0.05 ~ 0.10mm (1 #, 3 #, and # 4 bolt, no leakage of water; a copper of our country using ordinary sulfate cement mortar infusion bolt, due to the harsh corrosive environments, after 2a the surface of the mortar became like rubbish loose body; Yangyao River 1st tunnel of Chengdu-Kunming line, after applying spray bolt I0a later, the surface of the spray layer was etched into a 1cm thick layer of white crisp. Third research Institute of general Staff Corps of Engineers had the statistical analysis on material showed that: the service life of quality mortar bolt is 75 ~ 169a; the service life of poor quality mortar bolt is about 50a; the service life of poor quality mortar bolt in harsh environments is about 20 ~ 25a; Since some structural problems of this kind have been emerging, people pay more and more attention on safety and durability of bolts [1- 7].

In the Three Gorges project, 4204 pre-stressed bolt beams were installed to reinforce the rock slope. In one-stage project, 225 bolt beams of 1000 kN level and 203 bolt beams of 3000 kN level were installed; in two-stage project, 4 bolt beams of 1000 kN level and 3772 bolt beams of 3000 kN level were installed. Because of the vital role of pre-stressed bolt in the reinforcement of the rock slope, the durability of bolts had a large concern. Before the construction of the pre-stressed bolt cable, the designer conducted some experimental tests on the structure of the pre-stressed cable and the anti-corrosion materials. In 2000, the experts of the State Council Three Gorges Project affirmed the necessity to research on bolts' durability. To this end, China Yangtze Three Gorges Project Development Corporation proposed a

roadmap for the research on blots durability.

Literature review shows that the safety and durability of the bolt is very important. It requires theoretical studies, which cannot be confined to the construction technology. The durability of the bolt becomes an urgent issue. If we do not pay attention to this issue, we could have in the future severe damage to large infrastructure with important economic and human losses.

1.2 Introduction to the research history in bolt durability

1.2.1 Research outside China

Research on durability started in the early 19th century when Portland cement was invented. At that time it was widely used as a cementation material of concrete and Portland cement concrete. It was applied to the breakwater, pier, lighthouse and other marine structures. Due to the harsh working environment, offshore structures withstand long periods of strong influence of the external media, including the impact of physical effects (such as the impact of the waves, sediment erosion, as well as the role of ice and frost of the northern part) and chemical effects (effect of salt melting in seawater) [8], which may lead to the destruction of these structures in short period. In order to explore the causes of premature failure of offshore structures, important research was conducted on the corrosion of concrete of offshore structures.

In the nineteenth century, research in durability of concrete structures in the former Soviet was the most advanced in the world. In the study of the durability of offshore structures, the former Soviet conducted important work [8]: In 1902, the famous architect engineer A.P. Ke Shu Liangqin and B.N. Noam Chomsky found that Portland cement was used in the construction of marine hydraulic structures. In 1904, A.A. Pakistan Kauf and BH Cha Ernuo Rimsky conducted similar survey on ports structures in Russia, but reached an opposite conclusion. In 1840, a French excellent engineer and researcher Vicat published a book named “Study on chemical causes and protection methods of hydraulic components subjected to seawater corrosion”, which was the first book containing the research about seawater corrosion of hydraulic concrete cementations material damage. The AA Bykov's of the former Soviet Union played a major role in the development of concrete corrosion studies in terms of

basic theory and practical applications. In t he late nineteenth century, reinforced concrete structures were used in industrial buildings and structures. The durability of concrete structures faced a new challenge: how to solve the problem of safety of reinforced concrete used in chemically active substance corrosive conditions. In addition, the durability of reinforced concrete in the atmosphere of industrial zone became a prominent issue.

In the early 1920s, the form of concrete structures was constantly updated with design theory matured and their applications were increasingly widespread. Evolving concrete structures brought more and more new topics for durability research. In the 20th century, more countries started to pay attention to the durability of concrete structures [8]. In 1925, Miller performed in United States a long-term test in high sulfate content soil with the purpose to get 25 years, 50 years, resulting in a longer period of concrete corrosion data. The German Federal Reinforced Concrete Association used examples of concrete structures subjected to swamp water resulting in corrosion and damage; they also performed a long-term test about corrosion of concrete under natural conditions;. In the period 1934-1964, Kan Pisi performed a test on durability of concrete in seawater and O. Geer Fu wrote a report on durability of concrete of sea pier buildings, which provided more reliable data on concrete structures usage under natural conditions and more insights on the types of cement, concrete mixing ratio and some factors on the effects of corrosion on concrete resistance. Meanwhile, the former Soviet Union continued to carry out researches on concrete corrosion [8]. In 1937, the former Soviet Academy of Sciences held its first meeting on corrosion and protection methods of concrete; it also formulated a basic research method on concrete corrosion, prepared the first batch standards for hydraulic structures erosion in environmental water, and studied the corrosion resistance of cement concrete in natural water.

After the mid-20th century, the research on the durability of concrete structures expanded beyond the concrete corrosion studies [9]. In 1940, T.E.Stanton[9] discovered and defined the alkali aggregate reaction, and opened a new research field in concrete structures durability. In 1945, Powers and others researched on sub-microscopic of concrete, analyzed the effect of pore water to the hole wall, put forward the Hydrostatic hypothesis and osmotic hypothesis [10], and began the study of the mechanism of freeze-thaw damage. C.B. Sheth Torpey Love conducted a lot of research on concrete frost resistance, laying the theoretical basis of the

durability concrete and reinforced concrete structures in cold climates [8]. In 1951, the Bykov and Moskvin started the research on reinforcement corrosion. Purpose of the study is to solve corrosion problems of smallest thin protective layer of concrete structures and to use high-strength steel (including high-strength wire) to produce steel rebar [11], which marked the research on durability of concrete. MOSKVIN published a book named 'concrete corrosion' which put the basic of concrete corrosion process theory [8]. In 1954, the former Soviet Union set up a central laboratory of concrete and reinforced concrete science institute, which was the first institution of research on corrosion and anticorrosive methods of concrete and reinforced concrete in the world [8]. The former Soviet Union, on the basis of large-scale research work, developed standards to prevent corrosion of concrete and reinforced concrete in the construction industry, such as building construction standards of corrosion resistance CH262-63, CH262-67 et al[8], laid the foundation of the durability of concrete and reinforced concrete structures.

After the 1950s, the concrete structure enjoyed rapid development in the material, structural applications, construction standards and computing theory and became the most widely used structure in civil engineering construction. At the same time, the research on durability of concrete structures became independent new disciplines. Especially in the last twenty years, research on the durability of concrete structures gained considerable development; many international and domestic academic durability research institutions established, a large number of related literatures and books published, large-scale scientific research activities and academic exchanges conducted [12].

In 1957, the American Concrete Institute (ACI) established a committee named ACI201, responsible for directing of research on the durability of concrete. In 1960, the International Union of Laboratories and Experts in Construction Materials, Systems and Structures (RILEM) established the "Corrosion of Reinforced Concrete" Technical Committee (12-CRC), aiming to promote the development of research on the durability of concrete structures. In 1961 and 1969 RLIEM organized international conferences on the durability of concrete. In1970, Prague held the Sixth and Seventh International Conference of cement chemistry. From1978 to 1993, six conferences on the durability of building materials and components were held. In 1982, RLIEM and International Building Research Experimental

and Documentation Committee (CIB) composed Life Prediction of materials and components committee (CIBW80/ RILEM71-PSL), to study the problem of life prediction of the structure. In 1987, a new committee CIBW80 / RLIEM100-TSL was set up to promote the Committee's work and implement the research results; in the same year the International Association for Bridge and Structural (IABSE) organized the international conference "The Future of concrete" in Paris. In 1987, the first session of the durability of concrete was held in Atlanta. In 1988, Denmark organized the International Conference of "Re-evaluation of concrete structures". In 1989 an International Conference of the durability of structural was held in Lisbon. In 1991, the United States and Canada jointly held the second session of the International Conference on the durability of concrete structures, which proposed that the maintenance costs should be included into the total cost. In 1993, IABSE held an international conference on the residual capacity of the structure in Copenhagen. In 2000, Singapore hosted the Sixth International Conference on "durability and repair of structural defects ". In the same year, RLIEM held I France an international conference on "life prediction and durability design of concrete structures". In 2001 IABSE o the behalf of CIB, ECCS, FIB, RILEM and other organizations held an international conference on "security risk and reliability - engineering trends" in Malta.

At the same time, many countries developed relevant norms and regulations to ensure the durability of concrete structures, which marked the research of the durability of concrete structures. In 1991, the ACI437 Commission proposed a report on "resistance evaluate of existing concrete houses", developed a detailed testing methods and procedures [13]. In 1980, the Japan's Ministry of Construction conducted research on the "technology to improve the durability of the building," and submitted a report in 1985. In 1986 in Japan issued a document "The order to consider durability in buildings design, construction and maintenance". It is based on the building lifetime, including the whole process of building management, paying attention to preventive maintenance to extend the life of the building, followed by preparation of the "durability of concrete identification procedures" a series of durability design and identification procedures and methods. In 1989, the Japanese Society of Civil Engineers Concrete Committee formulated the "durability of concrete structure design criteria (Trial)" [14]. The Japan's Ministry of Construction proposed two structural integrated

technology projects on the durability of concrete in 1990 and 1997: "Improving the technology of the durability of concrete development," and "develop the technology of construction and renovation of long-term durability of urban apartment". In 1991, the Architectural Institute of Japan developed "high durability design of reinforced concrete structures, construction guide" (draft). In 1992, the "Building Survey, diagnosis, maintenance manuals" was launched. In the same year, the European Concrete Commission issued "durability of concrete structures Design Guide" [15], reflecting the level of Durability of concrete structures in Europe. In 1996, the RLIEMTC130-CSL Commission published the report" Calculation method of the service life design of concrete structures" and proposed design concept of the durability of concrete structures based on the Failure probability Design Theory.

In the late 1960s and early 1970s, France, Switzerland, Czech Republic and Australia established bolt technical regulations and specifications. In the late 1980s and early 1990s, the soil nail technology guide was established. These technical standards took full account of the anchorage type of structure protection issues in corrosive environments, where design and construction had strict rules. In 1975, R.Schach of the Norwegian Institute of Rock Blasting Techniques published the book "Rock Bolting-A Practical Hand Book". In 1980s, German published series of books including soil bolts and rock bolts, with explicit requirements on the comprehensive anticorrosive of rock bolt in foundation engineering. In the period 1974-1981, the ASTM Committee published a set of eight books on the effect of a variety of underground and ground corrosion to metallic materials, including the natural environment corrosion, stress corrosion and corrosion prevention measures that had a greater impact.

1.2.2 Research in China

In the1970s and early 1980s, the research in China focused on anticorrosive of hydraulic steel gates, as well as the research epoxy coating anticorrosive in hydraulic engineering [1]. In recent years, experts and researchers in civil engineering paid large attention to the safety and durability of civil engineering projects, promoting analysis of structural durability. In recent years, the research of structural durability and longevity became a major issue in the

development of structural engineering disciplines.

The research on durability of concrete structures in China began in the 1960s. From the 1960s to the late 1980s, many domestic researchers conducted comprehensive and systematic studies on the durability of harbor reinforced concrete structures and found that the steel corrosion leaded to structural premature destruction. Since the 1980s, the durability of reinforced concrete structures gained attention. In 1989, China promulgated the "reliability identification procedure of the steel industrial building" (YBJ219-89) [16], providing a method to predict the service life of reinforced concrete structures. In the early 1990s, the research on the durability of concrete structures entered the organized working stage. In 1990, the Ministry of Construction established a national identification and reinforcement of the building committee, with a conference every two years. In December 1991, China formulated a national design regulation for durability of reinforced concrete structures. In November 1992, the Concrete and Pre-stressed Concrete Society of Concrete Durability Professional Committee of China Civil Engineering Society was created. National and provincial research funding supported a number of researches on topics related to durability. The Ministry of Construction in the "Seven Five" and "Eighth Five" period has set up special research on durability of concrete. The "Seven Five" key issues concerned "the durability and service life of reinforced concrete structures under atmospheric conditions", include the survey of the durability of structure, corrosion, concrete carbonation, temperature and humidity on the carbonation etc. The "Eighth Five" key issues focused on " pre-stressed concrete structures and the durability of concrete technology," including the durability design method of reinforced concrete structural, durability testing and assessment of existing reinforced concrete structures, under certain conditions, the combined effects of factors to the durability of reinforced concrete structural and building databases of the durability of concrete. In the "Eighth Five" period, the State Science and Technology Commission, the National Natural Science Foundation established the "Safety and Durability basic research of major Civil Engineering" project (Climbing project Plan B) with chief scientist Professor Liu Xila. The main line concerned the three stages life process of structure, carrying out a series research on safety and durability, including structural durability, durability comprehensive testing system, mathematical and physical modeling, testing and simulation methods, existing structure

remaining life prediction methods, structure maintenance methods and durability set standards [12]. In 1996, Tsinghua University, Building Research of the Ministry of Construction, Highway Research Institute of Academy of Transportation Sciences, Building Research of Ministry of Metallurgical Industry and other units jointly completed the "durability of concrete structures detect Guide"[17] . In 1998, the Ministry of Construction approved this guide. The National Building appraisal reinforced standards committees started writing the "Durability Evaluation Criteria of concrete structures". The Ministry of Transportation began to write "durability of concrete structures and durability Design Guide" by the academician Chen Zhaoyuan.

However, the corrosion conditions of bolt structure are different from of the above study. Corrosion of anchorage structure results from aggressive media in soil and groundwater, the bimetallic effect and stray current in ground formation. Under certain conditions, the rock medium acidity (pH), chlorides and sulfates can cause corrosion of the anchorage structure. Bolt is generally pre-stressed. At present, some of the pre-stressed bolts have more than 10,000kN, with a trend towards higher capacity development. Therefore, stress corrosion of bolts can not be ignored. Due to the blind pursuit of the construction schedule and cutting corners, anchorage structure had very serious defects. In bolt installation, the industry usually uses cement mortar or pure mud, with more resistant to corrosion than concrete. The bolt protection suffers from different factors such as the thin bonding layer, the high water-cement ratio, and low injection pressure, improper use of bracket and shrinkage that did be serious. The minimum thickness of the bond could not be guaranteed with serious consequences on the local bonding.

Because of the different of engineering geological conditions, anchorage structure could be subjected to permanent immersion, alternating wet and dry and a variety of different environments. Preliminary studies indicate that: (i) Under permanent soaking conditions, the average corrosion rate of bolt body in the weakly acidic solution was at least 2-fold than in the neutral and weakly basic solution, while the corrosion rate in weak alkaline solution was slightly higher than neutral solution; (ii) Placed in a sealed and air relative humidity of 100% conditions, the corrosion rate of the bolt was about 1/5 of the time of in permanent immersion

and alternating wet and dry conditions; (iii)The bolt corrosion volume increased with time, and the corrosion rate decreased with time. Moreover, since the bolt structure belongs to hidden works, and its life was more difficult determine than the durability of general concrete structures, so the direct report of service life and protective countermeasures research work of anchorage structure were uncommon. From July 1985 to July 1987, the General Staff Corps of Engineers Third Research proposed a research on "Corrosion and Protection of mortar bolt", where some researchers carried out a preliminary study on bolt life, and got some useful results, but field sampling was not wide, and the laboratory tests were not systematic in-depth. From 1996 to 1997,the General Staff Corps of Engineers Third Research carried out a research on "underground engineering cement mortar durability test in corrosive environments", which produced 516 specimens for a period of 720d single factor corrosion tests. According to the test results, the trend strength loss rate of cement mortar in corrosive environments was estimated, so we can calculate the corrosion years of cement mortar of underground engineering under this condition [1].

Anchorage structure has been applied in various types of engineering and geological conditions in China for 40 years, but with few technical standards for their durability, life, and design life and protection measures. Based on long experience in pre-stressed bolt design and construction", General Staff Corps of Engineers Third Research prepared in 1999the national military standard "pre-stressed bolt Design and technical specifications for construction of geotechnical engineering"(GJB3635-99), one of the chapter concerned "corrosion and anticorrosive" of pre- stressed bolt. The protective measures and requirements were established on the basis of engineering experience, without adequately theoretical and experimental basis [1].

1.3 Introduction to the research status and results of bolt durability

Similar to concrete structures, bolts' structural deterioration is due to aggressive media together with self-protection deficiencies. Understanding this issue requires analysis of complex aspects such as aggressive media diffusion and reaction processes in the protective layer of mortar, reinforcement corrosion process, kinetic of steel corrosion process,

quantitative impact of steel corrosion on bolt bearing capacity, durability and life prediction after bolt corrosion.

1.3.1 Aggressive media diffusion and reaction process in the protective layer

1.3.1.1 Carbonized

In the atmosphere environment, carbon is one of the major predisposing factors leading to the corrosion of reinforced concrete structures. After filling the rock bolt with internal layer basically in closed state, the protective layer of mortar had minimal possibility to be carbonized, but in many ways the corrosion to bolts caused by carbonation is worth learning. The research on concrete carbonation includes carbonation mechanism, effect factors of carbonation, prediction model of carbonation depth and so on. Papadakos [18] described the mechanism of carbonation in molecular level, based on the reaction kinetics analysis the main physical and chemical reactions of the carbonation process, which laid the foundation for the quantitative analysis of the carbonization process. Three aspects affecting the degree of carbonation of concrete: variety and mix of concrete constituent material, construction factors: conservation methods and age and environmental factors (humidity, temperature and CO_2 concentration).

Because carbonation was the prerequisite of steel corrosion and the key premise of structure prediction of service life, models were developed for carbonation depth prediction. These models can be roughly divided into two categories. The first is based on experimental data or carbonation depth measured value of existing concrete structures, adopting mathematical statistics and neural networks and other methods to get empirical model. Niu Ditao et al. proposed a concrete carbonation probabilistic model[19], and consider the impact of environmental conditions and the quality of the concrete of double coefficients carbonation depth average prediction model and standard deviation of carbonation depth prediction model[20]; Li Qingfu used fuzzy analysis regression method to set up concrete carbonation depth prediction [21]; Yuan Qun used the random time series method to identify the carbonation depth of ARIMA (1,1,0) [22]; Jin Weiliang proposed a carbonation depth prediction model based on functional neural network[23]. Another theoretical model was

established on the basis of a quantitative analysis of carbonation process. For example, Alekseyev model [12], Papadakis model [18], the concrete carbonation depth practical mathematical model proposed by Zhang Yu [24]. Other models were proposed [25] for the concrete carbonation taking into account the influence of temperature and humidity. These models were based the CO_2diffusion in different types of concrete and the carbonization reaction kinetics.

Concrete carbonation depth prediction model can be writtenas follows:

$$D = \alpha t^{\beta}$$

Ddenotes the concrete carbonation depth (mm); t time (y); α、βdesignate the carbonation coefficient and carbonation index, respectively.

Carbonation rate coefficient considered the main factors on water-cement ratio, cement content, compressive strength of concrete, and impact of environmental conditions. From statistical analysis of 143 sets experimental data of concrete carbonation domestic and abroad, literature [26] proposed the Carbonization index uncertainty model. Concrete norms preparation group proposed concrete carbonation coefficient formula [27] based on a variety of research on concrete carbonation in recent years.

Although the empirical model was used conveniently, it yet suffers from the following (i) it does not considered the influence of the content of carbonized material on on the carbonation speed, (ii) The data used in this model is based on the specific environment and materials, (iii) the physical concepts of coefficients in the model are not very clear. Therefore the scope of the model is limited. Theoretical modeling should have clear concept with clear parameters. The selection and calculation of parameter of this model are controversial. We need to build a carbonation depth forecasting model with theoretical basis and strong applicability.

1.3.1.2 Chloride erosion

Chloride erosion analysis includes different topics, in particular chloride ion diffusion mechanism in concrete, diffusion depth, concentration predictions and critical concentration of chloride ions causing steel corrosion.

Bažant [28] first analyzed the physical and chemical processes of chloride ions causing corrosion of marine structures reinforced, and proposed a physical model. In 1970, Collepardi

[29] firstly applied Fick's diffusion second law on chloride ions in concrete diffusion model, and improved the existing models on this basis. Thutti[30] established a one-dimensional model of chloride ion diffusion process. Sun Wei deduced a new diffusion equation considering concrete chloride ion binding capacity, time-dependent of chloride diffusion coefficient and concrete structures of micro-defects affect [31].Funahashi[32] considered the parameters effects of temperature, the type of salt, the type and quality of the concrete, the amount of salt, and used the finite difference method to get the future distribution of the concentration of chloride ions. Chloride ions in concrete are influenced by internal and external factors. The internal factors refer to pore structure of concrete, the diffusion coefficient and the thickness of the protective layer. The external factors refer to the ambient temperature, humidity and the chloride concentration of the concrete surface, the structure of the splash zone. The diffusion process is also affected by the length of the air-dry and wet alternation time [33]. Chloride ion diffusion coefficient is an important indicator for the durability of concrete, and it is not only related to the composition of the concrete material, the quantity and characteristics of the internal pore structure, the degree of hydration and the other internal factors, but also related to external factors, including temperature, curing period, the type and quantity of admixture and the type of the chloride ion induced reinforcement corrosion [11]. Sun and Yu [31] obtained the statistical relationship between chloride diffusion coefficient and water-cement ratio by fitting the experimental data. Stephen et al. [34] obtained the solving diffusion coefficient formula taking into account the temperature.

According to the mechanism of chloride-induced corrosion of steel, it is known that the $[Cl^-]$ / $[OH^-]$ of concrete pore solution surrounding steel is the critical value of steel passivation [33]. Although this value is not determined, it is known that it is related to the water-cement ratio and the way chloride was introduced. Based on the comprehensive analysis of previous studies, the steel critical value of $[Cl^-]$ / $[OH^-]$ in different pH alkaline solution [33] should be considered.

1.3.2 Steel corrosion

Steel corrosion includes a variety of simultaneous chemical coupled processes. Analysis of

this phenomenon includes investigation of corrosion mechanism, amount of corrosion prediction and the mechanical properties of steel corrosion.

Based on chemical reaction mass conservation law, Fick first law of diffusion, Maxell static equation and chemical reaction kinetics, Bažant [28] completely described the steel corrosion process under marine environment.

Existing steel corrosion rate prediction models can be divided into two categories. The first is based on a theoretical model of corrosion electrochemical principles. For example, Bažant [35] proposed physical model of steel corrosion under the marine environment. Niu Ditao established a corrosion rate of reinforced concrete model before and after cracking under the general atmospheric [36, 37]. This model took into account the relative humidity and the water film on the steel surface to the absorption capacity of oxygen. Jin Weiliang treated the oxygen diffusion coefficient in concrete as a time-varying variable, considering radius changes after reinforcement corrosion and using a general expression of concrete carbonation, proposed a new uncracked concrete steel corrosion rate prediction model [38] and established steel corrosion rate prediction model of splitting concrete structure based on elasticity [39].

The second category is based experimental data and engineering research. Ling Huiyun obtained the relationship between weight loss, the crack width and various factors before and after steel corrosion cracking from a large number of specimens [40]. Morinaga got from experimental data the steel corrosion rate change with temperature, relative humidity, oxygen concentration, chloride ion content and other environmental parameters[12].Di Xiaotan proposed steel section loss rate formula in considering the basic parameters, the impact of environmental conditions and concrete materials [41].

Theoretical model more comprehensively reflects the corrosion process, but difficulties are encountered in the determination of the model parameters. Although the empirical formula is simple, it cannot fully consider the different environmental conditions. Consequently, the empirical models need further verification.

Zhang et al.[42] studied the variation of plastic properties of rust damage steel. Huiet al. [43] discussed the statistical relationships between the mechanical properties and steel damage after corrosion. Based on a large experimental study, they proposed a method for the determination of corroded reinforced elongation, tensile strength and yield strength through

Yuan et al. [44]studiedrapid corrosion, in particular the affect of pitting corrosion on degradation of reinforced mechanical. They showed that due to the stress concentration on rust pit, the yield strength and elongation decrease with the increase in the of steel corrosion rate. A reinforced stress - strain relationship was proposed. But this relationship did not consider the change of elastic modulus before and after the corrosion of corroded reinforced. In addition it was established on a limited number of trials. Ding and Cui [45] conducted long-term (10 years) experiments on concrete reinforcement corrosion. They analyzed the influence of the steel corrosion in concrete on the protective layer cracking and mechanical properties under atmospheric conditions.

1.3.3 Durability of components

Based on the durability study in engineering materials, the main purpose of the research on durability concerned the quantitative impact on the microstructure of the material damage, the bearing capacity of members, the foundation of structural durability assessment and remaining life prediction. The durability of the bolt structure is a system-engineering problem. In order to solve this problem, it is necessary to obtain the characteristics and laws of the various components, and grasp the contact and the laws between them for ultimately achieving structural durability assessment and remaining life prediction. The research on durability concerned the mechanical properties of corroded components, comparative analysis of elements corrosion damage form to the front and rear, the law of development of cracks and deformation of corrosion members, the capacity calculation method of corroded components and the recession laws of corroded reinforced and concrete bonding performance.

1.3.3.1 Research on bearing capacity of corroded components

Research on bearing capacity of corroded components can be divided into two categories: experimental and numerical. Xi'an Architecture and Technology University, China Mining University, Zhejiang University and Ministry of Metallurgical Construction Research Institute conducted researches on the impact of extent of corrosion to the bearing capacity and ductility of beams, columns and other elements. Results were obtained from rapid electrochemical corrosion [46-55], long-term exposure to natural [56] and the actual aging structure [57, 58]. They

showed that the bearing capacity, ductility and plastic performance of the corrosion components significantly reduced and brittleness performance significantly increased. Morinaga [59] and Nakayama et al. [63] conducted study on the bearing capacity decline of steel corrosion. Ting studied the effects of flexural capacity of corrosion reinforced concrete beam and prepared computer simulation program of curve *M-ϕ* under different degrees of corrosion [64]. Hui Zhuo assumed that the amount of steel corrosion along the beam was a parabolic distribution, and analyzed the effects of corrosion to the flexural capacity of beam by using three-dimensional nonlinear finite element [65]. Yuan Yingshu used the finite element method with a degradation mathematical model of reinforced concrete to study the structure degradation and properties of the beam [66]. Li Yong assumed that steel corrosion was ellipsoidal contour to any three-dimensional point of corrosion as a virtual board unit displacement discontinuity model. He established a three-dimensional numerical discrete model [67]. Most of the existing component capacity model can be integrated into the following forms:

$$M = kM_0$$

Among them:M -- bearing capacity of rust damage components;

M_0--bearing capacity of intact components;

k -- components bearing capacity reduction factor. The determination of the k value should consider the impact of the cross-sectional damage of component, mechanical properties of corrosion steel and reinforced concrete bonding performance deterioration and factors related to the geometric parameters of the member section, the function of the crack width and steel corrosion rate.

1.3.3.2 Bond performance of rusty member

Bonding between steel and concrete ensures the stress transfer. Steel corrosion can lead to a reduction in the steel-concrete adhesion. Anchorage structure performances rely on the bonding properties between bolt and grouting and grouting and bolted rock mass. The main factors that affect the bonding properties of components are concrete strength, the thickness of the protective layer and bar diameter.

Al-Sulaimani[68] conducted pull-out tests of partial corroded reinforced and loaded tests of

uniform corrosion of steel beams, and studied the bonding properties of four rust phases like without cracks, cracks, cracking, after cracking. Abrishamiand Mitchell [69] studied bond properties and failure modes under three different loading and proposed adhesion reduction factor to reflect the impact of corrosion cracks on bond strength [70]. Based on the bond failure test results of rapid corrosion of steel specimen, Pan Chenghua established constitutive model for ultimate bond strength and steel corrosion rate, from which the thickness of the protective layer of concrete, concrete strength, rebar diameter, the type and the location of the five kinds of factors were taken into account [71]. Yuan Yingshu through experimental research, considering the average corrosion rate of steel, protective layer thickness and reinforced diameter of three factors, established the bond stress - slip relationship degradation model of corrosion steel and concrete [66]. Bond corroded reinforced concrete constitutive relationship models proposed by Tongji University[72] and Zhejiang University[73] considered the effect of bolt position to the after the rust of reinforced concrete bond-slip relationship, and provided the basis for FEM calculation of reinforced concrete members after rust.

1.3.4 Structural durability assessment

Whether it is the bolted structure or concrete structure, it is a structural system, in which the durability assessment should reflect the impact of each component on the overall assessment. Determination of the durability index and selection of assessment methods is the key to Structural durability assessment.

Durability index is a qualitative or quantitative index, used to reflect the aging degree. Lu [74] divided structural durability index into two sets of index: the degree of deterioration and the rate of deterioration. Yuan and Zhao [75] used the fractal theory to analyze the uniformity and surface cracks of aging reinforced concrete. They presented ultrasonic velocity and rebound fractal dimension on behalf of the degree of uneven concrete, which fractal dimension of fracture can be used as two effective measure of the structure of the aging degree. Sabins et al. [76] assessed concrete structures according to the bonding condition of concrete and steel, the concrete surface cracks, weathered, peeling phenomenon and humidity.

Lu Mu used gray correlation for the guidelines and the Analytic Hierarchy Process (AHP) for the foundation, made the durability factors as durability index, the component durability as

structure durability index and structural durability rating as the target layer. He proposed structural durability of the multi-index weighted multi-level hierarchical evaluation method [74]. China's "reliable identification procedure of steel industry (structure) building" (YBJ219-89) [16]is based on the remaining useful life of the durability evaluation method to determine the next target life of Y_m according to the safe production and plant overhaul and predict remaining life of each component of natural life Y_r according to the extent of structure damage and injury rate, and finally by the structural durability factor $K_n = Y_r/Y_m$, the durability of structure can be divide into four grade. In recent years, more and more fuzzy theories were introduced into the structure durability assessment. Zhao Pengfei divided the durability into four grades according to the remaining life of the component (one grade: 50 years or more; two grade: 30 to 50 years; three grades: 10 to 30 years; four grade: 10 years or less). He used the fuzzy mathematics theory to establish multi-membership function durability rating method [77]. "Durability of Concrete Structure Evaluation Standards" (draft) assessed by project, component items, structure three grade four levels (project: a ~ d level, component: A ~ D level, structure: one ~ four level) step by step, in which industrial plants were assessed according to the failure tree analysis; and civil were assessed according to fuzzy comprehensive evaluation method [12]. Sun [78] considered the carbonation depth of concrete as normal distribution function. A membership function of carbonation to the durability injury and distribution function of degree of durability damage was established to assess the durability member according to the degree of injury. Tongji University proposed three fuzzy comprehensive evaluation methods for the reliability of existing building. The method used the analogy method to quantify the factors, according to the membership functions and weight of each factor adoption weighted average model as a comprehensive evaluation model [12]. Tongji University, Pan Liming and Shi Jiajun determined the weight using analytic hierarchy process (AHP), assessed rating according to the maximum membership principle, and classified the safety and durability of bridges as excellent, good, fair, poor, bad 5 grade, to establish a durability assessment model of steel - reinforced concrete composite beam cable-stayed bridge[12]. Adopting the similar approach, Sabins[76] established a durability rating method of culvert water components.

In order to assess the durability of structure, some countries established norms and regulations.

US ACI Committee 364 established a durability evaluation norms "Guide for Evaluation of Concrete Structure Prior to Rehabilitation" [80], which presents assessment of concrete structure before maintenance including the preliminary investigation, detailed investigation, documentation, site inspection and survey, sampling and material testing, evaluation and summary reports.

1.3.5 Service life prediction of structure

Life prediction of structure is an important basis for maintenance decisions. Based on the remaining life of the structure, different maintenance decisions are formulated to ensure the structural safety. For bolts used in medium-sized civil engineering, the structure service life prediction would result in considerable economic benefits.

1.3.5.1 Service life prediction of materials

Service life prediction of material is the basis of service life prediction of structure. Papadakis et al. [81] pointed out that the physical characteristics of the control of gas, liquid and ion inside the concrete diffusion process determined its durability in concrete. They studied the distribution of the molar concentration of carbonized materials, the porosity and pore size, and the formulas of the main parameters affecting the durability of concrete like pores saturation and concrete effective diffusion coefficient under the influence of temperature and relative humidity, which laid the foundation for the qualitative prediction and control of pre-corroded reinforced concrete aging process. The service life prediction of construction materials focused on concrete. Five main methods could be used [82]: empirical estimation method, similar extrapolation method, rapid test method, mathematical model method, stochastic process probabilistic analysis method.

Empirical estimation method is a semi-quantitative prediction method, based on testing, field testing and cumulative experience. Subjectivity of this method was strong, and its accuracy depends on the level of knowledge and the richness of the experience of the expert.

Similar extrapolation method was not widely used, but there had certain prospects. It is assumed that if a real life of material known, then another similar material exposed to similar environments should have the same life. However, due to the difference of the material, geometry, construction process and the use of the environment, the material life was discrete

largely, which would lead to a greater error on predictions, and could be only as a reference in service life prediction.

The premise to use rapid test method consist in that the deterioration mechanism of rapid test and use process is the same, and the degradation rate relationship between the two processes is linear (make sure to get the acceleration coefficient k). Under this condition, the natural life of the concrete is k times in rapid tests. But in fact due to the lack of long-term performance data of concrete, difficulties were encountered in the determination of k. In addition, external environment conditions and materials deterioration mechanism of rapid test were different from real environments.

The Mathematical models for the service life prediction are based on the material performance degradation law. Service life prediction models of concrete under different influence factors are available: concrete reinforcement corrosion service life prediction model established by Tuutti[83], concrete service life prediction model under sulfate attack established by Atknison and Hearne[84], dissolved leaching model of gypsum and anhydrite established by James and Lupton [85]. Yu and Sun [86] used the Fick's diffusion law to establish a diffusion equation considering chloride ion binding capacity of concrete, Time-dependent chloride ion diffusion coefficient and concrete structure micro-defects affect, and established chloride ion diffusion theory model for predicting the service life of concrete. Mathematical model method was reliable, less data requirement and wide range of applications.

Research works were conducted on the stochastic process probabilistic analysis method combined with mathematical statistics, reliability, and stochastic process theory. Sentler[87] established carbonized stochastic model. Siemes [88] adopted the average of deterministic model parameters to predict the service life of structure. Guan et al.[89] used the degree of damage as physical of durability of concrete, combined with reliability and damage theory. They proposed a prediction of the concrete life of suitable multivariate Weibull distribution model applied to different boundary conditions and univariate and multivariate conditions, and applied under freezing conditions [90]. Prezzi [91] established service life prediction method of concrete used in marine environment based on the concept of reliability and stochastic processes. Wu [92] proposed durability assessment methods of reinforced concrete service life under the chloride environment. However, lacking of sufficient data accumulation, random

parameters in stochastic process model were difficult to determine, which limited the application of this method.

1.3.5.2 Service life prediction of concrete elements and structures

Reasonable definition of the end life of structure was the premise to predict structure service life. The definition of the end life of structure largely varied according to the varying importance degrees of structure. According to the different Standard, the definition of the end life of structure can be divided into the aging life of the protective layer, the service life of cracking component, the service life of steel corrosion and the reliability life of component. The protective layer aging life is the time that carbonation to a depth of the steel surface or the chloride ion concentration in the steel surface reaches a critical value [93]. The corresponding prediction model was established based on the concrete carbonation depth prediction model and Fick's second law of chloride ion diffusion equation. Xu and Yang [94] proposed the pre-stressed structural design carbonation service life model. Maage [95] proposed the existing structure service life prediction model based on Fick's diffusion second law. Funahashi [32] used reinforcement corrosion as a sign of the end of life to calculate parking pre-stressed structural service life by the finite difference method.

Structural cracking life used the time of longitudinal crack development to a certain width caused by volume expansion of steel corrosion product as structure service life. Hui Yunling used the longitudinal cracks width 0.6mm as a sign of the end of bearing capacity, and proposed the remaining life of reinforced concrete structures prediction formula [96]; Qu and Zhang [97] used concrete corrosion splitting as the sign of the end of durability service life, and proposed concrete durability service life prediction method under aggressive environment based on the statistical distribution of the number of pitting corrosion on steel. Bažant [35] and Youping Liu [98] used the concrete surface corrosion cracking as the limit state to respectively proposed structure service life prediction models under each marine environment. Morinaga [99] used chloride ions due to steel corrosion that caused the rust cracks appearing on concrete surface as the failure criteria, and established the amount of steel corrosion and reinforcement corrosion rate of longitudinal test relational model to predict the structure service life. Xiao Congzhen, Liu Xila in Tsinghua University used longitudinal cracking (section loss rate reach

5%) as the end of life, using number Theory simulation combing with variance reduction techniques to predict the structure service life [100].

The Architectural Institute of Japan used the time when steel stress reaches the yield stress caused by cross-section decreases due to reinforcement corrosion as the end of life [12]. "Steel industrial building (structure) reliability identification procedure" (YJB219-89) used reinforced comprehensive corrosion (ϕ <10mm) or corrosion area more than 6% (ϕ> 10mm) as the sign of the end of life to proposed the theoretical prediction formula of remaining life [16]. Li [101] proposed a full life cycle assessment of the performance of corrosion concrete structures anti-aging model, used the strength and reliability limit state as structural performance evaluation criteria to determine the life cycle of corrosion concrete structures. Enright [102] adopted system reliability methods considering with the constant load and activity load change with time to predict the reliability service life of reinforced concrete highway bridges under erosion environment.

In addition Amey et al.[103] defined the service life of the structure as the time from it exposed to the environment to the production of significant damage, assumed that the life of the entire structure depends on one of the shortest life of member, and proposed to predict the service life of reinforced concrete in different environment especially in marine environment under the influence of the surface environment, chloride diffusion, ambient temperature, season and construction errors and other factors. Ahmad et al. [104] established a general method to predict the service life of reinforced concrete structures. Different laboratories and research institutions established their structural life prediction methods (Table 1.2).

Table 1.2 The method of service life perdition of structures proposed by foreign lab and research organization[104]

Research institutions Name	Method	The main content
RILEM TC 31-PCM	Materials performance standards	Materials performance analysis, evaluation and reinforcement countermeasures
RILEM TC 60-CSC	reinforced concrete corrosion	The exact definition of useful life, the requirements and the aging process
CIB W60	Performance concept of	The durability of the concept

	building structures	is divided into several sub-items: usage, materials, design and maintenance
ASTM E632-81	using the results of rapid test to predict Useful life of structural components and materials	problem definition, pre-experiment, experiment, interpret and report of data

Predicting the service life of structures requires considering the level of socio-economic development and people's risk tolerance. Zhao et al. [105] and Qu et Lu [106] proposed criteria for the remaining service life of existing concrete structures based on the combination of reliability and economic optimization.

1.4 Research features, significance and application value of this thesis

The study of the durability of bolt is a comprehensive edge science involving a number of areas like mathematics, mechanics, physics, chemistry, materials and structure. Therefore, it needs to study the issue from different angles, using a variety of research methods, then it may be have breakthrough.

The study of the durability of bolt is a multi-target, multi-factor system engineering problem. Many factors and mutual coupling affect the durability of the bolt; characterizing bolt durability index is often more than one (e.g. durability grade, residual life, reliability, etc.), so considering many factors in the premise the durability of anchorage system to achieve optimal is typical system engineering problems.

Durability of bolt is uncertainty, fuzziness and randomness. Feature of bolt technology determines its concealment, so when bolt construction is completed if we do not use special monitoring methods, it would difficult to know the work performance. And in the project of bolt production, we have a lot of unknown natural or man-made factors, resulting in material properties of bolt, protective systems, anchorage effects which existed a lot of unknown information, so the bolt durability problem was uncertain, fuzzy and random.

Research on the mechanical properties and durability assessment of bolt can reveal potential dangers and make timely maintenance decisions. Anchorage service life in general is more than 50 years, requiring a good durability. However, poor working conditions degraded the durability of bolts. Safety requires periodically comprehensive assessment of the remaining

life prediction on all aspects of the bearing capacity, the anchorage effect and the protection systems of the bolt by visual inspection and physical testing methods.

Research on the mechanical properties and durability assessment of bolts can be used. The empirical method was used in bolts' design, which resulted in conservative projects, but in other works, the durability of the bolt existed shortage. Results of the study on bolt durability can be applied to the design of pending construction durability, according to the service life and safety levels of pending project to find the best balance between durability and economy.

1.5 Research roadmap of the thesis

According to the statistical data, corrosion is a leading factor in durability degradation. It has tow effects on the capacity of bolts: (i) it leads to the cracking of the mortar cover due to the expansion of corrosion products; (ii) it results in the imperfect bonding between bolts and mortar. In the dissertation, some mechanical studies are conducted on the mechanical properties of corroded anchorage system by theoretical analysis, experiments and numerical analysis; and at the same time a method of evaluation of durability of corroded anchorage system is also proposed.

The principle issues of the dissertation are:

- Understanding of the mechanism of corrosion in reinforced concrete andestablishing theoretical formulas of corroded expansion force changes.
- Establishing a spatial bolt rust analytical model to study the three-dimensional stress field of the bolt due to bolting force and rust expansion force, to find the analytic solutions of each stress components in the bolt space issues.
- Use of the elastic-viscoplastic model to understand the corrosion process over time and determine the steady state of stress and strain. With the elastic-viscoplastic theory, the structural load - displacement curve gently changes. When compared to the period of instability curve, the sensitivity is not high, and therefore it is not easy to determine the safety factor. Application of the elastic-viscoplastic theory can avoid this shortcoming. For these reasons, the finite element program for corroded bolt of elastic viscoplastic potential theory will be used for the first time.

- Use of the composite element method for the analysis corroded anchorage systems.
- Validation of the finite element numerical modeling on experimental results.

References

1. Zeng X M, Chen Z Y, Wang J T. Research on safety and durability of bolt and cable-supported structures. Chinese Journal of Rock Mechanics and Engineering. 2004; 23(13):2235-2242.
2. Prestressed bolt durability domestic research special report.Armed Forces Gorge Hydropower Engineering Command.Yangtze Water Resources Commission gorge engineering representatives bureau, 2001
3. Zhang M. Analysis of safety and durability of China railroad tunnel structures. Forum of Engineering Science and Technology: Safety and Durability of Construction Structures. Beijing: Tsinghua University Press, 2001: 1-4.
4. Liu X L. Basic research on durability of structure works. In: Forum of Engineering Science and Technology: Safety and Durability of Construction Structures. Beijing: Tsinghua University Press, 2001: 200-206.
5. Wang A L, Yao Y. Research on durability of concrete in importance works and its application to engineering. Beijing: China Architecture and Building Press, 2001.
6. Yao Y. Durability of concrete material—research evolve on safety of concrete in importance work. Forum of Engineering Science and Technology: Safety and Durability of Construction Structures. Beijing: Tsinghua University Press, 2001: 266-273.
7. Zeng X M, Lei Z L, ZhangW J, et al. Discussion about “time bomb” question for bolt. Chinese Journal of Rock Mechanics and Engineering. 2002; 21(1):143-147.
8. Moskvin B M, et al. The corrosion and defending methods about concrete and reinforced concrete. Beijing: Chemical Industry Press, 1988.
9. Stanton D E. Process American Society, Civil Engineer, 1940.
10. Lu M. Recent study and research directions of concrete durability. Industrial Construction. 1997; 27(5):1-6.
11. Jin W L, Zhao Y X. Durability of concrete structures. Beijing: Science Press, 2002.
12. Zhang Y, Jiang L X, Zhang W P, et al. An introduction to durability of concrete structures. Shanghai: Shanghai Science & Technology Press, 2003.
13. ACI Committee 437. Strength Evaluation of Existing Concrete Building, 1991.

14. Duan S J. Introduction to Code for Durability Design of Concrete Structures (Trial) of Japan. Journal of North China Institute of Water Conservancy and Hydroelectric Power. 1991,25 (1): 56-60.

15 Zhou Y, et al. Translation of: Durable concrete structure: design guide (2th edition). Beijing: Institutes of Building Structures, China Academy of Building Research, 1991.

16 YBJZ19-89. Reliability evaluation procedures of iron and steel building. Beijing: Metallurgical Industry Press, 1991.

17 Gong J X, Zhao G F. State of the art of durability research of reinforced concrete structures. Industrial Construction. 2000; 30(5):1-5.

18 Papadakis V G, Vayenas C G, Fardis M N. Fundamental modeling and experimental investigation of concrete carbonation. ACI Material Journal. 1991; 88(4):363-373.

19 Niu D T, Shi Y C, et al. Reliability analysis and probability model of concrete carbonation. Journal of Xi'an University of Architecture &Technology. 1995; 27(2):252-256.

20 Niu D T, Chen Y Q, et al. Model and reliability analysis for carbonation of concrete structures. Journal of Xi'an University of Architecture &Technology. 1995; 27(4): 365-369.

21 Li Q F, Liu C G, Zhang Y L. Fuzzy analysis of durability for concrete carbonation. Journal of Zhengzhou University of Technology. 1996; 17(3):7-12.

22 Yuan Q, Zhao G F. Study on forecast model of time series analysis of concrete carbonization depth. Journal of Dalian University of Technology. 2000; 40(3):344-347.

23 Jin W L, Zhang L, Yan F. Application of functional-link neural network in analysis of concrete carbonization. Journal of Zhejiang University. 1998; 32(5):519-525.

24 Zhang Y, Jiang L X. A practical mathematical model of concrete carbonation depth based on the mechanism. Industrial Construction. 1998; 28(1):16-19.

25 Steffens A, Dinker D, Ahrens H. Modeling carbonation for corrosion risk prediction of concrete structure. Cement and Concrete Research. 2002; 32(6):935-941.

26 Jin W L, Yan F. Probabilistic model of carbonation Index on concrete durability.

Concrete. 2001,3(1):35-37.

27 Gong J X, Zhao G F, Zhao S C. Influence of corrosion of reinforcement on reliability of reinforced concrete structures in atmospheric environment. Journal of Dalian University of Technology. 2000; 40(2):210-213.

28 Bažant Z P, et al. Physical model for steel corrosion in concrete sea structures-theory. Journal of the Structural Division. 1979; 105(6):1137-1153.

29 Collpepard M, et al. Penetration of chloride ions into cement paste and concretes. American Ceramic Society. 1972(55).

30 Clifton J R. Predicting the service life of concrete. ACI Material Journal. 1993; 90(6):611-617.

31 Sun W, Yu H F. Study on development of durability and service life of concrete structure engineering. Proceeding of Engineering Forum on Security and Durability of Civil Engineering. Beijing: Tsinghua University Press. 2001:274-285.

32 Funahashi M. Predicting corrosion-free service life of a concrete structure in a chloride environment. ACI Materials Journal. 1990; 87(6):581-587.

33 Hong D H. Corrosion and protection of steel bars in concrete. Beijing: China Railway Publishing House, 1998.

34 Stephen L A, Johnson D A, et al. Predicting the service life of concrete marine structures: an environmental methodology. ACI Structure Journal. 1998; 95(2):205-214.

35 Bažant Z P, et al. Physical model for steel corrosion in concrete sea structures-application. Journal of the Structural Division. 1979; 105(ST6):1155-1166.

36 Niu D T, Wang Q L, Wang L K. Predeterminate model of steel corrosion extent in reinforced concrete structures before producing corrosion crack. Industrial Construction. 1996; 26(4):8-10.

37 Niu D T, Wang Q L, Wang L K. Predetermination of steel corrosion extent in reinforced concrete structures after corrosion crack. Industrial Construction. 1996; 26(4):11-13.

38 Jin W L, Yan F, Zhang L. A predeterminate model of steel bar corrosion ratio considered of concrete carbonation model. Journal of Zhejiang University. 2000;

34(2):430-434.

39 Zhao Y X, Jin W L. Corrosion ratio of reinforcement bar in reinforced concrete construction at the moment of cracking due to corrosion expansion. Journal of Hydraulic Engineering. 2004(11): 97-101.

40 Hui Y L. Assessment and predicted experimental study on corrosive degree of reinforcements in concrete structures. Industrial Construction. 1997; 27(6):6-9.

41 Di X T, Zhou Y．On corrosion of reinforcement in atmospheric environment．The 4th Conference on Concrete Durability in China．Beijing：China Concrete Durability Society, 1996.

42 Zhang P S, Lu M, Li X Y. Mechanical property of rustiness reinforcement steel. Industrial Construction. 1995; 2(9):41-44.

43 Hui Y L, Lin Z S, Li R. Experimental study and analysis on the property of corroded rebar. Industrial Construction. 1997; 27(6):10-13.

44 Yuan Y S, Jia F P, Cai Y. Deterioration of mechanical behavior of corroded steel bar. Industrial Construction. 2000; 30(1):43-46.

45 Ding W, Cui G H. Test and research of influences of reinforcing bar rust on the cracking of concrete protection layer and mechanics performances of reinforcing bar in concrete under the condition of atmosphere. Concrete. 2000(1):38-41.

46 Yuan Y S, Yu S. Deterioration of structural behavior in corroded reinforced concrete beam. Journal of Building Structures. 1997; 18(4):51-57.

47 Yuan Y S, Li G. Deterioration characteristics of corroded reinforced concrete columns. Building Structure. 2002; 32(10):18-20.

48 Jin W L, Chen J, et al. Corrosion Influence on Mechanical Property of Short Reinforced Concrete Beam. Journal of Huazhong University of Science and Technology. 2003; 20(1):1-3.

49 Shi Q X, Niu D T, Yan G Y. Experimental research on hysteretic characteristics of corroded R. C. members with flexural and compressive axial loads under repeated horizontal loading. Earthquake Engineering and Engineering Vibration. 2000; 20(4):44-50.

50 Hui Y L, Li R, et al. Experimental studies on the property before and after corrosion

of rebars in basic concrete members. Industrial Construction. 1997; 27(6):14-18.

51 Shi Q X, Li X J, Niu D T. Tentative study on the bearing capacity of R. C. eccentric compressive members before and after reinforcement corrosion. Journal of Xi'an University of Architecture &Technology. 1999; 31(3):218-221.

52 Jin W L, Zhao Y X. Test study on bending strength of corroded reinforced concrete beams. Industrial Construction. 2001; 31(5):9-11.

53 Lee H S, Noguchi T, Tomosawa F. Evaluation of the Bond Properties between Concrete and Reinforcement as a Function of the degree of Reinforcement Corrosion. Cement and Concrete Research. 2002(32):1313-1318.

54 Lundgren K. Modeling the Effect of Corrosion on Bond in Reinforced Concrete. Magazine of Concrete Research. 2002; 54(3):165-173.

55 Gabrera J G. Deterioration of Concrete due to Reinforcement Steel Corrosion. Cement and Concrete Composites. 1996; 18(1):47-59.

56 Niu D T, Zhai B, Wang L K, et al. Analysis for bearing capacity of RC beam with rusting steel- bar. Building Structures. 1999; 29(8):23-25.

57 Tao F, Wang L K, et al. Experimental study on the bearing capacity of existing reinforced concrete members. Industrial Construction. 1996; 26(4):17-20.

58 Jin W L, Chen J, et al. Experimental study on flexural capacity of reinforced concrete beams in marine environment. Journal of Zhejiang University. 2004; 38(5):603-609.

59 Morinaga S. Remaining life of reinforced concrete structure after corrosion cracking. Durability of Building Materials and Components. 1996(71):127-136.

60 Tachibana Y, Kajikawa Y, Kawamura M. The behavior of RC beams damaged by corrosion of reinforcement. Proceedings of Japan Society of Civil Engineers. 1989; 402(10):105-114.

61 Okada K, Kobayashi K, Miyagawa T. Influence of longitudinal cracking due to reinforcement corrosion on characteristics of reinforced concrete members. ACI Structural Journal. 1988: 134-140.

62 Katayama K, Maruyama K, Kimura T. Flexural behavior of RC beams with corrosion of steel bars. The 49th Annual Meeting of Japan Cement Association. Japan Cement Association, Tokyo, Japan, 1995:880-885.

63 Nakayama K, Yamakawa T, Iraha S, et al, An experimental study on elasto-plastic behavior of R/C columns damaged by electrochemical corrosion test. Proceeding of Japan Concrete Institutes of Annual Conference. 1995:880-885.

64 Ting S C, Nowak A S. Effect of reinforcing steel area loss on flexural behavior of reinforced concrete beams. ACI Structural Journal. 1991; 88(3):309-314.

65 Xi Z, Wang Q L. Computer simulation on load carrying capacity of damaged reinforced concrete members. Journal of Xi'an University of Architecture &Technology. 1997; 29(4): 431-434.

66 Yuan Y s, Jia F P, Cai Y. The structural behavior deterioration model for corroded reinforced concrete beams. China Civil Engineering Journal. 2000(3):47-52.

67 Li Y H, Ge X R. 3D corrosion layer model and numerical analysis for reinforced concrete structure in service. Science in China(Series E). 2002; 32(5):653–661.

68 AI-Sulaimani G J, et al. Influence of corrosion and cracking on bond behavior and strength of reinforced concrete members. ACI Structural Journal. 1990; 87(2):220-231.

69 Abrishami H H, Mitchell D. Analysis of bond stress distributions in pullout specimens. Journal of Structural Engineering. 1996(3):255-261.

70 Wang L K, Tao F, et al. Experimental study on bond and boltage of corroded reinforcement in concrete. Industrial Construction. 1996; 26(4):14-16.

71 Pan Z H, Niu D T, Wang Q L. Experimental study on relation between corrosion rate and ultimate bond strength. Industrial Construction. 2000; 30(5):10-12.

72 Zhang W P, Zhang Y. Bond-slip relationship between corroded steel bars and concrete. China Civil Engineering Journal. 2001; 34(5):40-43.

73 Zhao Y X, Jin W L. Test study on bond stress-slip relationship of concrete and steel bar. Journal of Building Structures. 2002; 23(1):32-37.

74 Lu M. Durability assessment based residual service life predication of existing R. C. structures. Building Science. 1999; 15(2):23-28.

75 Yuan Q, Zhao G F. Fractal characteristics of aged reinforced concrete structure. Journal of Hydraulic Engineering. 2000(12):21-25.

76 Sabnis G M, Sorokko R, Doshi K. A rating system for structural evaluation of

concrete buildings. Concrete International. 1990; 12(12): 63-65.

77 Zhao P F, Wang X M. A study on RC members durability appraise by fuzzy mathematics. Industrial Construction. 1997; 27(5):7-10.

78 Sun Z S. Analysis of evaluation method on durability of reinforced concrete structure. Journal of North China Institute of Water Conservancy and Hydroelectric Power. 1995; 16(3):85-88.

79 Zhu B X. The fuzzy evaluation of sluices water reinforced concrete members and durability grade. Water Resources and Hydropower Engineering. 2000; 31(7):29-32.

80 ACI Committee 364. Guide for evaluation of concrete structures prior to rehabilitation. ACI Materials Journal. 1993; 90(5):479-499.

81 Papadakis V G, Vayenas C G, Fardis M N. Physical and chemical characteristic affecting the durability of concrete.ACI Material Journal. 1991; 8(2):186-196.

82 Clifton J R. Predicting the service life of concrete. ACI Material Journal. 1993; 90(6):611-617.

83 Tuutti K. Corrosion of steel in concrete. Swedish Cement and Concrete Research Institute, Stoekholm, 1982.

84 Atkinson A, Hearne J A. Mechanistic model for the durability of concrete barriers exposed to sulphate-bearing groundwater. MRS Proceedings. Cambridge University Press. 1990: 149-156.

85 James A N, Lupton A R. Gypsum and anhydrite in foundation of hydraulic structures. Geotechnique. 1978; 28(3):249-272.

86 Yu H F, Sun W, et al. Prediction model for service life of reinforced concrete structures in salt lakes and its applications. Journal of Southeast University. 2002; 32(4):638-642.

87 Sentler L. Stochastic characterization of carbonation of concrete. 3rd International Conference on the Durability of Building Materials and Components. Technical Research Centre of Finland. 1984:569-580.

88 Siemes A, Vrouwenvelder A, Veukel A. Durability of buildings: a reliability analysis. Department of Civil Engineering, Delft University of Technology. 1985:3-48.

89 Guan Y G, Sun W, Miao C W. One service-life prediction model for the concrete

based on the reliability and damage theories Ⅰ: narration and establishment of the model. Journal of the Chinese Ceramic Society. 2001; 29(6):530-534.

90 Guan Y G, Sun W, Miao C W. One service-life prediction model for the concrete based on the reliability and damage theories Ⅱ: verification and application of the model. Journal of the Chinese Ceramic Society. 2001; 29(6):535-540.

91 Prezzi M, Geyskens P, et al. Reliability approach to service life prediction of concrete exposed to marine environments.ACI Materials Journal. 1996; 93(6):544-552.

92 Wu J, Wu S X. Durability assessment for reinforced concrete structures in chloride environment. China Civil Engineering Journal. 2005; 38(2):59-63.

93 Liu Z Y, Sun W, et al. Research and progress of modeling chloride ingress for corrosion risk prediction of marine concrete. Industrial Construction. 2004; 34(6):61-64.

94 Xu L, Yang X P. A service life model for prestressed structure design. Journal of Jiangsu University. 2002; 23(1):71-74.

95 Maage M, et al. Service life prediction of existing concrete structures exposed to marine environment. ACI Materials Journal. 1996; 93(6):602-608.

96 Hui Y L. Durability damage estimation and the method of life prediction for corrosion of reinforcements in concrete structures. Industrial Construction. 1997; 27(6):19-22.

97 Qu W J, Zhang Y. Discussion on the predicting method about durability life of concrete structure under erosion environment condition. Industrial Construction. 1999; 29(4):40-44.

98 Liu Y, Weyers R E. Modeling the time-to-corrosion cracking in chloride contaminated reinforced concrete structures. ACI Materials Journal. 1998; 95(6):675-681.

99 Morinaga S. Prediction of service life of reinforced concrete buildings based on the corrosion rate of reinforcing steel. Durability of Building Materials and Components, Proceedings of the 5th International Conference held in Brighton, UK. 1990.

100 Xiao C Z. Mechanism study and number-theoretic method for reinforcement

corrosion in the RC structures. PHD Thesis. Beijing: Tsinghua University, 1995.

101 Li C Q. Life-cycle modeling of corrosion-affected concrete structures: propagation. journal of structural engineering. 2003; 129(6):753-761.

102 Enright M P, Frangopol D M. Service-life prediction of deteriorating concrete bridges. Journal of Structural Engineering. 1998; 124(3):309-317.

103 Amey S L, Johnson D A, Miltenberger M, et al. Predicting the service life of concrete marine structures: an environmental methodology. ACI Structural Journal. 1998; 95(2):205-214.

104 Ahmad S, Bhattacharjee B, Wason R. Experimental service life prediction of rebar-corroded reinforced concrete structure. ACI Materials Journal. 1997; 94(4):311-316.

105 Zhao S C, Zhao G F, Gong J X. Analysis of remaining service life for concrete structures based on reliability and optimization theory. Industrial Construction. 2002; 32(4):37-39.

106 Qu W J, Luo X Q. Service life prediction of existing structure residual technology. China Journal of Highway and Transport. 1999; 12(4):29-36.

Chapter 2: Steel corrosion mechanism and model

2.1 Steel corrosion

Bolt is composed of steel and cement mortar, so in this essay, reinforcement corrosion mechanisms is used for reference by bolt corrosion mechanism. A large number of works has proved that steel corrosion is a major factor affecting the durability of existing structure in reinforced concrete. Fresh concrete is alkaline; the PH value is generally greater than 12.5, prone to inactivation in an alkaline environment, so that the steel surface produces a passive film to prevent corrosion of reinforcing steel in concrete. The transfer of carbon dioxide, water vapor and chlorine ions and other harmful substances from the concrete surface into the concrete through the gap and Neutralization with the alkaline substances in concrete materials reduces PH value of concrete and could become lower than 9. In this case, the passivation film of buried reinforced concrete surface is gradually destroyed. The steel corrosion occurs and could cause cracking of concrete cover. Also, bond strength between steel and concrete would be damaged; reinforced stress section reduced and structural strength decreased which result in reducing the structural durability. Under normal circumstances, reinforced concrete has more severe corrosion conditions subject to chloride contaminated.

Steel corrosion study is a very important part of study on the durability of reinforced concrete member. Large experimental research, engineering investigation and theoretical analysis were conducted. So far, there is no mathematical model considering both full theoretical basis and comprehensive range of practical factors, so the prediction of concrete reinforcement corrosion still requires important research.

2.1.1 Concrete reinforcement corrosion mechanism

Carbon dioxide, chloride and other corrosive media lead to alkaline reducing or concrete protective layer cracking, which result in passivity steel surface damaged. Different parts of the steel surface form a cathode and an anode. Under certain environmental conditions, the reinforcement corrosion starts. Generally, we observe porphyritic corrosion that rust distributed over a wider surface area. Steel corrosion damage characteristics can be summarized as [1]: crack extending along the reinforcement direction conduct; bond strength of steel and concrete decline and loss; loss of steel section; steel stress corrosion cracking.

2.1.1.1 Steel corrosion mechanism

Concrete reinforcement corrosion is generally electrochemical corrosion. Carbon dioxide and chloride ions on the concrete have no serious damaging effects, but these two substances are the most important and most frequently encountered environmental media for reinforced concrete passive film damaged. Therefore, concrete reinforcement corrosion mechanisms include mainly concrete carbonation and chloride intrusion.

Steel corrosion in concrete structures occurs in the condition that the presence of water molecules involved, and the steel corrosion of the electrode reaction is [2]:

Anode

$$Fe \rightarrow Fe^{2+} + 2e \quad (2.1)$$

Cathode

$$O_2 + 2H_2O + 4e \rightarrow 4OH^- \quad (2.2)$$

Secondary chemical processes for the anode surface

$$Fe^{2+} + 2OH^- \rightarrow Fe(OH)_2 \quad (2.3)$$

$$4Fe(OH)_2 + O_2 + 2H_2O \rightarrow 4Fe(OH)_3 \quad (2.4)$$

Under combined effect of oxygen and water vapor, the iron on the steel surface constantly lose electrons and insoluble in water by the electrochemical reaction above, thus gradually corrode, red rust on the steel surface is generated, causing the concrete to crack. Figure 2.1 shows a macroscopic process of reinforcement corrosion in concrete under atmosphere environment.

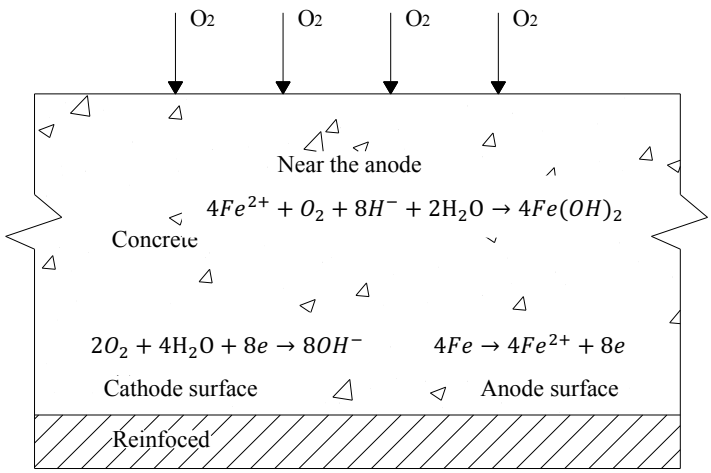

Figure 2.1 Steel corrosion processes in concrete

The most dangerous media of erosion during the service life of reinforced concrete structures is chloride ions. Its harm to concrete structure is multifaceted, and here only the mechanism of chloride to promote reinforcement corrosion is reviewed [3].

Chloride ions Cl^- and hydroxide ions OH^- competes corrosion producedFe^{2+}, forming patina$FeCl_2 \cdot 4H_2O$, and then patina migrate from the anode to the higher oxygen content of reinforced concrete pore, decomposed into brown rust$Fe(OH)_2$. Brown rust deposited around the anode, while release $H^+$and Cl^-, which went back to the anode region, so that resulting in the local acidification of the pore fluid near the anode region, and then Cl^- take out more Fe^{2+}. Thus, the chloride ion does not constitute corrosion products, nor consumed in corrosion, but as an intermediate product of corrosion, it plays a catalytic role in the corrosion. The reaction formula is

$$Fe^{2+} + 2Cl^- + 4H_2O \rightarrow FeCl_2 \cdot 4H_2O$$

(2.5)

$$FeCl_2 \cdot 4H_2O \rightarrow Fe(OH)_2 \downarrow + 2Cl^- + 2H^+ + 2H_2O \quad (2.6)$$

If there is a high concentration of chloride ion on the large area of the steel surface then the etching due to the chloride ion is uniform corrosion, but common the etching in the concrete is localized corrosion. First, form local damage in the small steel surface, which forming a small anode, when most of the steel surface had a passivation film, forming a large cathode. This particular corrosion galvanic consisting by large cathode and small anode, due to support fully of the large cathode, that iron on small anodic dissolves rapidly, produces deep erosion

pit and partial acidification on small anode area; meanwhile, due to the cathode reaction of the large cathode area, it generates OH^- and increases PH value; chloride improve concrete hygroscopicity, and ohmic resistance of the concrete pore solution between cathode and anode is reduced. Spontaneous changes in these three areas, making these localized corrosion galvanic ongoing in the form of partial depth, which is also known as localized corrosion or pitting corrosion (Figure 2.2).

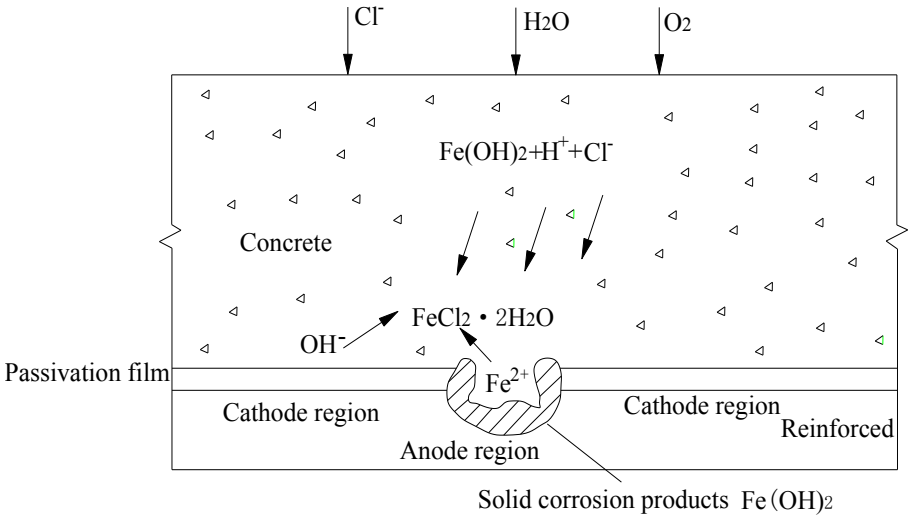

Figure 2.2 Reinforced chloride-induced corrosion points schematic

The environment of concrete structures can be divided into three types [3]:

(1) Dry environment. Moisture gradient of concrete is wet inside and dry outside. Steel has highest potential at the cracks along the bars, as the cathode increase the corrosion rate of deep reinforced and non-cracks reinforced, and accelerate produce cracks along the bars in other parts of the concrete. Due to the larger concrete resistance and its relatively large area of the anode and cathode when the various parts of steel surface as the Isolated electrode, low apparent corrosion rate, the steel corrosion problems is small under this environment.

(2) Surface moist environment. Reinforced concrete structure of this environment include frequent cycles of wet and dry environment, in which structure is exposed in the rainy season and long-term structural moist environment and so on. If these structures have cracks along the bars, their electrochemical corrosion characteristic of moisture gradient of concrete is wet outside and dries inside. Steel has lowest potential at the cracks along the bars, as the cathode increase the corrosion rate of deep reinforced and non-cracks reinforced, which showed a large cathode and a small anode characteristic, and with the widening cracks along the bars,

corrosion rate would accelerate growth on the basis of greater value.

(3) Long-term immersion environment. In this environment the corrosion electrochemical characteristics of reinforced concrete structures is basically the same like (2), but due to the small difference of inside and outside humidity and oxygen concentration, that the potential difference on different parts of the reinforcement is small. But if the width of the cracks along the bars is large, because of the greater concrete humidity, less resistivity, there may be a small potential difference at the same time produces a higher macro current. Macro current role will lead to greater growth of corrosion rate near the cracks along the bars.

2.1.1.2 Reinforcement corrosion process

Concrete reinforcement corrosion process can be divided into the following stages [3] (Figure 2.3)

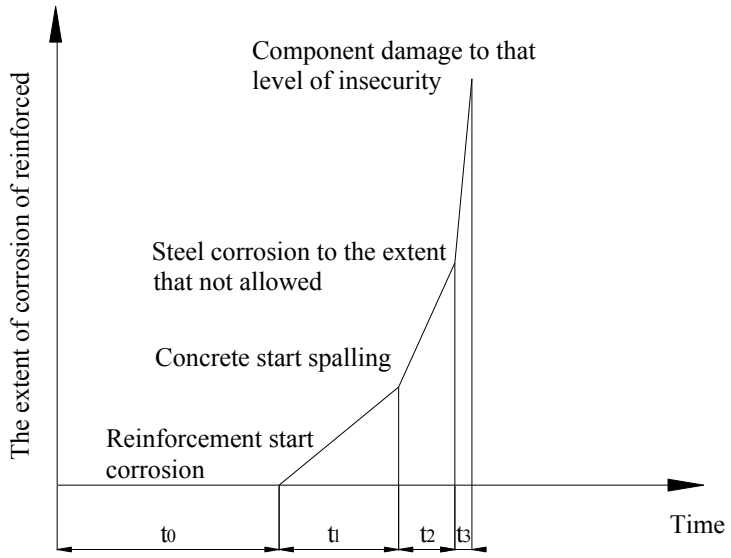

Figure 2.3 Concrete reinforcement corrosion process schematic

(1) Corrosion incubation period. From pouring concrete to concrete carbonation layer deep reaching reinforced or chloride ion intrusion resulting in steel depassivation beginning to rust so far, T_0 represents this time.

(2) Corrosion development period. From corrosion of steel beginning to protective layer on the surface of concrete damaged due to steel corrosion (such as smooth muscle split, spall or flake, etc.),T_1 represents this time.

(3) Corrosion damage period. From surface of concrete damaged due to steel corrosion to concrete severe spall, flake damage which has reached an intolerable degree and need a

comprehensive overhaul,T_2 represents this time.

(4) Corrosion hazard period. Steel corrosion of the concrete structure has been expanded to regional damage so that structure can not be used safely,T_3 represents this time.

Generally, T_0>T_1>T_2>T_3.

2.1.2 Factors affecting steel corrosion

In normal circumstances, the surface of the reinforced concrete has physical and mechanical protection to steel. At the same time, concrete provides a high alkalinity of the environment (PH> 12.5) for the reinforced, and make the steel surface to form a dense layer of passivation film, so it would not rust for a long time. When alkaline reduce, the passive film is gradually destroyed and reinforcement gradually begins to rust. When the PH value is less than 12, the corrosion rate significantly increases [5].

Reinforced concrete structure corrosion (is) affected by many factors, including reinforcing location, bar diameter, cement varieties, concrete compactness, protective layer thickness and integrity, the external environment and so on. According to Hong [4], the factors are summarized below:

(1) Concrete PH value of the liquid phase. Steel corrosion rate and concrete PH value of the liquid phase are closely related. When the PH value is greater than 10, steel corrosion rate is very small; while when the PH value is less than 4, the steel corrosion rate increases dramatically.

(2) Cl^-content in concrete. Cl^- content in concrete has enormous impact on steel corrosion. In normal circumstances, the chloride content of reinforced concrete structure should be less than 1% weight of cement (anhydrous state calculation), and mixed chloride concrete structures must be gotten by vibrated to compaction and also should not be cured by steam.

(3) Concrete density and thickness of the protective layer. Protective effects of concrete on the reinforcement include two main aspects: (i) high-alkaline of concrete forming passivation film on the surface of reinforced and (ii) protective layer preventing infiltration of outside corrosion media like oxygen and moisture. The latter role is mainly dependent on the density and thickness of the protective layer of concrete.

(4) The integrity of the concrete cover. It means whether the concrete has cracking or cellular holes. It has a significant effect on steel corrosion, especially greater impact on concrete structures in humid environments or corrosive medium. Surveys show that if the lateral fissure width is up to 0.2mm, the steel of the reinforced concrete structure used in wet conditions will corrode. Expansion of the volume of steel corrosion protection would increase the width of layer longitudinal cracks as the result of a vicious cycle which ultimately will lead to complete destruction of reinforced concrete structures.

(5) Varieties of cement and admixtures. Mineral admixtures such as fly ash can reduce concrete alkaline, thus affecting the durability of steel. Many researches show that when mixed with fly ash and other quality admixtures, and reducing concrete alkaline can also improve the density of concrete, changing the internal pore structure of concrete, which can prevent external corrosion medium, oxygen and moisture infiltration. This is favorable to prevent steel corrosion. In recent years, research has also showed that the incorporation of fly ash can enhance the corrosive effects of stray current on steel. Therefore, considering these effects, mixed with standard fly ash in the concrete structure does not affect the durability of concrete structures, and sometimes it will improve the durability.

(6) Environmental conditions. Environmental conditions concern temperature, humidity, dry alternation, seawater splash, chloride penetration are external factors causing steel corrosion. They have significant effect on the corrosion of reinforcement in concrete structures. Survey shows that the service life of the concrete structure in a dry non-corrosive media is 2 to 3 times longer than that in wet and corrosive media.

(7) Other factors. In addition to the above factors, reinforced stress state has a great influence on corrosion. Stress corrosion is more dangerous than the general corrosion. Stress corrosion appears in form of cracks, and continues to develop until destruction; which occurs suddenly without warning. In general, stress corrosion of steel is divided into two stages: the local electrochemical corrosion crack and development stage.

2.1.3 Changes in the mechanical properties of corroded bolts

Corrosion of steel embedded in concrete affects components' carrying capacity. It is

important to properly grasp the changes of various physical and mechanical properties of corrosion steel. In recent years, China has conducted large work on this issue [6 - 8].

Determination of the mechanical properties of corroded steel is usually achieved by weak corrosion test. The sample is also taken out for testing in the actual structure.

The experimental data from the Ministry of Metallurgical Industry Construction Research Institute and China Academy of Building Research show [6]:

(1) When a cross-section loss is less than 1%, the indicators of the reinforced are the same with base material.

(2) For a section loss less than 5% and uniform corrosion of weak corrosion steel, the hot-rolled steel stress - strain curves has obvious yield point. But after the severe corrosion, the stress - strain curve change significantly: absence of yield point, and yield strength and tensile strength are very close. It is easy to cause a sudden structural damage.

(3) Elongation is an important indicator of the intrinsic quality of the steel. The change in elongation causes changes in the work performance of structure. After corrosion, productivity decline significantly, while cross-sectional loss is less than 5%, elongation of steel is substantially greater than the minimum allowable value of specification; when the cross-sectional loss exceeds 10%, the elongation of steel is less than the minimum allowable value of specification, and the relationship between them can be fitted by exponential curve. Elongation decreases related to the square of the corrosion area, but the law between elongation and cross-sectional area is different from the law when reinforcement does not rust, and the elongation of corrosion steel is lower. After the steel corrosion, the partial section begins to weaken; the weakest section first reaches the yield. As the load increases, the weakest point reaches the tensile strength and starts to be broken, while the remaining parts may not have reached the yield. So the elongation of steel is low.

(4) The relationship between the yield strength of corroded steel and corresponding local weight ratio (or the ratio of the area of the cross-section) follows a linear relation; but with the increase in the corrosion loss, the yield strength decreases.

2.1.4 Steel corrosion testing

Investigation results show that the volume expansion due to corrosion layer significantly accelerates corrosion. When cracking occurs along the ribs, the steel section loss rate is generally less than 5%. In the absence of effective maintenance measures, the steel corrosion will significantly accelerate; the steel section loss rate could reach 10%o 20 %; the bond strength between steel and concrete can be reduced by 50% [9]. Therefore, the steel corrosion detection is essential for early diagnosis of structural durability and safety.

Currently, in addition to the traditional breakage detection method, a new technology of the steel corrosion state detection method, non-destructive testing, is explored in many countries. The nondestructive detection method on steel corrosion of concrete includes three categories: analysis, physical and electrochemical [10]. The analysis method is based on field measurement of bar diameter, cover thickness, concrete strength, harmful ion penetration depth and the content, longitudinal crack width data, by considering the environment conditions in which the members stay to infer the extent of corrosion. The physical method is adopted mainly by measuring the physical properties change of resistance, electromagnetic, thermal conductivity, acoustic wave propagation etc caused by steel corrosion to reflect the situation of steel corrosion. The electrochemical method is used by measuring electrochemical characteristics of concrete corrosion system to determine the extent or rate of corrosion in reinforced concrete.

Application of the analysis method depends on the establishment of reliable steel corrosion practical predictive models. For this reason, large experimental research, engineering investigation and theoretical analysis were conducted. Liu and Miao [2] conducted theoretical analysis on steel corrosion and proposed the component life prediction method. Based on the assumptions of oxygen diffusion obeying Fick's first law in concrete, Xiao [11] used Farady law to establish the steel corrosion model in atmosphere environment, but the formula needed power measurement with difficulties to be applied in engineering. Literature [12, 13] based on the same assumption, propose simple and practical of the basic parameters mathematical model of reinforcement corrosion of concrete structures. Niu et al. [14, 15]established the empirical formula of reinforced section loss rate in considering the thickness of the protective layer of concrete, rebar diameter, longitudinal crack width and other factors, Chen et al. [16]

assessed the amount of corrosion in reinforced concrete by the application of neural networks. Physical methods for the detection of reinforced concrete corrosion use the resistance bar method [4], the eddy current probe method [17], ray method [17], and infrared thermal imaging method [18]. Resistance bar method follows the resistance change caused by reinforced cross-sectional area and the surface state changing, using conducting principle to indirect projected the remaining area of the reinforcement. Eddy current detection method is used by measuring the phase relationship between the excitation current and the occurred in the reinforcement of second sound waves to determine the status of steel corrosion. Ray method shooting χ-rays or γ-rays radiographs of reinforced in concrete can be employed to directly observe corroded steel. Infrared thermal imaging method is adopted by measuring the temperature profile of the concrete surface to analysis of the extent of corrosion of reinforced. Physical methods are still remaining in the laboratory stage.

Concrete reinforcement corrosion is an electrochemical process and a powerful means of reflecting the essence of the process of electrochemical measurements. Comparison of analysis method, physical methods and electrochemical method has advantages such as fast test speed, high sensitivity, continuous tracking and in-situ testing, etc.. The electrochemical detection has been successfully used in both laboratory and field. They include[18] natural potential method, impedance spectroscopy method, linear polarization method, constant electricity method, electrochemical noise method, concrete resistance method and the harmonic method and so on.

2.1.5 Steel corrosion rate prediction model

Concrete is a highly alkaline materials (PH> 12.5). The reinforcement is buried in this highly alkaline environment, where the surface produces a layer of dense passive film, so rust could not occur. However, when reinforced concrete is surrounded by acid gases CO_2 and had neutralization action in atmospheric, the alkaline reduces, and the steel passivation film becomes unstable or even destroyed and the rust occurs. When the relative humidity of the atmosphere exceeds the critical relative humidity of the steel corrosion, steel becomes the anode; the oxygen dissolved in the water film on the steel surface becomes the cathode. Then the electrochemical reaction occurs, which could lead to steel corrosion.

Theoretical study of this dissertation will be based on the following assumptions [19]:

(1) Reinforced concrete carbonation is the only reason to produce corrosion.

(2) Oxygen diffusion in concrete follows Fick's first law.

(3) When the relative humidity is greater than the critical relative humidity of steel corrosion, the need of water for rust is plenty.

(4) Under atmospheric conditions the reinforcement corrosion wrapped in concrete is micro cell corrosion and the anode and cathode is in close contact.

According to Faraday's law [19], the cathode current density of steel corrosion cell i_c can be expressed as

$$\frac{i_c(\tau)}{n_0 F} = J_c(\tau) \tag{2.7}$$

where$i_c(\tau)$ represents the cathode current density at timeτ, $J_c(\tau)$ represents the diffusion flow rate of O_2 on the steel surface at timeτ, n_0 represents the number of electrons obtained in reaction of oxygen molecules participating, taking $n_0 = 4$, F represents the Faraday constant,$F = 9.6486 * 10^4 C/mol$.

According to electrochemical principles, the diffusion flow of A substance in the B substance should be equal to diffusion coefficient of A substance in the B substance multiplied by the first derivative of A substance concentration to diffusion direction, that is

$$J_c(\tau) = D_0 \frac{\partial C(x)}{\partial x} \tag{2.8}$$

whereD_0 is O_2diffusion coefficient in concrete (mm^2/ year), $C(x)$ is O_2concentration distribution in concrete, x is the diffusion direction axis.

It is assumed that O_2diffusion in concrete obey Fick's first law, which is within the range of the diffusion layer, and O_2 concentration from the maximum on concrete surface varies linearly to 0 at diffusion power forward, moreover, the diffusion layer thickness is completely carbonized zone depth D[12], then

$$\frac{\partial C}{\partial x} = \frac{C_0 - C_{st}}{D} \tag{2.9a}$$

Since it assumed that the steel corrosion is controlled by cathodic oxygen, in the formula (2.9a)C_s is taken 0, then:

$$\frac{\partial C}{\partial x} = \frac{C_0 - C_{st}}{D} = \frac{C_0}{D}$$

(2.9b)

where C_0 is the O_2concentration on the concrete surface, taking $8.93 * 10^{-9} mol/mm^3$, C_{st} is the O_2 concentration on the steel surface, *D* is the depth of the concrete completely carbonized area.

Substitute formula (2.8) and (2.9b) into formula (2.7), we obtain:

$$i_c(\tau) = n_0 F D_0 C_0 / D$$

(2.10)

According to Faraday's law, it can be written by the amount of steel corrosion in the period (*t*) as the formula (2.11), while as the cathode oxygen diffusion reaction process , so that the cathode current should be equal to the anode current:

$$dW_\tau = \frac{i_a(\tau)}{n_a F} M A_a dt = \frac{i_c(\tau)}{n_a F} M A_a d\tau \qquad (2.11)$$

$dW_\tau$is the steel corrosion amount (g) at the time $d\tau$, M is the atomic weight of iron (55.8 g/mol),n_a is the charge of iron ions, in fact, the value of n_a is obtained from the ratio of the weighted product of Fe_2O_3 and Fe_3O_4. It assumed that the product of two compounds have the same number of moles. It can be calculated thatn_a = 2.8, A_a is the reinforcement corrosion surface area at the timeτ.

CalculatingA_a, with 1mm per unit length, gives:

$$A_a = 2r \arccos \frac{R + c - D}{R} = d \arccos \frac{d + 2c - 2D}{d}$$

(2.12)

*R*is the reinforced diameter (mm), d is reinforced radius (mm), c is the concrete cover thickness (mm),*D* is the depth of carbonation, so:

$$D = \alpha \tau^{\lambda}$$

(2.13)

where, α is carbonation rate coefficient, λ is carbonized index.

For the parameter D in formula (2.10), the Niu et al.[20] give the following expression:

$$D_0 = 3.1536 * 10^5 \left(\frac{32.15}{f_{cu}} - 0.44\right) (mm^2/\text{year})$$

(2.14)

$f_{cu}$is the compressive strength of concrete cubes (N/mm^2).

Substitute formula (2.12) and (2.13) into formula (2.11) yields

$$dW_\tau = 7.118 * 10^7 \frac{D_0 d}{\alpha \tau^\lambda} \arccos \frac{d+2c-2\alpha\tau^\lambda}{d} d\tau \quad (2.15)$$

Formula (2.15) is integrated then the expression of the amount of steel corrosionW_t at *t* time is gotten, that is:

$$W_t = aP_{RH} \int_{t_0}^{t} dW_\tau$$

(2.16)

where, P_{RH} is taken into account that only when the atmospheric relative humidity is greater than the steel reinforcements corrosion critical relative humidity and amendments to the amount of steel corrosion. It takes atmospheric relative humidity greater than steel corrosion critical relative humidity (take 60%) occurred probability [12]. $a$takes into account only O_2 dissolved in water to be involved in steel corrosion reaction and amendment to the amount of steel corrosion, that O_2 solubility in water is 0.028 [21].

Note that the above equation is only for the case of$t_0 \le t \le t_1$, when$t \ge t_1$,$A_a = \pi d$, $D = c + d$, then

$$W_t = aP_{RH}(\int_{t_0}^{t_1} dW_\tau + \int_{t_1}^{t} dW_\tau')$$

(2.17)

where,$dW_\tau' = 7.118 * 10^{-7} \frac{\pi D_0 d}{c+d} d\tau$, t_0 for steel corrosion start time (years),$t_0 = (\frac{c}{\alpha})^{\frac{1}{\lambda}}$, t_1 for all steel surface rust starting time (years), $t_1 = (\frac{c+d}{\alpha})^{\frac{1}{\lambda}}$, t is the time to predict the amount of steel corrosion (years).

Usually measuring the extent of corrosion of reinforced is adopted to represent steel corrosion rate$\rho\left(= \frac{W_t}{W_0} * 100\%\right)$, W_0 is the theory weight of reinforcement. If we take $1mm$ unit length of steel, then$W_0 = \frac{1}{4}\pi d^2 * 7.8 * 10^{-3}$g , the expression of$\rho$is:

$$\left.\begin{aligned} &\rho = 0 \quad t < t_0 \\ &\rho = 3.254 * 10^{-4} \frac{D_0 P_{RH}}{\alpha d} \int_{t_0}^{t} \frac{\arccos \frac{d+2c-2\alpha\tau^\lambda}{d}}{\tau^\lambda} d\tau t_0 \le t \le t_1 \end{aligned}\right\}$$

$$\rho = 3.254 * 10^{-4} \frac{D_0 P_{RH}}{d} [\frac{\pi(t - t_1)}{c + d} + \int_{t_0}^{t_1} \frac{\arccos \frac{d + 2c - 2\alpha\tau^{\lambda}}{d}}{\alpha\tau^{\lambda}} d\tau \,] t \geq t_1$$

(2.18)

Determining carbonization index is difficult. Assumingλ = 0.5 and integrating the formula (2.18), A can be obtained.

$$\left.\begin{array}{l} \rho = 0 \quad t < t_0 \\ \rho = 3.254 * 10^{-4} \frac{D_0 P_{RH}}{d\alpha^2} (\sqrt{d^2 - \left(\mathrm{d} + 2\mathrm{c} - 2\alpha\sqrt{\mathrm{t}}\right)^2} \\ -\left(\mathrm{d} + 2\mathrm{c} - 2\alpha\sqrt{\mathrm{t}}\right)\arccos \frac{d + 2c - 2\alpha\tau^{\lambda}}{d}) \; t_0 \leq t \leq t_1 \\ \rho = 3.254 * 10^{-4} \frac{D_0 P_{RH}}{d} [\frac{\pi(t - t_1)}{c + d} + \frac{\pi d}{\alpha^2}] t \geq t_1 \end{array}\right\}$$

(2.19)

Formula (2.19) is more complex and does not be applied in engineering. For this reason, we use numerical simulation method, approximated the integral term of formula (2.18) as a function of τ . In contrast to the several possible functions such as power functions, exponential functions, polynomial, it is found that the exponential functions is the most simple and the fitting results are very satisfactory.

$$f(\tau) = \frac{\arccos (\frac{d+2c-2\alpha\tau^{\lambda}}{d})}{\tau^{\lambda}} = a(\tau - t_0)^b$$

(2.20)

where, a, b are undetermined parameters and are a function with respect to

parameters t,c,α,λ,c.

Substitute the formula (2.20) into the formula (2.18) gives a simplified prediction model of steel corrosion rate:

$$\left.\begin{array}{l} \rho = 0 \quad t < t_0 \\ \rho = 3.254 * 10^{-4} \frac{D_0 P_{RH}}{\alpha d} * \frac{a(\mathrm{t} - t_0)^{\mathrm{b}+1}}{b + 1} t_0 \leq t \leq t_1 \end{array}\right\}$$

$$\rho = 3.254 * 10^{-4} \frac{D_0 P_{RH}}{d} [\frac{\pi(t - t_1)}{c + d} + \frac{a(t_1 - t_0)^{b+1}}{a(b + 1)}] t \geq t_1 \quad (2.21)$$

A lot of parameters affect*a and b*; the formula is complicated to be used in engineering; further, since the parameter *b* is in the index position; its impact on the results is significant. There may be *a* large deviation between the calculated b from multi-parameter fitting equation and b obtained from formula (2.13), which affects the accuracy of the steel corrosion rate prediction model.

2.2 Durability of bolt members

Durability research of concrete members is the base of the durability research of concrete structures. Steel corrosion can cause concrete cover cracking; after rust expansion cracks the corrosion of steel will accelerate and will greatly affect the durability of the reinforced concrete members. Therefore, steel corrosion, concrete spalling and rust expansion crack width research is important for the analysis of concrete structures durability. Steel corrosion causes cracking of the concrete layer protection; the process is quite complex. Both theoretical analysis [22 - 26] and experimental research [27 - 33] were conducted for the determination of the relationship between the steel corrosion rates and crack width. They included the influencing factors and relationship between development of steel corrosion and surface concrete spalling, influencing factors of steel corrosion between the surface of the concrete spalling and the expression of steel corrosion rate at the concrete spalling moment.

Corrosion affects the bonding properties between concrete and steel. The reduction in bonding properties strength affects the steel strength, and consequently the durability of concrete structures. Because of restrictions of experimental conditions, early studies indicated that steel corrosion was favorable for the bonding between steel and concrete [34, 35]. Further research shows [36, 37] with the increasing of the amounts of steel corrosion, bond strength between deformed steel and concrete increase slightly in the beginning, but later it experiences a substantial drop. Yu, Tao and Wang [38 - 40] conduced experimental study on the bonding between concrete and steel. They showed an important influence of steel corrosion on adhesion.

The determination of the carrying capacity of reinforced concrete structures after rust

constitutes the main content of the assessment of the durability of concrete structures.Capozucca [41] conducted qualitative analysis on the impact of steel corrosion on the bending shear and torsion carrying capacity of reinforced concrete structures. Almusallam et al. [42] studied the flexural properties of reinforced concrete slab after steel corrosion by accelerated corrosion test. Okada et al. [43] conducted research on the mechanical behavior of reinforced concrete beams under cyclic loads before and after the steel corrosion. The study showed that under cyclic loads, the bearing capacity of corroded reinforced concrete beams degraded significantly. Construction Research Institute of the Ministry of Metallurgical in China realized bending experiment on three extent of corrosion roof [38]. Xi'an Architecture and Technology University conducted capacity test on 10 reinforced concrete beams and 10 reinforced concrete columns removing from the old house [39]. Zhejiang University [44] and the China Mining University [45] conducted bending experiments on corroded steel beams. Hui et al. [46] studied 24 rapid corrosion reinforced concrete beams 24 and 9 rapid corrosion reinforced concrete columns and had bearing capacity test. He proposed a method for the analysis of reinforced concrete members subjected to bending and compression.

2.2.1 Corroded expansion force model

The corrosion of reinforcement buried in concrete occur produces rust, whose volume is 2 to 4 of the corresponding volume [32]. The expansion occurs during four weeks. Since the concrete resists to this expansion, a pressure is created at the interface, which is called the corroded expansion force. Before the concrete protective layer of reinforced concrete member crack, corroded expansion force generation affects bond strength between steel and concrete. With the increase in the steel corrosion rate, corroded expansion force causes tension cracking of the concrete cover. Once the reinforced concrete structures appears by expansion force, steel corrosion rate accelerate [47], with catastrophic impact on the durability of the reinforced concrete members.

For buried deformation reinforced concrete structure, the presence of a beveled crush ribs produces radial forces. This leads to surrounding concrete cracking and steel corrosion. Therefore, the expansion forces of peripheral concrete before spalling impacts the durability of buried reinforced concrete structure.

2.2.1.1 Expansion force at concrete splitting time

When corroded expansion force reaches certain level, the concrete surface cracks, at this time the corroded expansion force of the reinforced has a great influence on the durability of reinforced concrete structures. Researchers [38- 50]suggests that at reinforced concrete cracking moment the corroded expansion force is related to steel diameter, concrete tensile strength and protective layer thickness. However, due to the discrete nature of the concrete materials, test methods and error, the test results are yet unsatisfactory. This area needs further researches. Elasticity is used here to study the uniform corrosion expansion force of smooth steel at concrete cracking moment.

After corroded expansion force, micro-cracks first produce near the reinforced, but do not expand to the surface of the protective layer of concrete, while with the increase in the corroded expansion force, cracks extends to the surface of the protective layer of concrete. Elasticity [47] can be applied to calculate the concrete hoop stress formula of uncracked concrete section in per unit length of the radius r of the circumference:

$$\sigma_t = \frac{e^2 * \frac{d}{2e} * [1 + \frac{(c+d/2)^2}{r^2}]}{(e+d/2)^2 - e^2} * q \qquad (2.22)$$

where the meaning of each symbol shown in Figure 2.4.

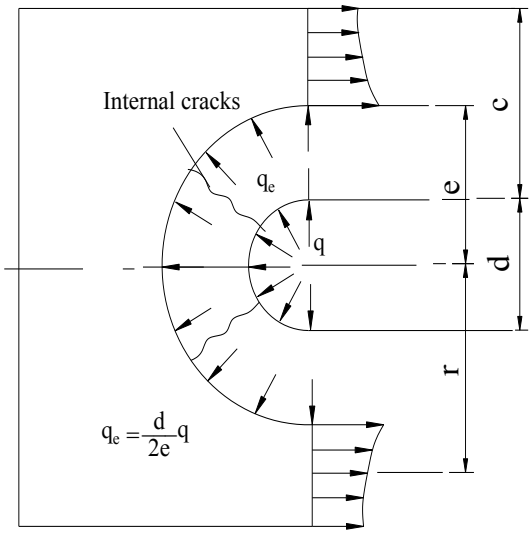

Figure 2.4

When r =e, the circle of the hoop stress reach the maximum, so

$$\sigma_{tmax} = \frac{d}{2e} * \frac{(c+d/2)^2 + e^2}{(c+d/2)^2 - e^2} * q$$

(2.23)

When σ_{tmax} =f_{tk}, the formula can be rewritten as:

$$q = \frac{2e}{d} * \frac{(c+d/2)^2+e^2}{(c+d/2)^2-e^2} * f_{tk}$$

(2.24)

Derivative formula (2.24) can obtained the value of e when$q$ =q_{max}, that

$$e = 0.486(c + d/2)$$

(2.25)

Substitute e into formula (2.24) and obtain corroded expansion force at concrete splitting time. At this point, e are not up to the entire thickness of the protective layer, but the thickness of the protective layer of concrete reached its maximum carrying capacity; when the corroded expansion force reachesq_{max}, the cracks will run through the entire concrete surface protective layer immediately.

When e approximates $0.5(c + d/2)$, it can derived per unit length of the concrete splitting time corroded expansion force formula by part cracking elastic computing:

$$q^* = (0.3 + 0.6c/d) * f_{tk}$$

(2.26)

where, q^* is corroded expansion force (N/mm^2), c is the concrete cover thickness (mm), f_{tk} is the standard value of tensile strength of concrete (N/mm^2).

2.2.1.2 Expansion Force of reinforced concrete before bursting

The corroded expansion force can be carried out as shown in Figure 2.5 shows, the thickness of protection is c and diameter of bolt is$d$.

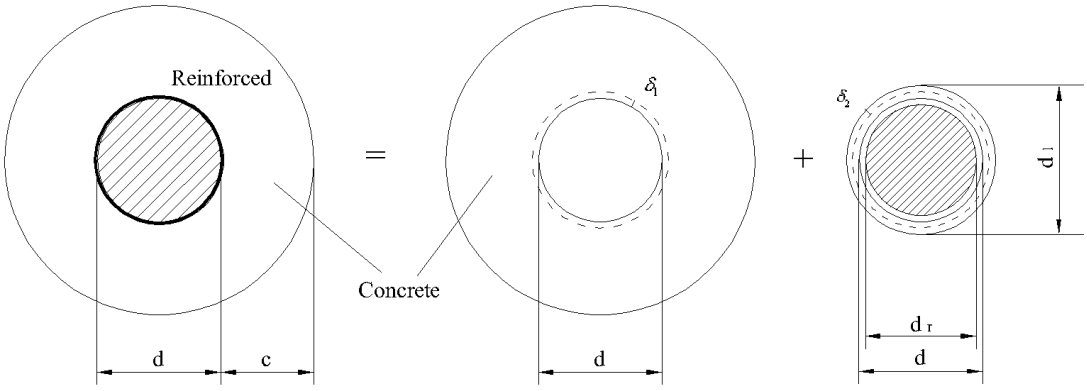

Figure 2.5Reinforced concrete structures due to corrosion expansion force deformation maps

Peripheral reinforced concrete bears a deformation of steel due to Expansion Force. The

nominal diameter of internal bolt after rusting and free expansion isd_1, net radius isd_ρ. Due to the steel rust, free expansion of d_1 sees a deformation ofδ_2.

Clearly, the relationship between the variables is in line with the deformation coordination, namely,

$$R + \delta_1 = R_1 - \delta_2$$

(2.27)

where,$R = \mathrm{d}/2, R_1 = d_1/2$.

As we know from analysis, when the steel corrosion rate isρ, then the nominal diameter of steel after corrosion isd_1,

$$d_1 = \sqrt{(n-1)\rho + 1 * d}$$

(2.28)

where, the volume expansion of steel after corrosion is$n$, typically 2-4. Steel corrosion ratio is valued by weight loss ratio of cross section. W_0 is the weight per unit length of steel before corrosion , W_ρ is the weight per unit length after corrosion, then

$$\rho = \frac{W_0 - W_\rho}{W_0}$$

$\delta_1$is the deformation of concrete under corroded expansion force after, the calculation results by elasticity are as follows:

$$\delta_1 = \frac{(1+\nu_c)Rc^2+(1-\nu_c)R^3}{E_c(c^2-R^2)} * q$$

(2.29a)

where, ν_c is the Poisson ratio of concrete, and generally 0.2, when plane strain is considered, $\nu_c = 0.25$; E_c is the modulus of elasticity of concrete, varies according to different concrete properties.

where

$$\mathrm{A} = \frac{(1+\nu_c)Rc^2 + (1-\nu_c)R^3}{E_c(c^2 - R^2)}$$

Then

$$\delta_1 = \mathrm{A} * \mathrm{q}$$

(2.29b)

δ_2 is deformation dues to corroded expansion force. Rust is a very complex compound; its

performance is inconsistent neither with the flexibility, nor with elastic-plastic or plastic. Rust generated under different conditions has different components, and their performance will change. Therefore, for simplicity, δ_2 is equivalently calculated according to the method of elastic mechanics, nominal Poisson's ratio v_r and nominal elastic modulus E_r of rust will optimize by fitting existing data. In this assumes

$$\delta_2 = \frac{n\rho(1-{v_r}^2)R_1}{E_r[(1+v_r)n\rho+(2-2\rho)]} * q$$

(2.30a)

where

$$B = \frac{n\rho(1-{v_r}^2)R_1}{E_r[(1+v_r)n\rho+(2-2\rho)]}$$

Then

$$\delta_2 = B * q$$

(2.30b)

Substituted formula (2.28)-(2.30) into deformation compatibility formula (2.27), available

$$q = \frac{[\sqrt{(n-1)\rho+1}-1]R}{\frac{(1+v_c)Rc^2+(1-v_c)R^3}{E_c(c^2-R^2)}+\frac{n\rho(1-{v_1}^2)R_1}{E_r[(1+v_r)n\rho+(2-2\rho)]}} \tag{2.31}$$

Where, q is corroded expansion force(N/mm^2),ρ is a rate of steel corrosion, R is the radius of the original steel(mm), R_1 is radius of bolt after rust free expansion(mm), v_c is concrete Poisson's ratio, c is the concrete cover thickness(mm), E_c is the elastic modulus of concrete(N/mm^2), n is rust expansion, E_r is rust nominal elastic modulus(N/mm^2), v_r is rust nominal Poisson .

where, the rust layer thickness$\delta = [\sqrt{(n-1)\rho+1}-1]R$, the physical meaning is the thickness of rust layer which is embedded in steel reinforcement, then

$$q = \frac{\delta}{A+B} \tag{2.32}$$

Through the fitting and slightly simplified, expression for Expansion Force is obtained as

$$q = \frac{K*\{[\sqrt{(n-1)\rho+1}-1]R\}^{1.71}}{\frac{(1+v_c)Rc^2+(1-v_c)R^3}{E_c(c^2-R^2)}+\frac{n\rho R}{140e^{-0.33n}(1.924n\rho+2-2\rho)}} \tag{2.33}$$

where, same symbol as in formula (2.10) has the same meanings of formula (2.10). K plays a role in adjusting the dimension, making the same dimension on both sides of the equation, in units of $mm^{1.71}$, in value of 1.

As the formula of corroded expansion force expression shows, factors affecting corroded expansion force are concrete grade, thickness of concrete cover, reinforcement diameter, thickness of rust and volume expansion of rust. Calculation example shows the main factors affecting the corroded expansion force of the rust layer thickness. Other factors, including grade concrete, concrete cover thickness, rust expansion, etc., impact lightly the corroded expansion force. Therefore corroded expansion force can be simplified in the following form:

$$q = K_c * \delta \tag{2.34}$$

Table 2.1 lists values of corroded expansion coefficient when the protective layer thickness is equal to 25 mm. When applying corroded expansion force to simplified formula, corroded expansion coefficient values vary according to Table 2.1. For the convenience to memorize and use, corroded expansion force can be simplified as the follows:

$$q = 35 * \delta \tag{2.35}$$

where, coefficient 35 has unit of N/mm^3.

The rust layer can be converted using geometrical relationship

$$\delta = d(\sqrt{n\rho + 1 - \rho} - 1)/2 \tag{2.36}$$

Table 2.1Corroded expansion coefficient K_c

Corroded expansion coefficient		Bolt diameter /mm				
		8	12	16	20	25
Concrete grade	C15	36.5	35.1	33.5	31.9	29.4
	C20	36.8	35.6	34.2	32.6	30.4
	C25	37.0	35.8	34.6	33.2	31.0
	C30	37.2	36.0	34.8	33.5	31.4
	C35	37.3	36.2	35.0	33.7	31.7
	C40	37.4	36.3	35.0	33.9	31.9
	C60	37.5	36.5	35.5	34.3	32.5

In summary, using the steel corrosion rate prediction formula (2.21), the simplified corroded

expansion force formula (2.35) and the rust layer thickness formula (2.36), we can determine expansion force using the formula:

$$\begin{cases} P = 0 & t < t_0 \\ P = K_c \cdot d \cdot \left(\sqrt{(n-1)\left[3.254 \cdot 10^{-4} \frac{D_0 P_{RH}}{\alpha d} * \frac{a(t - t_0)^{b+1}}{b+1}\right] + 1} - 1\right)/2 & t_0 \le t \le t_1 \\ P = K_c \cdot d \cdot \left(\sqrt{(n-1)\left\{3.254 \cdot 10^{-4} \frac{D_0 P_{RH}}{d}\left[\frac{\pi(t-t_1)}{c+d} + \frac{a(t_1 - t_0)^{b+1}}{\alpha(b+1)}\right]\right\} + 1} - 1\right)/2 & t \ge t_1 \end{cases} \quad (2.37)$$

This formula will be applied to finite element and compound element bolt corrosion calculation program.

2.3 Conclusions

A large number of engineering practices have proved that steel corrosion is a major factor that affecting the structural durability of reinforced concrete structures. In this chapter, the corrosion mechanism of reinforcement in concrete was analyzed with a particular focus on: Concrete carbonation and chloride ion ingress; Factors of steel corrosion; Changes in the mechanical properties of corroded steel; Detection of steel corrosion; Prediction model of steel corrosion rate; Corroded expansion force model. The corroded expansion force formula developed in this chapter will be used in the finite element method (chapter 4) and composite element method (Chapter) for the analysis of the impact of corrosion on the structural durability of reinforced concrete structures.

References

1. Hong N F. Steel corrosion and protective technology in concrete (1) ---damage of steel corrosion and failure effect on concrete. Industrial Construction. 1999; 29(8):66-68.
2. Liu X L, Miao P K. Steel corrosion and the durability calculation of reinforced concrete structures. China Civil Engineering Journal. 1990; 23(4):69-78.
3. Hong D H. HONG D H. Corrosion and protection of steel in concrete. Beijing: China Railway Press, 1998.
4. Gong L S, Liu C P. Durability, protection and repair of concrete structure. Beijing: Construction Industrial Publisher, 1990.
5. Hong N F. Concrete alkalinity and reinforcement corrosion. China Concrete and Cement Products. 1991(5):16-18.
6. Hui Y L. Approach to mechanical behavior of rusty reinforcement. Industrial Construction. 1992(10): 33-36.
7. Di X T, Zhou Y. On corrosion of reinforcement in atmospheric environment. The 4th Conference on Concrete Durability in China. Beijing: China Concrete Durability Society. 1996, 248-255.
8. Zhang P S, Lu M, Li X Y. Mechanical property of rustiness reinforcement steel. Industrial Construction. 1995; 25(9):41.
9. Zhu A M. Concrete carbonation and durability of RC. Concrete. 1992(6):18-22.
10. Zhang W P, Zhang Y, Liu Y Q. Electrochemical methods for investigation of reinforcement corrosion in concrete. Industrial Construction. 1998(12):21-25.
11. Xiao C Z. Research on the mechanism of steel corrosion in concrete and its simulation. PHD Thesis. Beijing: Tsinghua University, 1995.
12. Niu D T, Wang Q L, Wang L K. Predetermination of steel corrosion extent in reinforced concrete structures after corrosion crack. Industrial Construction. 1996(4):11-13.
13. Niu D T, Wang Q L, Wang L K. Predeterminate model of steel corrosion extent in reinforced concrete structures before producing corrosion crack. 1996(4):8-10.
14. Di X T, Zhou Y．On corrosion of reinforcement in atmospheric environment．The 4th Conference on Concrete Durability in China．Beijing：China Concrete Durability Society, 1996.

15. Hui Y L. Assessment and predicted experimental study on corrosive degree of reinforcements in concrete structures. The 4th Conference on Concrete Durability in Suzhou, China, 1996.
16. Chen H B, Niu D T, et al. Assessment on corrosive degree of reinforcement in concrete by artificial neural networks. Industrial Construction. 1999; 29(2):51-55.
17. Hou B L, Jiang Z F. Nondestructive Test of Concrete. Beijing: Earthquake Press, 1992.
18. Zhang W P, Zhang Y, Zhang X. Study on infrared ray testing theory for investigation of reinforcement corrosion in concrete. Structural Engineers, 1997(S).
19. Jiang Y H. General Chemistry, Higher Education Press: Beijing, 1982.
20. Niu D T, Wang L K, Wang Q L. Determination of oxygen diffusivity in concrete. Journal of Xi'an University of Architecture &Technology. 1996(1):10-13.
21. Kenji Kitade, KusumiYoshio. Translated by Li Y X, Wang Y F. Essentials of chemical calculation. Scientific and Technical Documentation Press: Tianjing, 1984.
22. Z.P. Bazant. Physical model for steel corrosion in concrete sea structures-theory. Journal of Structural Division, ASCE. 1979; 105(6):1137-1153.
23. H.J.Dagher, S.Kulendran. Finite element modeling of corrosion damage in concrete structures. ACI Structure Journal. 1992; 89(6):699-708.
24. Qu W J, Zhang Y. Determination of steel corrosion at the cracking of concrete cover. Engineering Mechanics (A02). 1997, 12-16.
25. Jin W L, Zhao Y X, Yan F. Corroded expansion force of reinforced concrete members and its influence factors. Industrial Construction. 2001; 31(5):6-8.
26. Jin W L, Zhao X Y, Yan F. The mechanism of corroded expansion force of reinforced concrete members. Journal of Hydraulic Engineering. 2001 (7): 57-62.
27. C. Andrade and C. Alonso. Cover cracking as a function of bar corrosion: part 1-experimental test. Materials and Structures. 1993; 26(8):453-464.
28. C. Alonso. , et al. Factors controlling cracking of concrete affected reinforcement corrosion. Materials and Structures. 1998; 31(7):435-441.
29. S. Al-Sandoun , et al. Corrosion cracking in relation to bar diameter, cover and concrete quality. Journal of Materials in Civil Engineering. 1992; 4(4): 327-342.
30. Y.P. Liu and R.E.Weyers. Modeling the time-to-corrosion cracking in chloride

contaminated reinforced concrete structures. ACI Materials Journal. 1998; 95(6): 675-680.

31. Li H B, Yan F, et al. Model of corroded expansion force at cracking on reinforced concrete structures. Journal of Zhejiang University. 2000; 34(4):415-422.
32. Han J Y, Cai L S. Research on the corroded rebar in reinforced concrete member. Institutes of Building Structures, China Academy of Building Research, 1991.
33. Wang S, Zhang W P, et al. Anticipating corrosion magnitude of reinforcement by crack width. Proceeding of the 9th Conference of CCES. Beijing: China Water power Press,2000.
34. Johnston B and Cox K C. The bond strength of rusted deformed bars. ACI Journal Proceedings. 1941(37):57-72.
35. Kemp L, et al. Effect of rust and scale on the bond characteristics of deformed reinforcing bars. ACI Journal Proceedings. 1968; 65(9):743-756.
36. Al-Sulaimani G J, et al. Influence of corrosion and cracking on bond behavior and strength of reinforced concrete members. ACI Structural Journal. 1990; 87(2):220-231.
37. Yuan Y S, Yu S, Jia F P. Deterioration of bond behavior of corroded reinforced concrete. Industrial Construction. 1999; 29(11):47-50.
38. Yu M Y. The property of the aging and damage reinforced concrete. Industrial Construction. 1990(2):15-19.
39. Tao F, et al. Experimental study on the bearing capacity of existing reinforced concrete members. Industrial Construction. 1996(4):17-20.
40. Wang K L, et al. Experimental study on bond and boltage of corroded reinforcement in concrete. 1996(4):14-16.
41. Capozucca R. Damage to reinforced concrete due to reinforcement corrosion. Construction & Building Materials. 1995; 9(5):295-303.
42. Almusallam A, et al. Effect of reinforcement corrosion on flexural behavior of concrete slabs. Journal of Materials in Civil Engineering. 1996; 8(3):123-127.
43. Okada K, Kobayashi K, Miyagawa T. Influence of longitudinal cracking due to reinforcement corrosion on characteristics of reinforced concrete members. ACI Structural Journal. 1998; 85 (2): 134–140.
44. Jin W L, Zhao Y X. Test study on bending strength of corroded reinforced concrete beams.

Industrial Construction. 2001; 31(5):9-11.

45. Yuan Y S, et al. Deterioration of structural behavior in corroded reinforced concrete beam. Journal of Building Structures. 1997(4):51-57.
46. Hui Y L, Li R, Lin Z S, et al. Experimental studies on the property before and after corrosion of rebars in basic concrete members. Industrial Construction. 1997; 27(6):14-18.
47. Wang C Z, Teng Z M. Theory of reinforced concrete structure. Beijing: China Architecture & Building Press, 1985.
48. Yan F. Studies on the durability of the reinforced concrete structural members in atmosphere circum stances.PHD Thesis. Hangzhou: Zhejiang University, 1999.
49. Zhang W P. Damage prediction and durability estimation for corrosion of reinforcement in concrete structures. PHD Thesis. Shanghai: Tongji University, 1999.
50. Nilson A H. Internal measurement of bond slip. ACI Journal Proceedings. 1972; 69(7): 439-441.

Chapter 3: Analytical model for bolting force and Expansion Force of corroded bolt

3.1 Introduction

Analytical solution, especially for practical engineering problems, is widely used and occupies a vital position in all disciplines. This chapter presents the development of analytical solution for both bolting force and Expansion Force of corroded bolt. Shear stress between the bolt and surrounding mortar changes along the axis of the bolt, and stress field in mortar protective layer changes in the axial and radial directions. Therefore, three-dimensional corroded bolt model must be established for detailed analysis. In the past, 2D and 1D model were used to study this problem. Few studies were based on 3D model. Little attention was paid to the durability of bolts. The existing analytical models rarely consider the impact of corrosion expansion forceon the stress field.

For instance, Li and Stillborg[1]proposed 1D analytical model of shear stress distribution in rock bolt. This model aimed at studying how the size of pullout strength affects the bonding mechanisms and the shear stress distribution between bolt and mortar. However, it neglected the influence of corrosion expansion force to the bond stress distribution. Heyett et al. [2] conducted bolt pull-out test to study the influence of binding effect of the surrounding rock on the bond strength and radial displacement of mortar cover, but the mathematical model, did not consider the change of displacement state along axial direction. Tepfers[3] analyzed the stress state of bolt in concrete during elastic deformation, the plastic deformation and the cracking stage; a two-dimensional model was established, without considering the stress state changein the protective layer along the axial direction. Other researchers [4-6] also discussed this issue. On the basis of previous studies, I tried to establish a three-dimensional analytical model to study the three-dimensional stress field of the bolt under the influence of the bolting force and the corrosion expansion force, and propose mathematical solution for the bolt space issues and each stress components. The study has a certain reference value for the design and analysis of the mechanism of bolting structure.

3.2 spatial analytical model of corroded bolt

3.2.1 Model building

3.2.1.1 Model simplification

Wnidsor[7]considers that the reinforcement system includes four elements: rock, reinforcement elements, internal fixation devices and external fixation devices. When bolts are used in reinforcement (Figure 3.1(a)), reinforcement element refers to bolt, external fixation device refers to parts of the bolt head jigs, and internal fixation devices typically refers to "friction" behavior on interface of cement mortar, resin or other material. As referring to internal fixation devices, Wnidsor divides them into three groups: continuous mechanical coupling (CMC), continuous friction vortex composites (CFC) and discrete mechanical vortex composites (DMFC) system. According to the classification, based cement mortar-bolt system belongs to CMC systems.

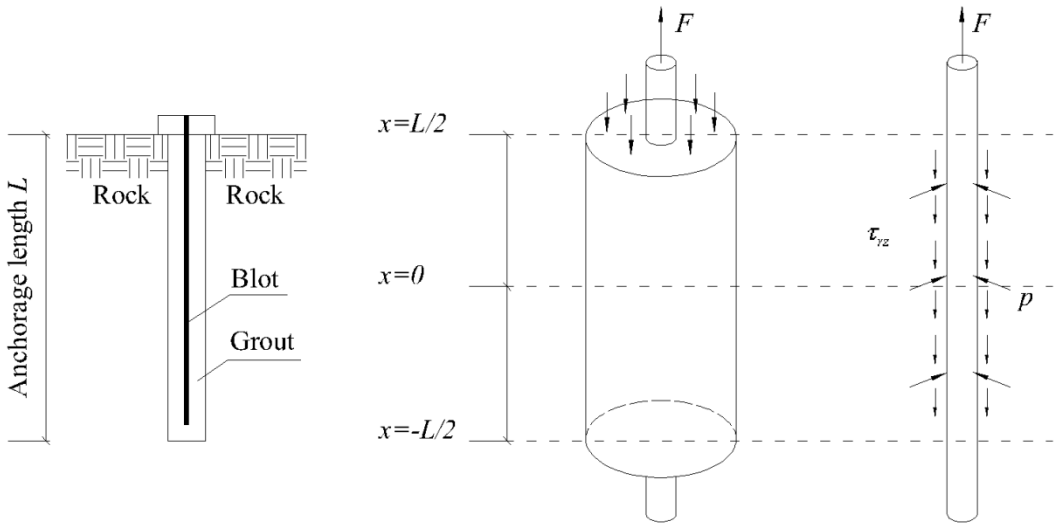

Figure 3.1 The 3-D model of corroded boltage system

In order to facilitate the establishment of the model, the actual force bolting device (Figure.3.1 (a)) can be simplified as in Figure3.1 (b) and Figure3.1(c). In the bolt head position, the end of bolt bears bolting force F, the mortar around bolt end bears the join force of F brought by pressure plate. On the bolt, bolting force F acts on bolt end. Due to the corrosion of the bolt surface, Expansion Force P acts on the interface between rod and mortar cover. Besides, shear stress acts on the surface of the rod and changes along the boltage length. Shear stress on the external surface of mortar cover and bolting force need to meet the

balance between of the periphery, without regard to the specific form of shear stress distribution on the external surface of the mortar covers.

3.2.1.2 Fundamental Assumption

Spatial model of corroded bolt is established using the following assumptions:

1) Stress field of corroded bolt is axisymmetric;

Surface corrosion of rod is uniform, rust layer is thin and does not lead to cracking of the mortar cover;

2) Rust layer is very thin, so there is no obstruction of transfer between the bolt and mortar, which means the conditions of stress is continuous on the bolt and mortar interface;

3) Material forces are in the elastic stage;

4) We focus on the critical state of bond slip between bolt and mortar, consequently points along the length of the bolt reaches a critical state at the same time, so contact conditions between bolt and cement is consistent with the Coulomb friction model;

5) Bonding is effective on the whole anchorage length. The value of bond stress on the surface between bolt and mortar interface peaks when unlimited approaching to the bolt end. The model in this dissertation only study anchorage bond stress and stress distribution from the peak to the free end, that is to say, to study declining segment of bond stress distribution curve.

3.2.2 Solution

The stresses are assumed in the elastic stage. According to the stress state of corroded bolt, the problem is decomposed into two elasticity problems (Figure. 3.2):

Problem 1: An inner wall of a thick-walled cylinder is in intimate contact with a solid cylinder, and a uniform distribution pressure P acts on the contact surface of the thick-walled cylinder and the solid cylinder, as shown in Figure. 3.2 (a);

Problem 2: The inner wall of a thick-walled cylinder is in intimate contact with a solid cylinder, a pulling F acts on a solid cylinder at x = L / 2, so the cylindrical surface bears the pressure force F, as shown in 3.2 (b).

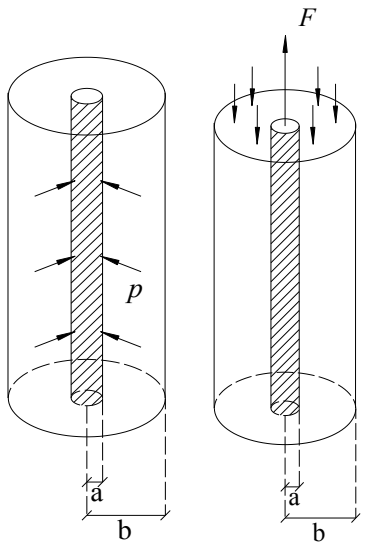

Figure 3.2 The decomposition of the 3-Dmodel of corroded bolt age device

3.2.2.1 Solution of Expansion Force

Stress generated by the Expansion Force can also be reduced to a plane strain (Figure 3.3), with the cylinder radius a; the inner cylinder of radius *a*, outer radius *b*, on the cylinder and cylinder interface there is pressure *P*.

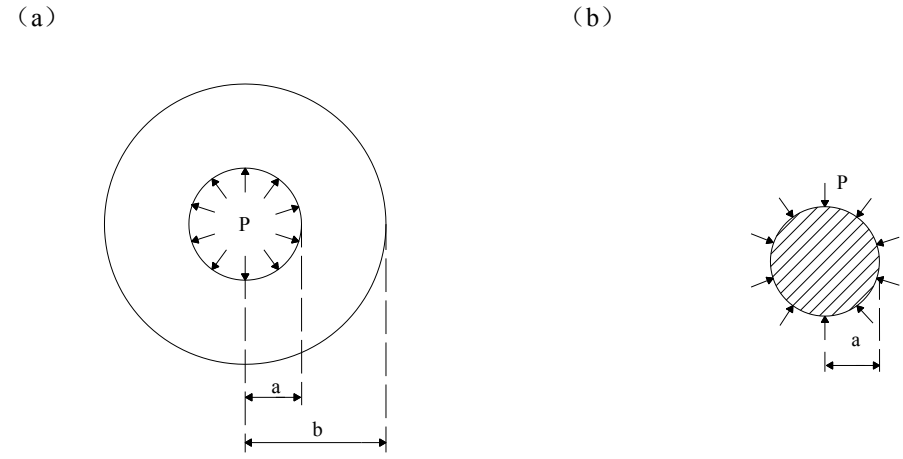

Figure 3.3 The solution of the second question

Obviously, the stress distribution is axisymmetric. Thus, according to the elasticity, the stress components reinforcement and the radial displacement could be determined using formula (3.1) and (3.2). Since the stress in the reinforcement does not change with *r*, A = 0. Stress and radial displacement component of mortar can be express using formula (3.3) and (3.4).

$$\begin{cases} \sigma_r^m = \frac{A'}{r^2} + 2\,C' \\ \sigma_\theta^m = -\frac{A'}{r^2} + 2C' \\ \tau_{r\theta}^m = \tau_{\theta r}^m = 0 \end{cases} \tag{3.3}$$

Radial displacement expression is

$$u_r^m = \frac{1+\mu_2}{E_2}[2aC'(1-\ 2\mu_2) - \frac{A'}{a}]$$

(3.4)

where, E_1 and μ_1 is elastic modulus and Poisson's ratio of mortar.

Boundary conditions require

$$\begin{cases} (\sigma_r^s)_{r=a} = -P \\ (\sigma_r^m)_{r=a} = -P \\ (u_r^s)_{r=a} = (u_r^m)_{r=a} \end{cases} \tag{3.5}$$

Substitution the stress component expressions of cylinder and cylinder (3.1) and (3.3), and radial displacement component expressions of axisymmetric stress state (3.2) and (3.4) into the boundary conditions (3.5) have equations

$$\begin{cases} 2C = -P \\ \frac{A'}{a^2} + 2C' = -P \\ \frac{1+\mu_1}{E_1}[2a(1-\ 2\mu_1)C] = \frac{1+\mu_2}{E_2}[2aC'(1-\ 2\mu_2) - \frac{A'}{a}] \end{cases} \tag{3.6}$$

Then

$$\begin{cases} 2C = -P \\ A' = \frac{a^2[-(1+\mu_2)(1-2\mu_2)\,E_1 + (1+\mu_1)(1-2\mu_1)\,E_2]}{2(1-\mu_2{}^2)\,E_1} P \\ C' = \frac{(1+\mu_2)E_1 + (1+\mu_1)(1-2\mu_1)\,E_2}{2(1-\mu_2{}^2)\,E_1} P \end{cases} \tag{3.7}$$

Substitution into (3.1) and (3.3), a little finishing, that reinforced and mortar answer stress components formula respectively as follows (3.8) and (3.9):

$$\sigma_r^s = \sigma_\theta^s = -P$$

(3.8)

$$\begin{cases} \sigma_r^m = \frac{P}{2(1-\mu_2{}^2)\,E_1} \cdot \{-a^2[(1+\mu_2)(1-2\mu_2)\,E_1 - (1+\mu_1)(1-2\mu_1)\,E_2]\frac{1}{r^2} - [(1+\mu_2)E_1 + (1+\mu_1)(1-2\mu_1)\,E_2]\} \\ \sigma_\theta^m = \frac{P}{2(1-\mu_2{}^2)\,E_1} \cdot \{a^2[(1+\mu_2)(1-2\mu_2)\,E_1 - (1+\mu_1)(1-2\mu_1)\,E_2]\frac{1}{r^2} - [(1+\mu_2)E_1 + (1+\mu_1)(1-2\mu_1)\,E_2] \end{cases}$$

(3.9)

where the expansion Force P expression is

$$\begin{cases} P = 0 & t < t_0 \\ P = K_c \cdot d \cdot (\sqrt{(n-1)[3.254 \cdot 10^{-4}\,\frac{D_0 P_{RH}}{\alpha d} * \frac{a(\mathrm{t}-t_0)^{\mathrm{b}+1}}{b+1}] + 1} - 1)/2 & t_0 \le t \le t_1 \\ P = K_c \cdot d \cdot (\sqrt{(n-1)\{3.254 \cdot 10^{-4}\,\frac{D_0 P_{RH}}{d}[\frac{\pi(t-t_1)}{c+d} + \frac{a(t_1-t_0)^{\mathrm{b}+1}}{\alpha(b+1)}]\} + 1} - 1)/2 & t \ge t_1 \end{cases}$$

(3.10)

Substitution expansion Force P that reinforced and mortar answer stress components formula respectively as follows (3.11) - (3.13):

When $t < t_0$, that

$$\begin{cases} \sigma_r^s = \sigma_\theta^s = 0 \\ \sigma_r^m = 0 \\ \sigma_\theta^m = 0 \end{cases} \tag{3.11}$$

When $t_0 \le t \le t_1$, that

$$\begin{cases} \sigma_r^s = \sigma_\theta^s = -K_c \cdot d \cdot (\sqrt{(n-1)[3.254 \cdot 10^{-4}\,\frac{D_0 P_{RH}}{\alpha d} * \frac{a(\mathrm{t}-t_0)^{\mathrm{b}+1}}{b+1}] + 1} - 1)/2 \\ \sigma_r^m = \frac{K_c \cdot d \cdot (\sqrt{(n-1)[3.254 \cdot 10^{-4}\,\frac{D_0 P_{RH}}{\alpha d} * \frac{a(\mathrm{t}-t_0)^{\mathrm{b}+1}}{b+1}] + 1} - 1)/2}{2(1-\mu_2{}^2)\,E_1} \cdot \{-a^2[(1+\mu_2)(1-2\mu_2)\,E_1 - (1+\mu_1)(1-2\mu_1)\,E_2]\frac{1}{r^2} - [(1+\mu_2)E_1 + (1+\mu_1)(1-2\mu_1)\,E_2]\} \end{cases}$$

$$\sigma_\theta^m = \frac{K_c \cdot d \cdot (\sqrt{(n-1)[3.254 \cdot 10^{-4} \frac{D_0 P_{RH}}{\alpha d} * \frac{a(\mathrm{t} - t_0)^{\mathrm{b}+1}}{b+1}] + 1} - 1)/2}{2(1 - \mu_2{}^2)\, E_1}$$
$$\cdot \{a^2[(1 + \mu_2)(1 - 2\mu_2)\, E_1 - (1 + \mu_1)(1 - 2\mu_1)\, E_2]\frac{1}{r^2} - [(1 + \mu_2)E_1$$
$$+ (1 + \mu_1)(1 - 2\mu_1)\, E_2]\}$$

(3.12)

When $t \geq t_1$, that

$$\begin{cases} \sigma_r^s = \sigma_\theta^s = -K_c \cdot d \cdot (\sqrt{(n-1)\{3.254 \cdot 10^{-4} \frac{D_0 P_{RH}}{d}[\frac{\pi(t-t_1)}{c+d} + \frac{a(t_1 - t_0)^{\mathrm{b}+1}}{a(b+1)}]\} + 1} - 1)/2 \\ \sigma_r^m = \dfrac{K_c \cdot d \cdot (\sqrt{(n-1)\{3.254 \cdot 10^{-4} \frac{D_0 P_{RH}}{d}[\frac{\pi(t-t_1)}{c+d} + \frac{a(t_1 - t_0)^{\mathrm{b}+1}}{a(b+1)}]\} + 1} - 1)/2}{2(1 - \mu_2{}^2)\, E_1} \\ \quad \cdot \{-a^2[(1 + \mu_2)(1 - 2\mu_2)\, E_1 - (1 + \mu_1)(1 - 2\mu_1)\, E_2]\frac{1}{r^2} - [(1 + \mu_2)E_1 \\ \quad + (1 + \mu_1)(1 - 2\mu_1)\, E_2]\} \\ \sigma_\theta^m = \dfrac{K_c \cdot d \cdot (\sqrt{(n-1)\{3.254 \cdot 10^{-4} \frac{D_0 P_{RH}}{d}[\frac{\pi(t-t_1)}{c+d} + \frac{a(t_1 - t_0)^{\mathrm{b}+1}}{a(b+1)}]\} + 1} - 1)/2}{2(1 - \mu_2{}^2)\, E_1} \\ \quad \cdot \{a^2[(1 + \mu_2)(1 - 2\mu_2)\, E_1 - (1 + \mu_1)(1 - 2\mu_1)\, E_2]\frac{1}{r^2} - [(1 + \mu_2)E_1 \\ \quad + (1 + \mu_1)(1 - 2\mu_1)\, E_2]\} \end{cases}$$

(3.13)

3.2.2.2 Solution of Anchoring Force

Stress field of anchoring force F generated in the anchor is axisymmetric problems. Stress components σ_r , σ_θ , σ_z and τ_{rz} should satisfy the equilibrium equations (excluding physical) [9] (3.14) :

$$\begin{cases} \frac{\partial \sigma_r}{\partial r} + \frac{\partial \tau_{zr}}{\partial z} + \frac{\sigma_r - \sigma_\theta}{r} = 0 \\ \frac{\partial \tau_{rz}}{\partial r} + \frac{\partial \sigma_z}{\partial z} + \frac{\tau_{rz}}{r} = 0 \end{cases}$$

(3.14)

Introduction of axisymmetric problems stress function φ, when it satisfies the biharmonic equation [9-11] (3.15)

$$\left(\frac{\partial^2}{\partial r^2}+\frac{1}{r}\frac{\partial}{\partial r}+\frac{\partial^2}{\partial z^2}\right)\left(\frac{\partial^2\varphi}{\partial r^2}+\frac{1}{r}\frac{\varphi}{\partial r}+\frac{\partial^2\varphi}{\partial z^2}\right)=0$$

(3.15)

That is, when $\nabla^2(\nabla^2\varphi)=0$, the stress component using the following expression

$$\begin{cases}\sigma_r=\frac{\partial}{\partial z}(\mu\nabla^2\varphi-\frac{\partial^2\varphi}{\partial r^2})\\ \sigma_\theta=\frac{\partial}{\partial z}(\mu\nabla^2\varphi-\frac{1}{r}\frac{\partial\varphi}{\partial r})\\ \sigma_z=\frac{\partial}{\partial z}[(2-\mu)\nabla^2\varphi-\frac{\partial^2\varphi}{\partial z^2}]\\ \tau_{rz}=\frac{\partial}{\partial r}[(1-\mu)\nabla^2\varphi-\frac{\partial^2\varphi}{\partial z^2}]\end{cases} \quad (3.16)$$

Regardless of what kind of function ofφ, the stress components can always satisfy the equilibrium equations (3.14) and the biharmonic equation (3.15). Of course, the stress component should also satisfy the boundary conditions of stress and displacement single value condition. Adopt the stress function [12] to satisfy (3.14) and (3.15):

$$\varphi(r,z)=A_1(8z^5-15zr^4)+A_2(8z^5-40z^3r^2+15zr^4)+A_3(8z^4-3r^4)+A_4(2z^4-3r^2z^2)+A_5z\ln r+A_6z^3+A_7r^2z+A_8r^2z\ln r+A_9z^3\ln r+A_{10}r^2\ln r+A_{11}z^2\ln r \quad (3.17)$$

The above equation is substituted into Equation stress components, and sort through the operation have [12

$$\begin{cases}\sigma_r=3\left(160\mu A_1+80A_2+\frac{A_9}{r^2}\right)z^2-[60(4\mu-3)A_1+180A_2]r^2\\ +\left[192\mu A_3+12(2\mu+1)A_4+\frac{2A_{11}}{r^2}\right]z+\frac{A_5}{r^2}+6\mu A_6+2(2\mu-1)A_7\\ +[2(2\mu-1)\ln r+(4\mu-3)]A_8+6\mu\ln rA_9\end{cases}$$

$$\sigma_\theta = 3\left(160\mu\, A_1 + 80\, A_2 - \frac{A_9}{r^2}\right)z^2 - [60(4\mu-1)\, A_1 + 60\, A_2]r^2$$
$$+ \left[192\,\mu A_3 + 12(2\mu+1)A_4 - \frac{2A_{11}}{r^2}\right]z - \frac{A_5}{r^2} + 6\,\mu A_6 + 2(2\mu-1)A_7$$
$$+ [2(2\mu-1)\ln r + (4\mu-1)]A_8 + 6\,\mu \ln r A_9$$
$$\sigma_z = 3[160(1-\mu)\, A_1 - 160\, A_2]z^2 + [-240(2-\mu)\, A_1 + 240\, A_2]r^2$$
$$+ [192(1-\mu)A_3 - 24\mu A_4]z + \frac{A_5}{r^2} + 6\,(1-\mu)A_6 + 4(2-\mu)A_7$$
$$+ 4(2-\mu)(\ln r + 1)A_8 + 6\,(1-\mu)\ln r A_9$$
$$\tau_{rz} = 2[-240(1-\mu)\, A_1 + 240\, A_2]zr + [-96(1-\mu)\, A_3 + 12\,\mu A_4]r$$
$$+ \left[\frac{4(1-\mu)}{r}\, A_8 - \frac{6\mu}{r}\, A_9\right]z + \frac{4(1-\mu)}{r}\, A_{10} - \frac{2\mu}{r}\, A_{11}$$

(3.18)

Consider the actual stress situation of the anchor and equation solvability, boundary conditions using the following three categories:

1. Cylinder stress boundary conditions:

   When z = L / 2, the cylinder pull force on pull side is F, that is

   $$\iint_S \sigma_z^s|_{z=L/2}\mathrm{d}s = F$$

   (3.19)

   When z = -L / 2, the pulling force on free end of the cylinder is 0, that is

   $$\iint_S \sigma_z^s|_{z=-L/2}\mathrm{d}s = 0$$

   (3.20)

   When z = -L / 2, the shear force on free end of the cylindrical section is 0. The direction of the shear stress is taken into account, which cannot be integrated over the entire cross-section. Since the distribution of shear stress on cross-sectional associated with r only, stress conditions can be expressed as

   $$\int_0^a \tau_{zr}^s|_{z=-L/2}\mathrm{d}r = 0$$

(3.21)

   Considering the cylinder by the force balance, as shown in Figure 3.4, there

   $$F + \int_z^{L/2} 2\pi a \cdot \tau_{zr}^s|_{r=a}\mathrm{d}z = \iint_S \sigma_z^s(z)\mathrm{d}s$$

   That is

$$\int_0^a \sigma_z^s(z)rdr - a\int_z^{L/2} \tau_{rz}^s|_{r=a}\ dz = \frac{F}{2\pi}$$

(3.22)

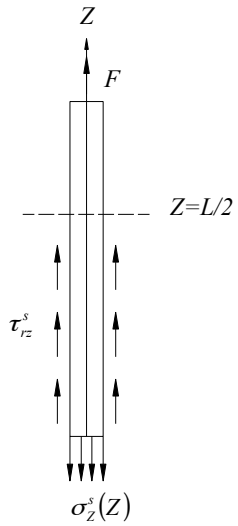

Figure 3.4 The equilibrium of force of the bolts

2. Thick-walled cylinder stress boundary conditions:

   When r = b, the cylinder outer pressure is zero, that is

$$\sigma_r^m|_{r=b} = 0$$

   (3.23)

   When z = L / 2, the pressure force on cylinder surface is F, that is

$$\iint_s \ \sigma_z^m|_{z=L/2}\, ds = -F \tag{3.24}$$

   When z = -L / 2, the force on cylindrical surface is 0, that is

$$\iint_s \ \sigma_z^m|_{z=-L/2}\, ds = 0 \tag{3.25}$$

   When z = -L / 2, the shear on cylindrical surface is 0, that is

$$\int_a^b \tau_{zr}^m|_{z=-L/2}\ ds = 0 \tag{3.26}$$

3. Thick-walled cylinder and cylinder contact conditions:

   Thick-walled cylinder and cylinder radial remain in contact, and thus there is

$$\sigma_r^s|_{r=a} = \sigma_r^m|_{r=a} \tag{3.27}$$

$$u_r^s|_{r=a} = u_r^m|_{r=a} \tag{3.28}$$

Due to the derivation process of expressions u in space axisymmetric problems is very complicated; there is no recognition of expressions available. Thus during the solution

process, the problem can be approximated. The boundary condition shown in the formula (3.28) weakens radial strain equal on contact surface of bolt and mortar, that

$$\varepsilon_{\mathrm{r}}^{\mathrm{s}}|_{r=a} = \varepsilon_{\mathrm{r}}^{\mathrm{m}}|_{r=a} \tag{3.29}$$

According to the model assumption, the contact conditions of thick-walled cylinder and cylinder in the axial direction meet basic Coulomb friction model, that

$$\tau = c - k \cdot \sigma \tag{3.30}$$

where, τ -- Shear stress on shear slip plane, MPa;

c --Cohesion on shear sliding surface, MPa;

σ --Normal stress on shear sliding surface, tension is positive, pressure is negative, MPa;

k --Coefficient of friction.

So contact conditions of thick cylinder and cylinder can be written as

$$\tau_{\mathrm{rz}}^{\mathrm{s}}|_{r=a} = \tau_{\mathrm{rz}}^{\mathrm{m}}|_{r=a} \tag{3.31}$$

$$\tau_{\mathrm{rz}}^{\mathrm{s}}|_{r=a} = c - k \cdot \sigma_{\mathrm{r}}^{\mathrm{s}}|_{r=a} \tag{3.32}$$

$$\tau_{\mathrm{rz}}^{\mathrm{m}}|_{r=a} = c - k \cdot \sigma_{\mathrm{r}}^{\mathrm{m}}|_{r=a} \tag{3.33}$$

On behalf of the stress component of the formula (3.18) into the boundary conditions and contact stress conditions, after finishing operations and get the following equation:

According to the stress boundary conditions of the cylinder, obtained from formula (3.19), we have:

$$\begin{aligned}[60L^2a^2(1-\mu_1) - 60a^4(2-\mu_1)]A_1 + [-60L^2a^2 + 60a^4]A_2 + 48La^2(1-\mu_1)A_3 \\ - 6La^2\mu_1 A_4 + 3a^2(1-\mu_1)A_6 + 2a^2(2-\mu_1)A_7 \\ + a^2(2\ln a + 1)(2-\mu_1)A_8 + \frac{3}{2}a^2(2\ln a - 1)(1-\mu_1)A_9 = \frac{F}{2\pi}\end{aligned} \tag{3.34}$$

Obtained from formula (3.20), we have

$$\begin{aligned}[60L^2a^2(1-\mu_1) - 60a^4(2-\mu_1)]A_1 + [-60L^2a^2 + 60a^4]A_2 - 48La^2(1-\mu_1)A_3 \\ + 6La^2\mu_1 A_4 + 3a^2(1-\mu_1)A_6 + 2a^2(2-\mu_1)A_7 \\ + a^2(2\ln a + 1)(2-\mu_1)A_8 + \frac{3}{2}a^2(2\ln a - 1)(1-\mu_1)A_9 = 0\end{aligned} \tag{3.35}$$

Obtained from formula (3.21), we have

$$\begin{aligned}-120La^2(1-\mu_1)A_1 + 120La^2A_2 - 48a^2(1-\mu_1)A_3 + 6a^2\mu_1 A_4 + 2L\ln a(1-\mu_1)A_8 \\ - 3L\ln a\,\mu_1 A_9 + 4\ln a(1-\mu_1)A_{10} - 2\ln a\,\mu_1 A_{11} = 0\end{aligned} \tag{3.36}$$

Obtained from formula (3.22), we have

$$\begin{cases} 4(1-\mu_1)A_{10} - 2\mu_1 A_{11} = 0 & (3.37) \\ [60L^2a^2(1-\mu_1) - 60a^4(2-\mu_1)]A_1 + [-60L^2a^2 + 60a^4]A_2 + 48La^2(1-\mu_1)A_3 \\ \quad - 6La^2\mu_1 A_4 + 3a^2(1-\mu_1)A_6 + 2a^2(2-\mu_1)A_7 \\ \quad + [a^2(2\ln a + 1)(2-\mu_1) - 0.5L^2(1-\mu_1)]A_8 + [\frac{3}{2}a^2(2\ln a - 1)(1-\mu_1) \\ \quad + 0.75L^2\mu_1]A_9 - 2L(1-\mu_1)A_{10} + L\mu_1 A_{11} = \frac{F}{2\pi} & (3.38) \end{cases}$$

According to the stress boundary conditions of thick cylinders, obtained from formula (3.23), we have

$$\begin{cases} 160\mu_2 B_1 + 80 B_2 + \frac{1}{b^2} B_9 = 0 & (3.39) \\ 192\mu_2 B_3 + 12(2\mu_2 + 1)B_4 + \frac{2}{b^2} B_{11} = 0 & (3.40) \\ -60b^2(4\mu_2 - 3)B_1 - 180b^2 B_2 + \frac{1}{b^2} B_5 + 6\mu_2 B_6 + 2(2\mu_2 - 1)B_7 \\ +[2(2\mu_2 - 1)\ln b + (4\mu_2 - 3)]B_8 + 6\ln b\,\mu_2 B_9 = 0 & (3.41) \end{cases}$$

Obtained from formula (3.24), we have

$$\begin{aligned} &[60L^2(b^2-a^2)(1-\mu_2) - 60(b^4-a^4)(2-\mu_2)]B_1 + [-60L^2(b^2-a^2) + 60(b^4-a^4)]B_2 \\ &\quad + 48L(b^2-a^2)(1-\mu_2)B_3 - 6L(b^2-a^2)\mu_2 B_4 + 3(b^2-a^2)(1-\mu_2)B_6 \\ &\quad + 2(b^2-a^2)(2-\mu_2)B_7 + [b^2(2\ln b + 1) - a^2(2\ln a + 1)](2-\mu_2)B_8 \\ &\quad + \frac{3}{2}[b^2(2\ln b - 1) - a^2(2\ln a - 1)](1-\mu_2)B_9 = -\frac{F}{2\pi} \end{aligned} \quad (3.42)$$

Obtained from formula (3.25), we have

$$\begin{aligned} &[60L^2(b^2-a^2)(1-\mu_2) - 60(b^4-a^4)(2-\mu_2)]B_1 + [-60L^2(b^2-a^2) + 60(b^4-a^4)]B_2 \\ &\quad - 48L(b^2-a^2)(1-\mu_2)B_3 + 6L(b^2-a^2)\mu_2 B_4 + 3(b^2-a^2)(1-\mu_2)B_6 \\ &\quad + 2(b^2-a^2)(2-\mu_2)B_7 + [b^2(2\ln b + 1) - a^2(2\ln a + 1)](2-\mu_2)B_8 \\ &\quad + \frac{3}{2}[b^2(2\ln b - 1) - a^2(2\ln a - 1)](1-\mu_2)B_9 = 0 \end{aligned} \quad (3.43)$$

Obtained from formula (3.26), we have

$$-120L(b^2-a^2)(1-\mu_2)B_1+120L(b^2-a^2)B_2-48(b^2-a^2)(1-\mu_2)B_3 + 6(b^2-a^2)\mu_2 B_4+2L(\ln b-\ln a)(1-\mu_2)B_8-3L(\ln b-\ln a)\mu_2 B_9 + 4(\ln b-\ln a)(1-\mu_2)B_{10}-2(\ln b-\ln a)\mu_2 B_{11}=0 \quad (3.44)$$

According to the contact conditions of thick-walled cylinder and cylinder, Obtained from formula (3.27), we have

$$\begin{cases} 160\,\mu_1 A_1+80\,A_2+\frac{1}{a^2}A_9-160\,\mu_2 B_1-80\,B_2-\frac{1}{a^2}B_9=0 & (3.45)\\ 192\,\mu_1 A_3+12(2\mu_1+1)A_4+\frac{2}{a^2}A_{11}-192\,\mu_2 B_3-12(2\mu_2+1)B_4-\frac{2}{a^2}B_{11}=0 & (3.46)\\ -60a^2(4\,\mu_1-3)A_1-180a^2A_2+\frac{1}{a^2}A_5+6\,\mu_1 A_6+2(2\mu_1-1)A_7 & \\ +[2\ln a(2\mu_1-1)+(4\,\mu_1-3)]A_8+6\ln a\,\mu_1 A_9+60a^2(4\,\mu_2-3)B_1+180a^2B_2-\frac{1}{a^2}B_5 & \\ -6\,\mu_2 B_6-2(2\mu_2-1)B_7-[2\ln a(2\mu_2-1)+(4\,\mu_2-3)]B_8-6\ln a\,\mu_2 B_9=0 & (3.47)\end{cases}$$

Obtained from formula (3.29), we have

$$\begin{cases} \frac{1+\mu_1}{E_1}\left(240A_2+\frac{3}{a^2}A_9\right)-\frac{1+\mu_2}{E_2}\left(240B_2+\frac{3}{a^2}B_9\right)=0 & (3.48)\\ \frac{1+\mu_1}{E_1}\left(12A_4+\frac{2}{a^2}A_{11}\right)-\frac{1+\mu_2}{E_2}\left(12B_2+\frac{2}{a^2}B_{11}\right)=0 & (3.49)\\ \frac{1+\mu_1}{E_1}\left(180a^2A_1-180a^2A_2+\frac{1}{a^2}A_5-2A_7-(2\ln a+3)A_8\right) & \\ -\frac{1+\mu_2}{E_2}\left(180a^2B_1-180a^2B_2+\frac{1}{a^2}B_5-2B_7-(2\ln a+3)B_8\right)=0 & (3.50)\end{cases}$$

Obtained from formula (3.32) we have

$$\begin{cases} 160\,\mu_1 A_1+80\,A_2+\frac{1}{a^2}A_9=0 & (3.51)\\ -480a(1-\mu_1)A_1+480a\,A_2+192k\,\mu_1 A_3+12k(2\mu_1+1)A_4+\frac{4(1-\mu_1)}{a}A_8 & \\ -\frac{6\,\mu_1}{a}A_9+\frac{2k}{a^2}A_{11}=0 & (3.52)\end{cases}$$

$$-60ka^2(4\,\mu_1-3)\,A_1-180ka^2\,A_2-96ka(1-\,\mu_1)\,A_3+12a\,\mu_1\,A_4+\frac{k}{a^2}\,A_5+6k\,\mu_1\,A_6$$
$$+2k(2\,\mu_1-1)\,A_7+k[2\ln a(\,2\mu_1-1)+(4\,\mu_1-3)]\,A_8+6k\ln a\,\mu_1\,A_9+\frac{4(1-\,\mu_1)}{a}\,A_{10}$$
$$-\frac{2\,\mu_1}{a}\,A_{11}=c \tag{3.53}$$

Obtained from formula (3.33) we have

$$\begin{cases} -480a(1-\,\mu_2)\,B_1+480a\,B_2+192k\,\mu_2\,B_3+12k(\,2\mu_2+1)\,B_4+\frac{4(1-\mu_2)}{a}\,B_8-\frac{6\,\mu_2}{a}\,B_9 \\ +\dfrac{2k}{a^2}\,B_{11}=0 \end{cases} \tag{3.54}$$

$$\begin{cases} -60ka^2(4\,\mu_2-3)\,B_1-180ka^2\,B_2-96ka(1-\,\mu_2)\,B_3+12a\,\mu_2\,B_4+\dfrac{k}{a^2}\,B_5+6k\,\mu_2\,B_6 \\ +2k(2\,\mu_2-1)\,B_7+k[2\ln a(\,2\mu_2-1)+(4\,\mu_2-3)]\,B_8+6k\ln a\,\mu_2\,B_9+\dfrac{4(1-\,\mu_2)}{a}\,B_{10} \\ -\dfrac{2\,\mu_2}{a}\,B_{11}=c \end{cases} \tag{3.55}$$

From above 22 simultaneous equations (3.34) - (3.55), A1-A11, B1-B11 can be determined. Because of the complexity of the equation solving, equations are written under the vector equation

$$Cx=t \tag{3.56}$$

where, C is the coefficient matrix of the equation.

Solution vector of equations are $x=[\,A_1,\Lambda,\,A_{11},\,B_1,\Lambda,\,B_{11}]^T$

$$t=[\frac{F}{2\pi},0,0,0,0,0,0,-\frac{F}{2\pi},0,0,0,0,0,0,0,0,0,0,0,c,0,c]^T$$

Rank of coefficient matrix and augmented matrix in vector equations is equal, so the equation has a solution. Using linear algebra arithmetic functions in mathematical software MATLAB for solving equations, solution vector of vector equation is obtained.

In order to solve the vector equation (3.54), the expressions of the coefficients A1-A11、B1-B11 are given by (To simplify the coefficient expressions, the Poisson's ratio substitution of steel and mortar is used by 0.3 and 0.2, respectively). Because in general, changes in the magnitude of both the Poisson's ratio are small, which have less impact on the calculation results):

$$A_1 = 0.425\times10^{-3}\frac{E_1}{(a^2-b^2)L^2E_2}F\ ;$$

$$A_2 = 0.850\times10^{-5}\frac{35a^2\,E_1+78(b^2-a^2)\,E_2}{a^2(a^2-b^2)L^2E_2}F\ ;$$

$$A_3 = -6.376\times10^{-5}\frac{-a(175b^2-105a^2+35akL)\,E_1+26(b^2-a^2)kL\,E_2+26a(b^2-a^2)\,E_2}{a^2(a^2-b^2)k\,L^2E_2}F;$$

$$A_4 = -1.7\times10^{-4}\frac{-a(175b^2-105a^2+35akL)\,E_1+78(a^2-b^2)kL\,E_2+182a(b^2-a^2)\,E_2}{(a^2-b^2)k\,L^2E_2};$$

$$(1.25a^6-3.333a^4b^2+2.083a^2b^4)c\,L^2E_1$$

$$+(-1.167a^6+2.333a^4b^2-1.167a^2b^4)c\,L^2E_2$$

$$+(-0.057a^4-0.153a^4b^2+0.221a^2(\ln a)b^4-0.221a^2b^4(\ln b)+0.21a^2b^4)k\,E_1F$$

$$+[-(0.033a^6-0.033a^2b^2)kL^2+(0.199a^5-0.53a^3b^2+0.332ab^4)L\,]E_1F$$

$$+(0.068a^6-0.136a^4b^2+0.068a^2b^4)k\,E_2F$$

$$A_5 = \frac{+[-(0.04a^4-0.08a^2b^2+0.04b^4)kL^2-(0.186a^5-0.381a^3b^2+0.186ab^4)L\,]E_2F}{(a^2-b^2)^2k\,L^2E_2};$$

$$(-0.545a^6+1.453a^4b^2-0.908a^2b^4)c\,L^2E_1$$

$$+(0.944a^6-1.889a^4b^2+0.944a^2b^4)c\,L^2E_2$$

$$+(0.044a^6(\ln a)+0.09a^6-0.044a^4(\ln a)b^2+0.083a^4b^2)k\,E_1F$$

$$+(-0.096a^2(\ln a)b^4+0.096a^2b^4(\ln b)+0.092a^2b^4)k\,E_1F$$

$$+[(0.014a^4-0.014a^2b^2)kL^2-(0.087a^5-0.231a^3b^2+0.145ab^4)L\,]E_1F$$

$$+(-0.053a^6(\ln a)-0.051a^6+0.106a^4(\ln a)b^2)k\,E_2F$$

$$+(0.102a^4b^2-0.053a^2(\ln a)b^4-0.051a^2b^4)k\,E_2F$$

$$A_6 = \frac{+[-(0.013a^4-0.027a^2b^2+0.013b^4)kL^2+(0.15a^5-0.301a^3b^2+0.15ab^4)L\,]E_2F}{a^2(a^2-b^2)^2k\,L^2E_2};$$

$$(0.337a^6-0.897a^4b^2+0.561a^2b^4)c\,L^2E_1$$

$$-(0.583a^6-1.167a^4b^2+0.583a^2b^4)c\,L^2E_2$$

$$+(0.028a^6(\ln a)+0.003a^6-0.028a^4(\ln a)b^2-0.059a^4b^2)k\,E_1F$$

$$+\big(0.06a^2(\ln a)b^4+0.057a^2b^4-0.06a^2b^4(\ln b)\big)k\,E_1F$$

$$+[-(0.009a^4-0.009a^2b^2)kL^2+(0.054a^5-0.143a^3b^2+0.089ab^4)L\,]E_1F$$

$$+(-0.034a^6(\ln a)+0.043a^6+0.068a^4(\ln a)b^2)k\ E_2F$$

$$+(-0.085a^4b^2-0.034a^2(\ln a)b^4+0.043a^2b^4)k\ E_2F$$

$$A_7 = \frac{+[(0.02a^4-0.04a^2b^2+0.02b^4)kL^2-(0.093a^5-0.186a^3b^2+0.093ab^4)L\ ]E_2F}{a^2(a^2-b^2)^2k\ L^2E_2};$$

$$A_8 = -5.684\times10^{-3}\frac{5a^2\ E_1+6(b^2-a^2)\ E_2}{(a^2-b^2)L^2E_2}F\ ;$$

$$A_9 = -8.842\times10^{-3}\frac{5a^2\ E_1+6(b^2-a^2)\ E_2}{(a^2-b^2)L^2E_2}F\ ;$$

$$A_{10} = 2.842\times10^{-3}\frac{(15a^3-5a^2kL-25ab^2)\ E_1+[14a(b^2-a^2)-6(b^2-a^2)kL\ ]E_2}{(a^2-b^2)k\ L^2E_2}F;$$

$$A_{11} = 1.326\times10^{-2}\frac{(15a^3-5a^2kL-25ab^2)\ E_1+[14a(b^2-a^2)-6(b^2-a^2)kL\ ]E_2}{(a^2-b^2)k\ L^2E_2}F;$$

$$B_1 = 5.305\times10^{-4}\frac{F}{(a^2-b^2)L^2}\ ;$$

$$B_1 = -2.653\times10^{-4}\frac{F}{(a^2-b^2)L^2}\ ;$$

$$B_3 = 6.631\times10^{-4}\frac{a+3kL}{(a^2-b^2)kL^2}F\ ;$$

$$B_4 = 5.305\times10^{-3}\frac{3a-kL}{(a^2-b^2)kL^2}F\ ;$$

$$(-a^4b^2+a^2b^4)c\ L^2-(0.159a^3b^2+0.159ab^4)\ LF$$

$$B_5 = \frac{+\big(0.111a^6b^2-0.106a^2(\ln a)b^4-0.111a^2b^4+0.106a^2b^4(\ln b)\big)kF}{(a^2-b^2)^2kL^2};$$

$$B_6 = \frac{0.467a^2c\ L^2+[0.005kL^2+0.074aL-(0.042a^2-0.032b^2)k]F}{(a^2-b^2)kL^2};$$

$$(-0.3a^6+0.3a^2b^4)c\ L^2$$

$$+[(0.008a^2-0.008b^2)kL^2-(0.048a^3-0.048ab^2)L]F$$

$$B_7 = \frac{+\big(0.048a^6-0.106a^2(\ln a)b^4-0.101a^2b^4+0.053b^6+0.106b^4(\ln b)\big)kF}{(a^2-b^2)^2kL^2};$$

$$B_8 = 1.061\times10^{-1}\frac{b^2}{(a^2-b^2)L^2}F\ ;$$

$$B_9 = 0$$

$$B_{10} = -2.653\times10^{-2}\frac{(a-2kL)b^2}{(a^2-b^2)kL^2}F\ ;$$

$$B_{11} = -1.592\times10^{-1}\frac{ab^2}{(a^2-b^2)kL^2}F\ ;$$

Substitute A1-A11 into (3.18) and get all stress components of bolt under bolting force. Substitute B1-B11 into (3.18) and get all stress components of mortar protective layer under bolting force. The Expansion Force P and bolting force F in the bolt in causing stress

components are superimposed and can be obtained from analytical solutions for each stress component.

3.3 Examples Analysis

We present the application of formula developed in section 3.2on the an bolt example with the following values : bolting force F = 700Nk at the ends of the bolt, bolt length L = 10m, radius r = 8mm, reinforced elastic modulus E_s = 200GPa, Poisson's ratio = 0.3, friction coefficient of the surface of reinforced k = 0.8, thickness of the mortar cover = 25mm, mortar elastic modulus E_g = 25GPa, Poisson's ratio = 0.2, cohesion between reinforced and mortar c = 1.0MPa, the expansion Force is P.

The results of the axial stress distribution at the critical state of bolt bond-slip are shown in Table 3.1 and Figure3.5. Value of the axial stresses along the length of the bolt matches the exponential decay function. The pull force in the bolt decreases rapidly in the first part of bolt, then slowly.

Stress caused by Expansion Force P in mortar is two-dimensional; its distribution is only related to radius r and is unrelated to the length of the bolt, it changes with time. Corroded after a year, the results of Expansion Force simulation are shown in Figure3.2, Figure3.6.

Table3.1The axial stress distribution in the bolt

Bolt length/m	L=0(bolt end)	L=1	L=2	L=3	L=4	L=5
axial stress/MP	999.30	802.14	633.79	485.25	356.51	247.58
Bolt length/m	L=6	L=7	L=8	L=9	L=10(free end)	
axial stress/MP	158.45	89.13	36.61	9.90	0.00	

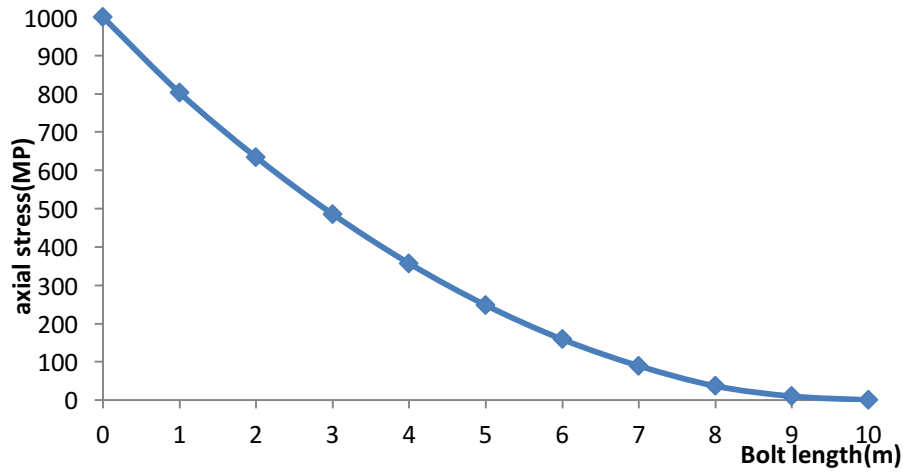

Fig.3.5 The axial stress distribution in the bolt

Table3.2 The stress distribution in the mortar cover under *P*

Bolt edge distance/(mm)	Expansion Force *p*	
	radial stress/(MP)	hoop stress/(MP)
r=0.0	-0.100	-0.042
r=4.5	-0.088	-0.054
r=9.0	-0.082	-0.059
r=13.5	-0.079	-0.063
r=18.0	-0.077	-0.065
r=22.5	-0.075	-0.066
r=27.0	-0.075	-0.067
r=31.5	-0.074	-0.068
r=36.0	-0.073	-0.068
r=40.5	-0.073	-0.069
r=45.0	-0.073	-0.069

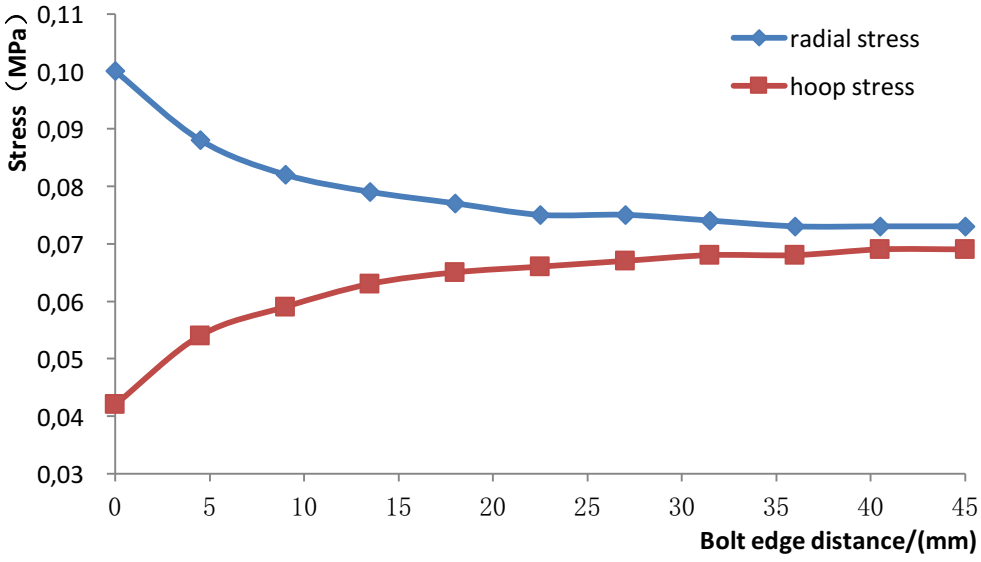

Fig.3.6 The stress distribution in the mortar aroused by *P*

Stress due to the bolting force *F* is three-dimensional. Relevant results are shown in Form3.3, Figure3.7 and Figure3.8. On the plane perpendicular to the bolt, the radial tensile stress and hoop stress reach maximum in the mortar near bolt edge.

Stress fields caused by the Expansion Force *P* and the bolting force *F*are combined. Results are show in Form3.4, Figure3.9 and Figure3.10. We observe that the radial stress within the mortar protective layer transfers from tensile stress to compressive stress, the tensile stress peak is in the mortar near bolt edge. Along the length of the bolt, the compressive stress peaks in the mortar around the bolt end. And in any plane perpendicular to the bolt along bolt length, the compressive stress peaks in the mortar near bolt edge.

Values of shear stress caused by bolting force *F* match the linear distribution along the length of bolt, the vector direction is opposite to that of bolting force(as shown in Figure3.11).

According to presumptions in the model, bond-slip condition of bolt and mortar contact at the critical state is in accordance with the basic Coulomb friction model. In the joint action of Force *P* and Force *F*, the value of the shear stress between the bolt and mortar in bond slip critical state is in line with the following formula:

$$\tau_{rz}|_{r=a} = c - k \cdot \sigma_{rz}|_{r=a} (3.57)$$

Where, $\sigma_{rz}|_{r=a}$ in the interface of bolt and mortar is generated by the common product of *P* and *F*.

Under the common product of *P* and *F*, the results of shear stress on the interface between the bolt and mortar is shown as Table3.5 and Figure3.12, the value of shear stress follows linear distribution.

Table3.3 The stress distribution in the mortar covers under *F*

	Bolt edge distance /(mm)	Bolt length/(m)					
		L=0(bolt end)	L=2	L=4	L=6	L=8	L=10(free end)
radial stress /(MP)	r=0	3.107	2.735	2.364	1.993	1.621	1.250
	r=4.5	1.754	1.544	1.335	1.125	0.915	0.706
	r=9	1.087	0.957	0.828	0.698	0.568	0.438

	r=13.5	0.711	0.626	0.541	0.456	0.371	0.286
	r=18	0.478	0.421	0.364	0.306	0.249	0.192
	r=22.5	0.323	0.285	0.246	0.207	0.169	0.130
	r=27	0.216	0.190	0.164	0.138	0.113	0.087
	r=31.5	0.138	0.121	0.105	0.088	0.072	0.056
	r=36	0.080	0.070	0.061	0.051	0.042	0.032
	r=40.5	0.035	0.031	0.027	0.022	0.018	0.014
	r=45	0.000	0.000	0.000	0.000	0.000	0.000
hoop stress /(MP)	r=0	-3.523	-3.102	-2.682	-2.261	-1.840	-1.419
	r=4.5	-2.170	-1.911	-1.652	-1.392	-1.133	-0.874
	r=9	-1.503	-1.324	-1.144	-0.965	-0.785	-0.606
	r=13.5	-1.127	-0.992	-0.858	-0.723	-0.589	-0.454
	r=18	-0.893	-0.787	-0.680	-0.573	-0.467	-0.360
	r=22.5	-0.739	-0.650	-0.562	-0.474	-0.386	-0.298
	r=27	-0.631	-0.556	-0.480	-0.405	-0.330	-0.255
	r=31.5	-0.553	-0.487	-0.421	-0.355	-0.289	-0.223
	r=36	-0.495	-0.436	-0.377	-0.318	-0.259	-0.200
	r=40.5	-0.450	-0.396	-0.343	-0.289	-0.235	-0.182
	r=45	-0.415	-0.366	-0.316	-0.267	-0.217	-0.168

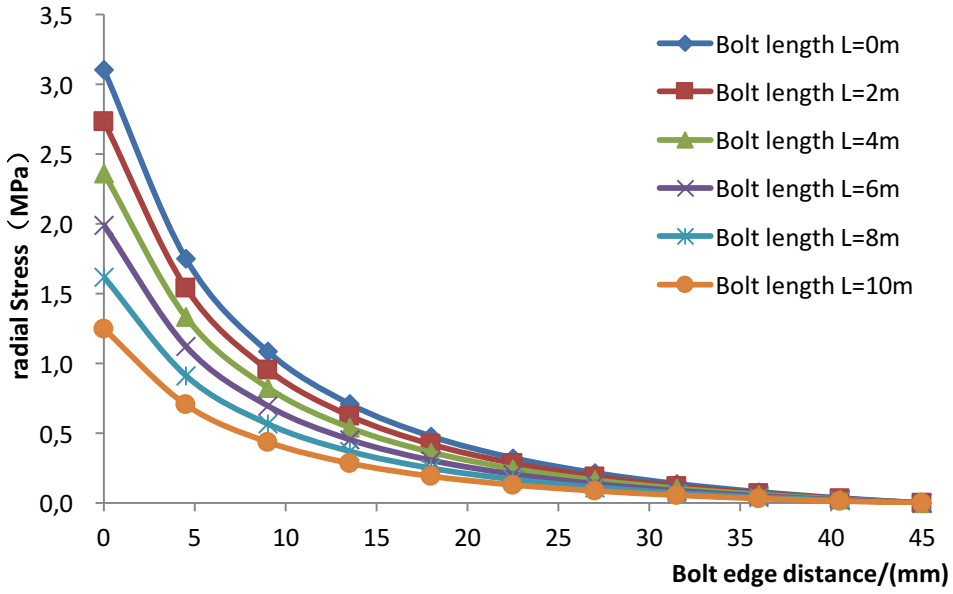

Fig.3.7 The radial stress in the mortar aroused by *F*

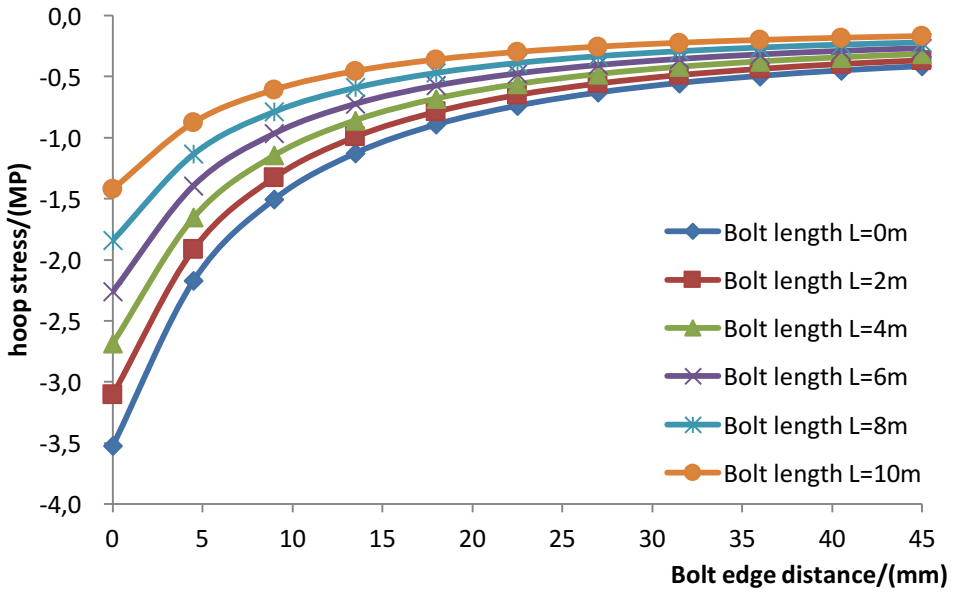

Fig.3.8 The hoop stress in the mortar aroused by *F*

Table3.4 The stress distribution in the mortar cover under *P* and *F*

	Bolt edge distance /(mm)	Bolt length/(m)					
		L=0(bolt end)	L=2	L=4	L=6	L=8	L=10(free end)
radial	r=0	3.007	2.635	2.264	1.893	1.521	1.150

stress /(MP)	r=4.5	1.666	1.456	1.247	1.037	0.827	0.618
	r=9	1.005	0.875	0.746	0.616	0.486	0.356
	r=13.5	0.632	0.547	0.462	0.377	0.292	0.207
	r=18	0.401	0.344	0.287	0.229	0.172	0.115
	r=22.5	0.248	0.210	0.171	0.132	0.094	0.055
	r=27	0.141	0.115	0.089	0.063	0.038	0.012
	r=31.5	0.064	0.047	0.031	0.014	-0.002	-0.018
	r=36	0.007	-0.003	-0.012	-0.022	-0.031	-0.041
	r=40.5	-0.038	-0.042	-0.046	-0.051	-0.055	-0.059
	r=45	-0.073	-0.073	-0.073	-0.073	-0.073	-0.073
hoop stress /(MP)	r=0	-3.565	-3.144	-2.724	-2.303	-1.882	-1.461
	r=4.5	-2.224	-1.965	-1.706	-1.446	-1.187	-0.928
	r=9	-1.562	-1.383	-1.203	-1.024	-0.844	-0.665
	r=13.5	-1.190	-1.055	-0.921	-0.786	-0.652	-0.517
	r=18	-0.958	-0.852	-0.745	-0.638	-0.532	-0.425
	r=22.5	-0.805	-0.716	-0.628	-0.540	-0.452	-0.364
	r=27	-0.698	-0.623	-0.547	-0.472	-0.397	-0.322
	r=31.5	-0.621	-0.555	-0.489	-0.423	-0.357	-0.291
	r=36	-0.563	-0.504	-0.445	-0.386	-0.327	-0.268
	r=40.5	-0.519	-0.465	-0.412	-0.358	-0.304	-0.251
	r=45	-0.484	-0.435	-0.385	-0.336	-0.286	-0.237

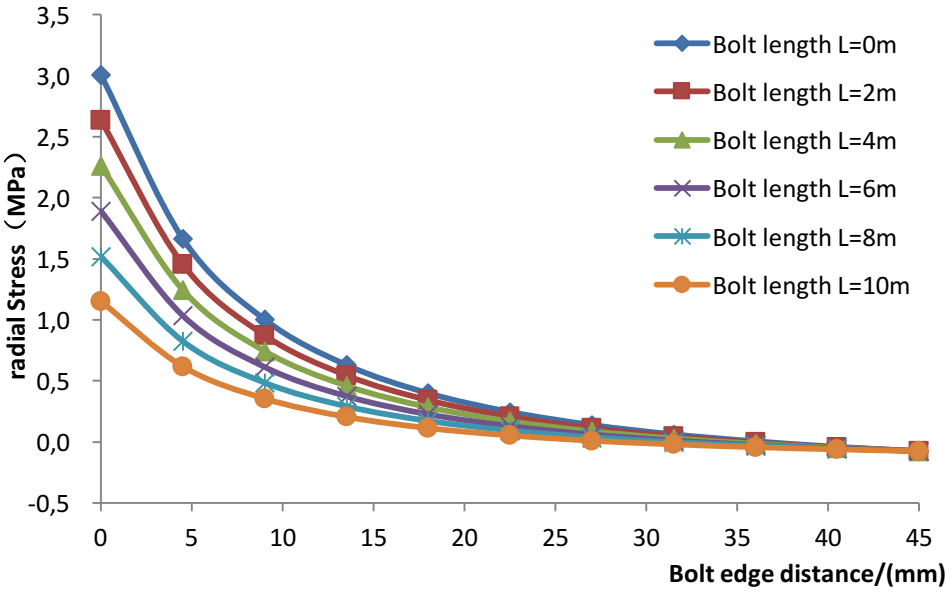

Fig.3.9 The radial stress in the mortar aroused by *P* and *F*

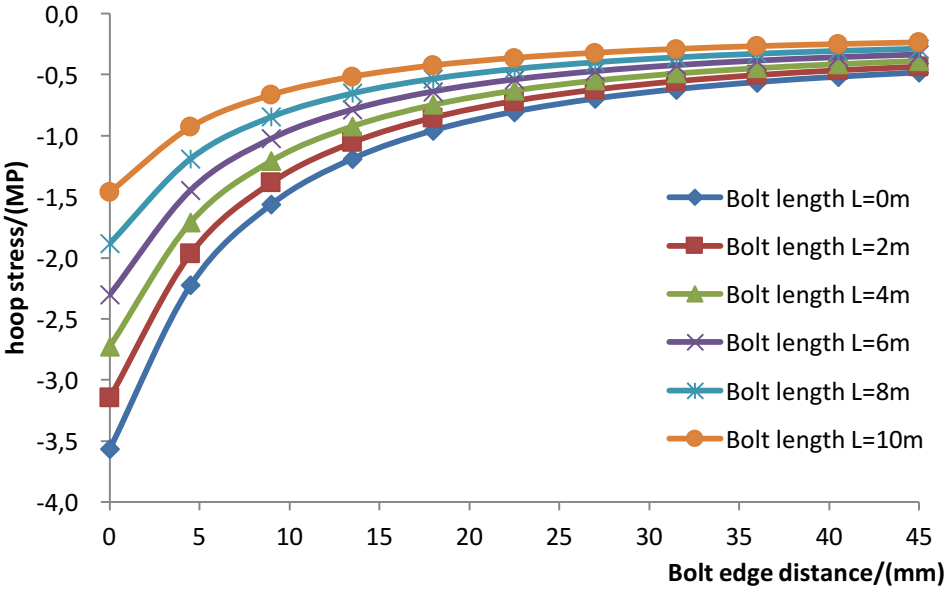

Fig.3.10 The hoop stress in the mortar aroused by *P* and *F*

Table3.5 The Shear stress distribution between the bolt and mortar

Bolt length/m	*L*=0(bolt end)	L=1	L=2	L=3	L=4	L=5
Shear stress/MP	-1.406	-1.272	-1.108	-0.969	-0.811	-0.669
Bolt length/m	L=6	L=7	L=8	L=9	L=10(free end)	
Shear stress/MP	-0.514	-0.363	-0.219	-0.068	0.080	

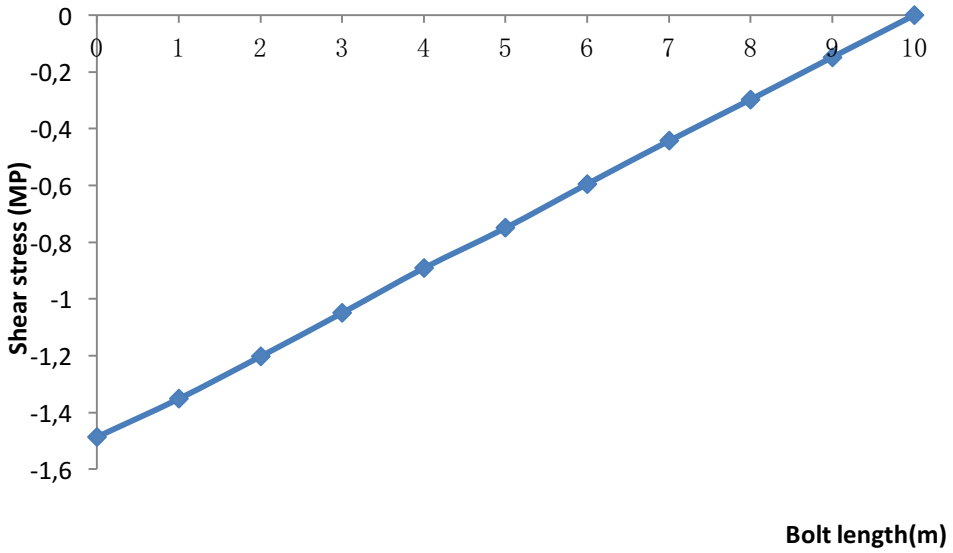

Fig.3.11 The Shear stress between the bolt and mortar aroused by *F*

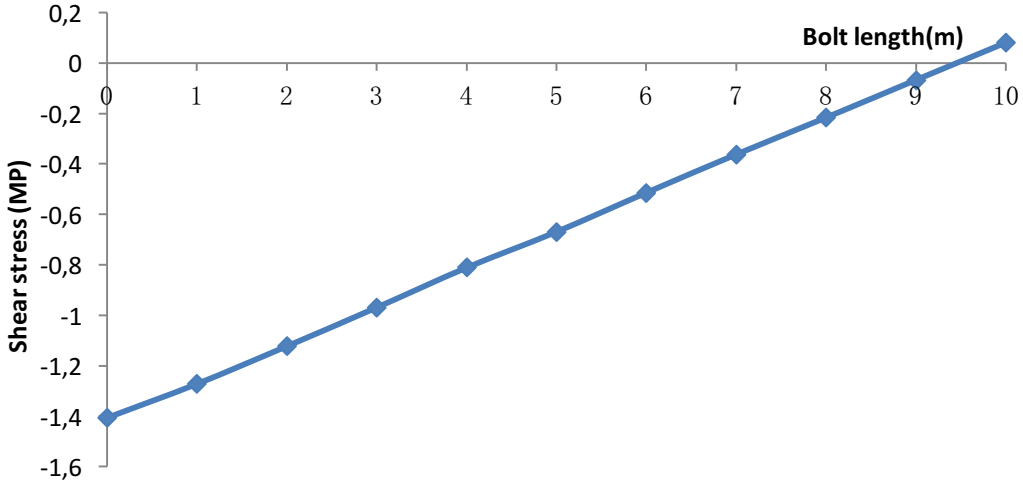

Fig.3.12 The Shear stress between the bolt and mortar aroused by *P* and *F*

Under the joint action of *P* and *F*, the results of shear stress on the interface between the bolt and mortar are shown in Figure3.5 and Figure3.12. The shear stress follows linear distribution. Most bolt surface shear stress is negative, in the opposite direction to that of the bolting force, and the shear stress peak occurs at the bolt end. In the transition from negative values to positive ones, the shear stress goes through a 'neutral point', at this point, the size of the shear stress is zero. Confining pressure and Expansion Force on reinforced mortar interface will lead to radial compressive stress, which is beneficial to improving the bolt pullout before

cracking according to the Coulomb friction model.

3.4 Conclusions

In this chapter, we established bolt space rust analytical in order to study the three-dimensional stress field of the bolt under the joint action of bolting force and rust expansion force.

According to numerical analysis, stress distribution in rusting bolt body is given:

① the axial stress of the bolt is distributed in the form of exponential decay function;

②On the plane perpendicular to the bolt, the radial stress within the mortar protective layer is in transition from tensile stress to compressive stress, tensile stress peaks occur at the radial edge of the mortar bolt;

③Along the length of bolt, compressive stress within the mortar peaks occur at the end of the bolt, but on the plane perpendicular to the bolt, hoop stress peaks occur near the edge of the bolt in the mortar;

④ Shear stress between the bolt and mortar follows linear distribution. Most values of the shear stress on the bolt surface are negative; peaks occur at the bolt end, vectors of shear stress are in opposite direction to that of bolting force. In the transition from negative values to positive ones, the shear stress goes through a 'neutral point', at this point, the size of the shear stress is zero.

Confining pressure and Expansion Force on reinforced mortar interface will lead to radial compressive stress, which is beneficial for improving the bolt pullout before cracking according to the Coulomb friction model.

Shear stress obtained by the stress function matches linear distribution along the bolt length, which does not agree with experimental results: The distribution of the shear stress in most tests along the length follows exponential decay function. Although the results obtained in this chapter reflects the roughly law of shear stress distribution along the length of the bolt, there are some errors with the actual distribution of the shear stress. To improve the

description of the distribution of the shear stress, quadratic functions of z or exponential decay function of the expression should be used. In other words, the stress function need to be further modified, so that the form of the shear stress components obtained by the stress function can reflect the distribution of the shear stress more accurately on the interface between bolt and mortar.

References

1. Li C, Stillborg B. Analytical models for rock bolts. International Journal of Rock Mechanics and Mining Sciences. 1999(36):1013-1029.
2. Hyett A J, Bwaden W F, Macsporran G R, Moosvai M. A constitutive law for bond failure of full-grouted cable bolts using a modified Hoek cell. International Journal of Rock Mechanics and Mining Sciences & Geomechanics Abstracts. 1995; 32(1):11-36.
3. Tepfers R. Cracking of concrete cover along bolted deformed reinforcing bars. Magazine of Concrete Research. 1979; 31(106):3-12.
4. Nielsen C V, Bićanić N. Radial fictitious cracking of think-walled cylinder due to bar pull-out.Magazine of Concrete Reseacrh. 2002; 54(3):215-221.
5. Cairns J, Jones K. An evaluation of the bond-splitting action of ribbed bars. ACI Material Joumal. 1996; 93(1):10-19.
6. Bahnolzer B, Barmeshuber W, Jung W. Analytical simulation of pull-out test----the direct problem. Cement & Concrete Composites. 2005(27):93-101.
7. Windsor C R. Rock Reinforcement System. International journal of rock mechanics and mining sciences. 1997; 34(6):919-51.
8. Xu Z L. Elasticity. Beijing: High Education Press, 1979.
9. Timoshenko S P, Goodier J N. Theory of Elasticity. New York: McGraw-Hillnle, 1970.
10. Xu Z L. Applied Elasticity. Mew Delhi: Wiley Eastern Limited, 1992.
11. Shan R, Liu Z B, Liu W. A solution of hyperbolic cosine pressures on a hollow cylinder and the limit when $k \rightarrow 0$. China Mechanical Engineering. 2003; 14(17):1526-1529.
12. Liu Z B, Shan R, Liu W, et al. A solution of arbitrary quadratic function pressures on a hollow cylinder and the limit when $k \rightarrow 0$. Science in China. 2004; 34(3):298-304.

Chapter 4 Equivalent finite element method to study bolt corrosion

4.1 Introduction

This chapter introduces the basic principles of finite element method, then describes the equivalent mechanical model and the constitutive relation usedin finite element method. The method is then used for the analysis of a bolt subjected tocorroded expansion force. Through examples, we analyze the method performances.

4.2 Finite element method

Figure4.1 shows a homogeneous domain, such as a block of intact rock, which has definite hydraulic and mechanical properties. According to the theory of the Finite Element Method (FEM), the domain is meshed as a finite element, in which the hydraulic potential ϕ_r and the displacement vector $\{\Delta u\}_r$ are interpolated from the nodal values $\{\phi\}_r$ and $\{\Delta\delta\}_r$ respectively as the Equations (4.1) and (4.2).

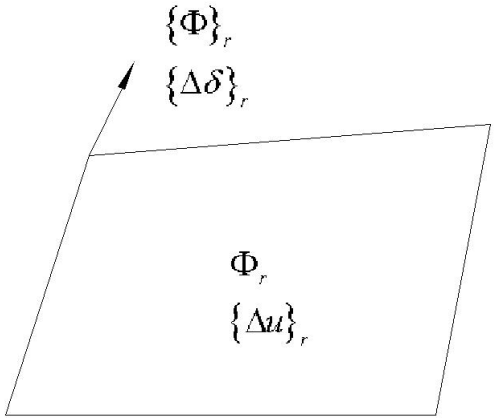

Figure 4.1 Interpolation of the hydraulic potential and the displacement vector in a finite element

$$\phi_r = [N]\{\phi\}_r \tag{4.1}$$

$$\{\Delta u\}_r = [N]\{\Delta\delta\}_r \tag{4.2}$$

in which $[N]$ is the shape function matrix defined as

$$[N] = \begin{pmatrix} N_1 & 0 & 0 & N_2 & 0 & 0 & \cdots & N_n & 0 & 0 \\ 0 & N_1 & 0 & 0 & N_2 & 0 & \cdots & 0 & N_n & 0 \\ 0 & 0 & N_1 & 0 & 0 & N_2 & \cdots & 0 & 0 & N_n \end{pmatrix} \tag{4.3}$$

Where, n is the node number in an element.

For a three-dimensional element with 8 nodes, the shape function of each node is expressed in local coordinates as

$$N_1(\xi,\eta,\varsigma)=\frac{1}{8}(1+\xi_i\xi)(1+\eta_i\eta)(1+\varsigma_i\varsigma) \qquad (i-1,2,\quad ,8) \tag{4.4}$$

$$\xi=(-1)^i\eta_i=(-1)^{[i/2+0.5]}\xi_i=(-1)^{[i/4+0.75]} \tag{4.5}$$

For seepage analyses, the governing equations are established using the variational principle [1]:

$$[h]_r\{\phi\}_r=\{f\}_r \tag{4.6}$$

$$\{\mathrm{h}\}_r=-\iiint_{\Omega_r}(\{S\}[N])^T[H]_r(\{S\}[N])d\Omega \tag{4.7}$$

$$\{\mathrm{f}\}_r=-\iiint_{\Omega_r}[N]fd\Omega-\iint_{\Gamma_r}[N]d\Gamma \tag{4.8}$$

f is the point convergence density; q is the flow rate normal to boundary surfaces and pointing outwards; $\{\mathrm{S}\}$ is the differential operator and $[N]_r$ is the permeability coefficient matrix as:

$$\{\mathrm{S}\}=\{\frac{\partial}{\partial x},\frac{\partial}{\partial y},\frac{\partial}{\partial z}\} \tag{4.9}$$

$$[H]_r=\begin{pmatrix}k_{xx} & k_{xy} & k_{xz}\\ & k_{yy} & k_{yz}\\ S & & k_{zz}\end{pmatrix} \tag{4.10}$$

For stress/strain analyses, the governing equations are established by the virtual work principle [2]:

$$[k]_r\{\Delta\delta\}_r=\{\Delta f\}_r+\{\Delta f^{vp}\}_r \tag{4.11}$$

$$\{\mathrm{k}\}_r=\iiint_{\Omega}[B]^T[D]_r[B]d\Omega \tag{4.12}$$

$$\{\Delta f^{vp}\}_r=\iiint_{\Omega_r}[B]^T[D]_r\{\varepsilon^{\mathrm{vp}}\}_r\Delta td\Omega \tag{4.13}$$

$$\{\Delta f\}_r=\iiint_{\Omega_r}[N]^T\{f\}d\Omega+\iint_{\Gamma_r}[N]^T\{p\}d\Gamma-\iiint_{\Omega_r}[B]^T\{\sigma_0\}d\Omega+\iiint_{\Omega_r}[B]^T[D]_r\{\varepsilon_0\}d\Omega \tag{4.14}$$

$\{\mathrm{f}\}$ is the body force vector; $\{\mathrm{p}\}$ is the surface force vector; $\{\sigma_0\}$ is the initial stress vector; $\{\varepsilon_0\}$ is the initial strain vector; $[D]_r$ is the elastic matrix as the Equation (4.15) formed by the Lame Coefficients, i.e. λ and G; $[B]$ is the differential matrix of the shape functions as the

Equations(4.16) and (4.17); $\{\varepsilon^{vp}\}_r$ is the viscoplastic flow rate vector as the Equations (4.18) and (4.19), where γ , F , Q are the fluidity parameter, yield function and potential function, respectively.

$$[D]_r = \begin{pmatrix} \lambda+2G & \lambda & \lambda & 0 & 0 & 0 \\ \lambda & \lambda+2G & \lambda & 0 & 0 & 0 \\ \lambda & \lambda & \lambda+2G & 0 & 0 & 0 \\ 0 & 0 & 0 & G & 0 & 0 \\ 0 & 0 & 0 & 0 & G & 0 \\ 0 & 0 & 0 & 0 & 0 & G \end{pmatrix} \tag{4.15}$$

$$[B] = [[B]_1 [B]_2 \quad [B]_n] \tag{4.16}$$

$$[B]_i = \begin{pmatrix} \frac{\partial N_i}{\partial x} & 0 & 0 \\ 0 & \frac{\partial N_i}{\partial y} & 0 \\ 0 & 0 & \frac{\partial N_i}{\partial z} \\ 0 & \frac{\partial N_i}{\partial z} & \frac{\partial N_i}{\partial y} \\ \frac{\partial N_i}{\partial z} & 0 & \frac{\partial N_i}{\partial x} \\ \frac{\partial N_i}{\partial y} & \frac{\partial N_i}{\partial x} & 0 \end{pmatrix} \tag{4.17}$$

$$\{\varepsilon^{vp}\}_r = \gamma < F > \left\{ \frac{\partial Q}{\partial \{\sigma\}} \right\} \tag{4.18}$$

$$< F > = \begin{cases} F & if \quad F > 0 \\ 0 & if \quad F < 0 \end{cases} \tag{4.19}$$

4.3Constitutive relation

The constitutive relation shown in Figure 4.2 was firstly proposed by Chen and Pande[3], the aim of the new model is to describe the bolt's behavior in more detail with the equivalent continuum approach.

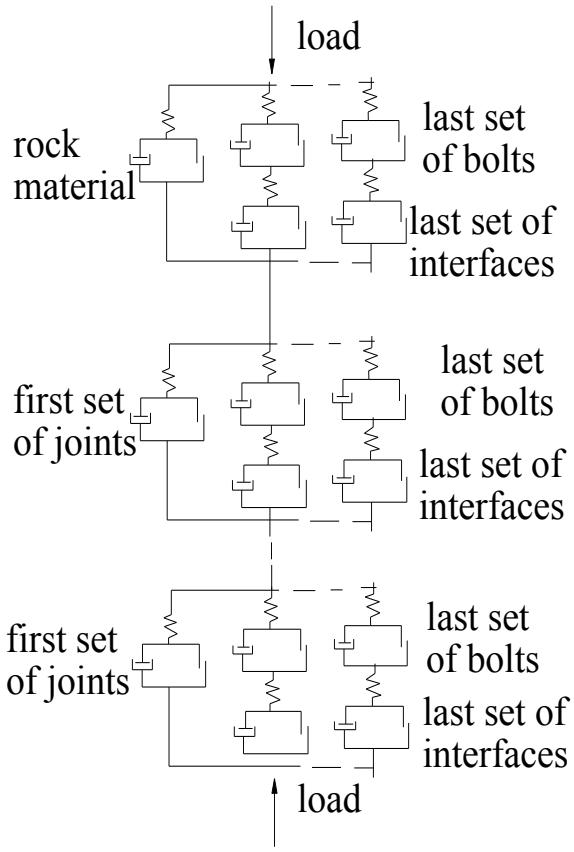

Figure 4.2 The new rheological model

In the present study the influence of the interfaces is not taken into consideration, so from the proposed rheological model four basic principles can be obtained for the jointed rock masses reinforced by the passive, fully grouted bolts:

(1) The strain increment of the bolted jointed rock is given as the sum of the incremental strains of the reinforced rock material and the reinforced joints.

(2) The load increment is shared among the bolt and the rock material in the reinforced rock material, the same applies to the reinforced joint.

(3) The mean stress in the bolted rock material is equal to the mean stress in the bolted joint.

(4) The strain of the bolt is equal to the strain of the rock material in the bolted rock material; similarly, the relative displacement of the two hinges is equal to the relative displacement of the joint.

Under the co-ordinate systems specified above, these principles can be formulated as follows:

(1)

$$\{\Delta\varepsilon\}^n = \{\Delta\varepsilon\}^n_{R(B)} + \sum_j \{\Delta\varepsilon\}^n_{J(B)} \tag{4.20}$$

(2)

$$\left.\begin{aligned}\{\Delta\sigma\}^n_{R(B)} &= A_R\{\Delta\sigma\}^n_R + \sum_b A_b[T]^{\mathrm{T}}_b\{\Delta\sigma\}^n_{(br)}\\ \{\Delta\sigma\}^n_{j(b)} &= A_R\{\Delta\sigma\}^n_j + \sum_b A_b[T]^{\mathrm{T}}_{(bj)}\{\Delta\sigma\}^n_{(bj)}\end{aligned}\right\} \tag{4.21}$$

Where A_R and A_b are the volumetric proportions of rock and bolt, with

$$A_R + \sum_b A_b = 1$$

(3)

$$\{\Delta\sigma\}^n = \{\Delta\sigma\}^n_{R(B)} = \{\Delta\sigma\}^n_{J(B)} \tag{4.22}$$

(4)

$$\left.\begin{aligned}\{\Delta\varepsilon\}^n_{R(B)} &= \{\Delta\varepsilon\}^n_R = \{\Delta\varepsilon\}^n_{(BR)}\\ \{\Delta\varepsilon\}^n_{j(b)} &= \{\Delta\varepsilon\}^n_j = [T]^{-1}_{(bj)}\{\Delta\varepsilon\}^n_{(bj)}\end{aligned}\right\} \tag{4.23}$$

In which the reverse calculation $[T]^{-1}_{(bj)}$ can be carried out only for its submatrix $[T]^{*}_{(bj)}$.

4.4 The Formulation of the elasto-viscoplatic constitutive equation for bolted jointed rock masses

According to the elasto-viscoplastic potential theory [8], at time t_n, the constitutive equation takes the following forms:

$$\{\Delta\sigma\}^n = [D](\{\Delta\varepsilon\}^n - \{\varepsilon^{vp}\}^n\Delta t_n)$$

or (4.24)

$$\{\Delta\varepsilon\}^n = [S]\{\Delta\sigma\}^n + \{\varepsilon^{vp}\}^n\Delta t_n$$

Where Δt_n is the time-stepping length, and [D] and [S] are the elastic matrix and compliance matrix, respectively. The viscoplastic flow rate is:

$$\{\Delta\varepsilon^{\mathrm{vp}}\}^n = \gamma < F > \left\{\frac{\partial Q}{\partial\{\sigma\}}\right\} \tag{4.25}$$

Where γ is the fluidity parameter, F and Q are the yield and potential functions respectively, and the function $<F>$ is defined as

$$< F > = \begin{cases} F & if \quad F > 0 \\ 0 & if \quad F < 0 \end{cases} \tag{4.26}$$

In the study of practice problems, if the fluidity parameter could be obtained by the laboratory and field tests or by the back analysis, the histories as well as the steady-state results of the

deformation and failure of a structure could be calculated. However, in some cases it is not easy to get the appropriate fluidity parameter or only the elasto-plastic solution is of importance, under such circumstances we can simply assume that the fluidity parameter $\gamma = 1$. In this way the histories are not applicable, but the steady-state results of the deformation and failure are identical to the corresponding conventional static elasto-plastic solution [8].

4.4.1 The constitutive equation of intact rock

The rock material is taken as an isotropic material whose elastic matrix is:

$$[D]_R = \begin{bmatrix} \lambda & +2G & \lambda & \lambda & 0 & 0 & 0 \\ & \lambda & +2G & \lambda & 0 & 0 & 0 \\ & & \lambda & +2G & 0 & 0 & 0 \\ & & & & G & 0 & 0 \\ & & SYM & & & G & 0 \\ & & & & & & G \end{bmatrix} \tag{4.27}$$

For the yield of the intact rock, both the Mohr- Coulomb and the Drucker-Prager criteria are widely used; in the present study the latter is implemented in the FEM program:

$$\begin{aligned} F_R &= \mathrm{a}I_1 + \sqrt{J_2} - k = 0 \\ a &= \sin\varphi_R / \sqrt{3(3+\sin^2\varphi_R)} \\ k &= \sqrt{3}c_R\cos\varphi_R / \sqrt{3(3+\sin^2\varphi_R)} \end{aligned} \tag{4.28}$$

The associate flow rule is adopted:

$$Q_R = F_R \tag{4.29}$$

so the flow rate of viscoplastic strain is

$$\{\Delta\varepsilon^{\mathrm{vp}}\}_R^n = \gamma_R < F_R > \left\{\frac{\partial F_R}{\partial\{\sigma\}}\right\} \tag{4.30}$$

In equations (4.28)-(4.30) c_R, φ_R, γ_R are the cohesion, friction angle and Fluidity parameter of intact rock, respectively.

4.4.2 The constitutive equation of joint

The relative displacement of the joint walls will be interpreted as equivalent strain according to the joint spacing. The elastic matrix of the *j*th joint in its local co-ordinate system can be

expressed by the normal stiffness k_{nj}, the tangential stiffness k_{sj}, and the joint spacing d_j as

$$[D]_j = d_j \begin{bmatrix} 0 & 0 & 0 & 0 & 0 & 0 \\ 0 & 0 & 0 & 0 & 0 & 0 \\ 0 & 0 & k_{nj} & 0 & 0 & 0 \\ 0 & 0 & 0 & k_{sj} & 0 & 0 \\ 0 & 0 & 0 & 0 & k_{sj} & 0 \\ 0 & 0 & 0 & 0 & 0 & 0 \end{bmatrix} \tag{4.31}$$

Non-associate flow rule is considered for the joint:

$$\{\Delta\varepsilon^{vp}\}_j^n = \frac{\gamma_j}{d_j} < F_j > \left\{ \frac{\partial Q_j}{\partial \{\sigma\}_j} \right\} \tag{4.32}$$

where the yield function F_j and potential function Q_j are expressed by the cohesion c_j, friction angle φ_j, dilatance angle ϕ_j and tension strength σ_{Tj}:

$$F_j = \sqrt{\tau_{zxj}^2 + \tau_{zyj}^2} + \sigma_j tg\varphi_j - c_j \qquad if\ \sigma_j < \sigma_{Tj}$$

$$Q_j = \sqrt{\tau_{zxj}^2 + \tau_{zyj}^2} + \sigma_j tg\phi_j + const \tag{4.33}$$

$$\begin{matrix} F_j = \sigma_j - \sigma_{Tj} & if\ \sigma_j \geq \sigma_{Tj} \\ Q_j = \sqrt{\tau_{zxj}^2 + \tau_{zyj}^2} + \sigma_j^2 & +const \end{matrix} \tag{4.34}$$

4.4.3 The constitutive equation of Bolt

4.4.3.1 The bolt in a joint

A series of laboratory tests for a reinforced joint has been conducted at the Swiss Federal Institute of Technology in Lausanne [4-7]. The main conclusions are:

1. For samples with a bolt forming a small angle to the normal of the joint, bending of the bolt becomes predominant even when the shear force is small, which will create two hinges above and below the joint plane (Figure 4.3). As the stress level is approximately constant in the zone between the two hinges, the exact location of failure cannot be predicted. Failure may occur by bending in one of the plastic hinges or by combined shear and tension near the shear surface. Test results showed the occurrence of both failure types for tests under apparently the same conditions, the ultimate loads and displacements at failure were nearly identical.

2. For samples with a bolt being inclined at a large angle to the normal of the joint, two hinges also developed in the tests, but the bending phenomena are not so strong. The great majority of the inclined bolts failed in tension near the shear surface.

3. The vertical height of the bended bolt is about 2-4 times the bolt diameter d_b, i.e. $h_b = 2-4d_b$. It is named 'effective height', corresponding to an 'effective length' of $L_b = 2-4d_b$ (Figure 4.3). This height depends on the quality of the rock (or the grout mortar) and the bolt, on the bolt's diameter and the inclined angle, etc.

4. The sample in which the bolt forms a small angle with the normal of the joint show larger shear displacements, i.e. the inclined bolts react in a stiffer way than the normal ones. Besides, the maximum shear resistance of the bolted joint increases with the inclination of the bolt provided there is considerable friction along the joint.

5. Large bolt diameters reduce the shear displacements required for obtaining a given shear force, and the maximum shear force increases linearly with the section of the bolt.

From the above conclusions it is natural to assume that there is an 'effective length' of the bolt at a joint (nearly the same quantity as the length between the hinges) within which nearly all deformations will take place (Figure 4.3). By the general assumption (1) of the equivalent material, the relative displacement between the two hinges is equal to the relative displacement of the joint walls at the intersection point. For the tension stress in this part, the uniform distribution along the effective length L_b seems a good and reasonable approach (Figure 4.4(a)), for the shear stress distribution we think two types are applicable as shown in Figures 4.4(b) and 4.4(c).

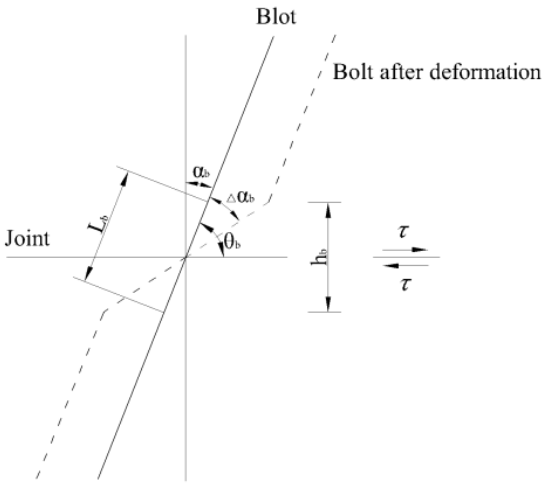

Figure 4.3 The deformation of the bolt near a joint

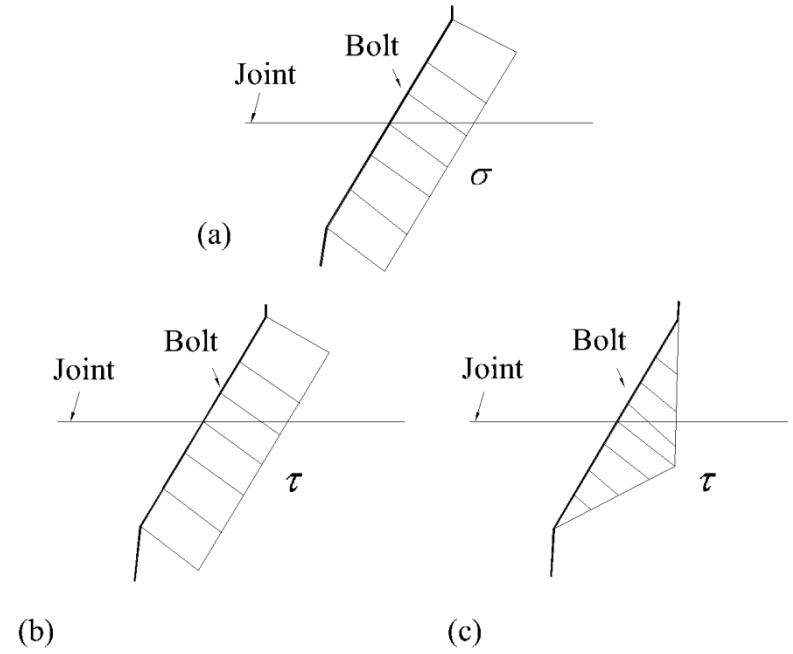

Figure 4.4 The ideal stresses distribution along the effective length of a bolt: (a) normal stress distribution; (b) shear stress distribution (uniform): (c) shear stress distribution (triangular)

The elastic relationship between strains and average stresses would be

$$\begin{aligned} \sigma_b &= E_b \varepsilon_b \\ \tau_b &= G_b \frac{1}{A\beta} \gamma_b \end{aligned} \tag{4.35}$$

where $A = 4/3$ for solid round bar, and:

$$\begin{aligned} &\beta = 1 \text{ for uniform shear stress distribution (Figure 5(b))} \\ &\beta = 1/2 \text{ for triangular shear stress distribution (Figure 5(c))} \end{aligned} \tag{4.36}$$

By what has been analyzed above, it is clear that in the implementation of the numerical model more attention should be paid to the bolt's behavior in the joint; especially the dip direction deflection $\Delta\phi_b$ and the dip angle deflation $\Delta\theta_b$ as well as the deformability of the bolt should be taken into account.

According to the above assumptions, on the bolt only normal stress σ_b and shear stress τ_{zxb}, τ_{zyb} can be transmitted (Figure 4.6), therefore the constitutive equation of the bolt set *b* at the joint set *j* expressed in 'real' stress and strain would be

$$\{\Delta\sigma\}_b^{*_n} = [D]_{(bj)}^{*} (\{\Delta\varepsilon\}_b^{*_n} - \{\Delta\varepsilon^{\text{vp}}\}_b^{*_n} \Delta t_n) \tag{4.37}$$

where

$$[D]^{*}_{(bj)} = \begin{pmatrix} 0 & & & \\ & 0 & & \\ & & [D]^{**}_{(bj)} & \\ & & & 0 \end{pmatrix}$$
$$[D]^{**}_{(bj)} = \begin{pmatrix} E_b & 0 & 0 \\ 0 & G_b / A\beta & 0 \\ 0 & 0 & G_b / A\beta \end{pmatrix} \tag{4.38}$$
$$\{\Delta\varepsilon^{\mathrm{vp}}\}^{*_n}_{b} = \gamma_b < F_b > \left\{ \frac{\partial F_b}{\partial \{\sigma\}_b} \right\}$$

The Von Mises criterion with isotropic working hardening is used:

$$F_b = \left[3(\tau^2_{zxb} + \tau^2_{zyb}) + \sigma^2_b \right]^{1/2} - \sigma$$
$$\sigma = \sigma_y + (\sigma_u - \sigma_y)\gamma^{vp} / \gamma^{vp}_u \tag{4.39}$$

in which σ_y, σ_u, γ^{vp}, γ^{vp}_u are the yield strength, ultimate strength, ultimate plastic general shear strain, and present plastic general shear strain respectively.

The strain increment of the bolt set *b* in the joint set *j* should be made equivalent to that of the rock mass according to the effective length and the joint spacing:

$$\{\Delta\varepsilon\}_b = \frac{L_b}{d_j}\{\Delta\varepsilon\}^{*}_{b} \qquad or$$
$$\{\Delta\varepsilon\}^{*}_{b} = \frac{d_j}{L_b}\{\Delta\varepsilon\}_b \tag{4.40}$$

Equation (4.43) becomes

$$\{\Delta\sigma\}^{n}_{b} = [D]_{(bj)}(\{\Delta\varepsilon\}^{n}_{b} - \{\Delta\varepsilon^{\mathrm{vp}}\}^{n}_{b}\Delta t_n) \tag{4.41}$$

in which

$$[D]_{(bj)} = \frac{d_j}{L_b}[D]^{*}_{(bj)}$$
$$\{\varepsilon^{\mathrm{vp}}\}^{n}_{b} = \frac{L_b}{d_j}\{\varepsilon^{\mathrm{vp}}\}^{*_n}_{b} \tag{4.42}$$

During the viscoplastic deformation, the length of hinge L_b, the dip direction ϕ_b and dip angle θ_b should be updated at definite time steps to simulate the effect of the change of the bolt's geometry characteristics. At any time step *n*, the corresponding quantities should be calculated as follows:

$$
\begin{aligned}
L_b^n &= L_b^{n-1} + d_j \Delta\varepsilon_b \\
\phi_b^n &= \phi_b^{n-1} + \arctg(\frac{d_j \Delta\gamma_{zxb}}{L_b^{n-1}}) \\
\theta_b^n &= \theta_b^{n-1} + \arctg(\frac{d_j \Delta\gamma_{zyb}}{L_b^{n-1}})
\end{aligned}
\tag{4.43}
$$

4.4.3.2The bolt in the rock material

For the bolt set *b* in the rock material, it can be written directly:

$$
\{\Delta\sigma\}_{(br)}^n = [D]_{(br)}(\{\Delta\varepsilon\}_{(br)}^n - \{\varepsilon^{\mathrm{vp}}\}_{(br)}^n \Delta t_n) \tag{4.44}
$$

where:

$$
[D]_{(br)} = \begin{bmatrix}
0 & 0 & 0 & 0 & 0 & 0 \\
0 & 0 & 0 & 0 & 0 & 0 \\
0 & 0 & E_b & 0 & 0 & 0 \\
0 & 0 & 0 & G_b & 0 & 0 \\
0 & 0 & 0 & 0 & G_b & 0 \\
0 & 0 & 0 & 0 & 0 & 0
\end{bmatrix}
$$

$$
\{\varepsilon^{\mathrm{vp}}\}_{(br)}^{*_n} = \gamma_b < F_{(br)} > \left\{ \frac{\partial F_{(br)}}{\partial \{\sigma\}_{(br)}} \right\} \tag{4.45}
$$

4.4.4The constitutive equation of equivalent material

Substituting the constitutive equation of each component into equation (4.21), and making strain transforming the constitutive equations of the bolted rock material and the bolted joint can be written as

$$
\begin{aligned}
\{\Delta\sigma\}_{R(B)}^n &= A_R[D]_R\{\Delta\varepsilon\}_R^n - A_R[D]_R\{\varepsilon^{\mathrm{vp}}\}_R^n \Delta t_n \\
&\quad + \sum_b A_b[T]_b^{\mathrm{T}}[D]_{(br)}[T]_b\{\Delta\varepsilon\}_{(BR)}^n - \sum_b A_b[T]_b^{\mathrm{T}}[D]_{(br)}\{\varepsilon^{\mathrm{vp}}\}_{(br)}^n \Delta t_n \\
\{\Delta\sigma\}_{j(b)}^n &= A_R[D]_j\{\Delta\varepsilon\}_j^n - A_R[D]_j\{\varepsilon^{\mathrm{vp}}\}_j^n \Delta t_n \\
&\quad + \sum_b A_b[T]_{(bj)}^{\mathrm{T}}[D]_{(bj)}[T]_{(bj)}\{\Delta\varepsilon\}_{(bj)}^n - \sum_b A_b[T]_{(bj)}^{\mathrm{T}}[D]_{(bj)}\{\varepsilon^{\mathrm{vp}}\}_b^n \Delta t_n
\end{aligned}
\tag{4.46}
$$

Taking equation (4.29) into account, the above constitutive equation can be rewritten as

$$
\begin{aligned}
\{\Delta\sigma\}_{R(B)}^n &= [D]_{R(B)}\{\Delta\varepsilon\}_{R(B)}^n - \{\Delta\sigma^{vp}\}_{R(B)}^n \\
\{\Delta\sigma\}_{j(b)}^n &= [D]_{j(b)}\{\Delta\varepsilon\}_{j(b)}^n - \{\Delta\sigma^{vp}\}_{j(b)}^n
\end{aligned}
\tag{4.47}
$$

or

$$
\begin{aligned}
\{\Delta\varepsilon\}_{R(B)}^n &= [D]_{R(B)}^{-1}\{\Delta\sigma\}_{R(B)}^n + [D]_{R(B)}^{-1}\{\Delta\sigma^{vp}\}_{R(B)}^n \\
\{\Delta\varepsilon\}_{j(b)}^n &= [D]_{j(b)}^{-1}\{\Delta\sigma\}_{j(b)}^n + [D]_{j(b)}^{-1}\{\Delta\sigma^{vp}\}_{j(b)}^n
\end{aligned}
\tag{4.48}
$$

where

$$[D]_{R(B)} = A_R[D]_R + \sum_b A_b[T]_b^{\mathrm{T}}[D]_{(br)}[T]_b$$
$$[D]_{j(b)} = A_R[D]_j + \sum_b A_b[T]_{(bj)}^{\mathrm{T}}[D]_{(bj)}[T]_{(bj)} \tag{4.49}$$

and

$$\{\Delta\sigma^{vp}\}_{R(B)}^n = A_R[D]_R\{\varepsilon^{\mathrm{vp}}\}_R^n\Delta t_n + \sum_b A_b[T]_b^{\mathrm{T}}[D]_{(br)}\{\varepsilon^{\mathrm{vp}}\}_{(br)}^n\Delta t_n$$
$$\{\Delta\sigma^{vp}\}_{j(b)}^n = A_R[D]_j\{\varepsilon^{\mathrm{vp}}\}_j^n\Delta t_n + \sum_b A_b[T]_{(bj)}^{\mathrm{T}}[D]_{(bj)}\{\varepsilon^{\mathrm{vp}}\}_b^n\Delta t_n \tag{4.50}$$

Transforming the constitutive equation of the bolted joint in equation (4.54) using the matrix $[T]_j$ defined in equation (4.20), then putting it into equation (4.26) together with the constitutive equation of the bolted rock material, the constitutive equation of the bolted jointed rock masses can be obtained:

$$\{\Delta\varepsilon\}^n = [S]\{\Delta\sigma\}^n + \{\Delta\varepsilon^{vp}\}^n \tag{4.51}$$

where

$$[S] = [D]_{R(B)}^{-1} + \sum_b([T]_j)^{-1}[D]_{j(b)}^{-1}([T]_j^T)^{-1} \tag{4.52}$$

and

$$\{\Delta\varepsilon^{vp}\}^n = [D]_{R(B)}^{-1}\{\Delta\sigma^{\mathrm{vp}}\}_{R(B)}^n + \sum_j[T]_j^{-1}[D]_{j(b)}^{-1}\{\Delta\sigma^{\mathrm{vp}}\}_{j(b)}^n \tag{4.53}$$

The above constitutive model has been implemented in a three-dimensional FEM program CORE3 in which the common 8-node hexahedral iso-parametric element is used, the formulation of the FEM for the elasto-viscoplastic problem is the same as in the literature [8].

4.5Expansion Force

Unit volume withstands the expansion force:

$$\{p\} = \begin{pmatrix} p_x \\ p_y \\ p_z \end{pmatrix}$$

With the virtual displacement $\{r^*\}$, the expansion force $\{p\}$ is

$$\iiint\{r^*\}^T\{p\}dxdydz = (\{\delta^*\}^e)^T\iiint\{N\}^T\{p\}dxdydz$$

It should be equal to the equivalent nodal loads of work, that is

$$(\{\delta^*\}^e)^T\{p\}_q^e = (\{\delta^*\}^e)^T \iiint \{N\}^T\{p\}dxdydz \tag{4.54}$$

Because virtual displacement $\{\delta^*\}$is arbitrary, we can obtain from the formula (4.54), the expansion force $\{p\}$on-containing bolt units of the equivalent nodal loads:

$$\{p\}_q^e = \iiint \{N\}^T\{p\}dxdydz \tag{4.55}$$

Equation (4.55) concerns the volume element of *e*.

4.6Algorithm

The main procedure of the equivalent finite element method for modeling bolt corrosion includes:

(1)Input the information of elements, nodes, material constants, boundary conditions and loading steps of the model.

(2) Determine whether there are bolts in the model, if no, go to (8), otherwise, moved to (3).

(3) Input strike, dip angle and coordinates of bolts.

(4) Find the elements crossed through by bolts in the model and calculate the information and coordinates of bolts crossing through.

(5) Generate the stiffness matrix of bolts.

(6) Generate the load vector; determine whether the loads are concentrated forces or equivalent body forces; determine whether bolt corrosion expansion forces will be applied or not.

(7) Assemble the whole stiffness matrix and the whole load vector, Solve the equilibrium equation by FEM.

(8) Output the final results of stress and strain after all load steps applied.

Fig. 4.5 summarizes the algorithm.

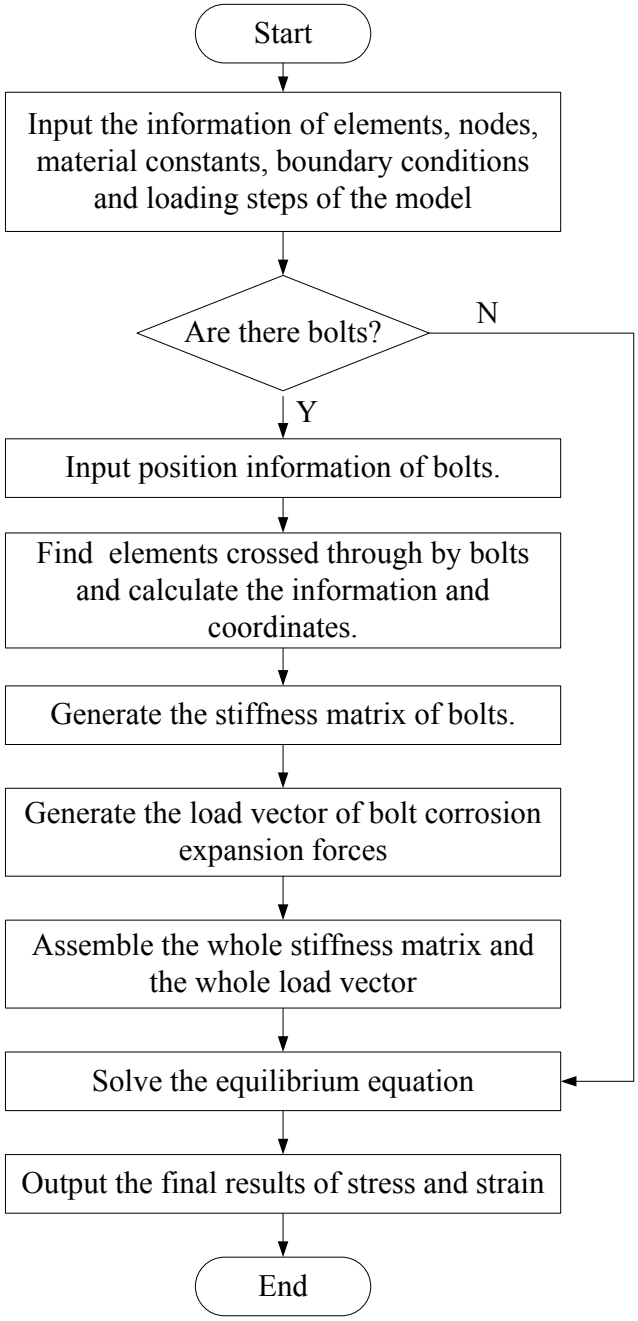

Fig. 4.5 Flowchart of the FEM for modeling bolt corrosion

4.7Case study

4.7.1 Model condition

In this case, a rock mass sample 5m×5m×5m is reinforcement by a 3m length hollow bolt (Fig 4.6). With this sample, a drawing test is numerically simulated by the FEM. A discrete model of the bolt is used. The mesh is refined around the bolt. The FEM model includes 5057 nodes and 4392 elements (Fig 4.7).

Material properties used in this example are summarized in Tables 4.1 and 4.2.

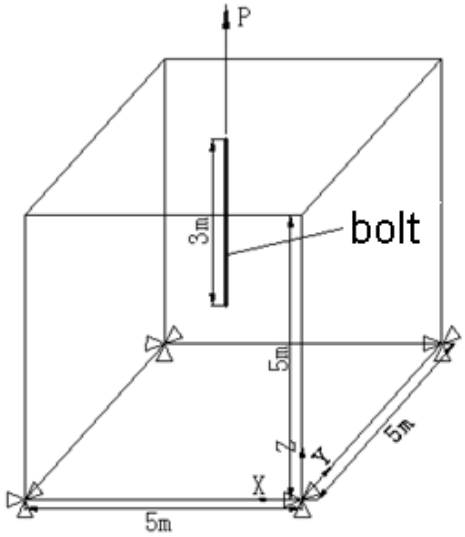

Fig 4.6 Load conditions and boundary conditions of the simulated rock sample

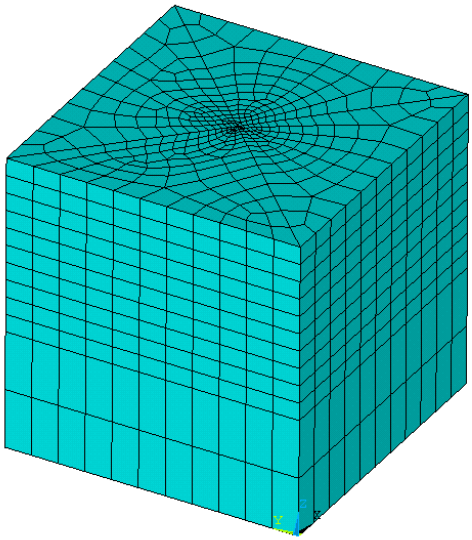

Fig 4.7 The FEM model of the simulated rock sample

Table 4.1 Elastic material constants

material	E[MPa]	ν
steel	200 000	0.30
grout	25 000	0.20

Table 4.2 Material constants of the interfaces

material	Kn [MPa]	Ks [MPa]	C [MPa]	φ [°]	ϕ [°]	σ_T [MPa]
grout-bolt	1000000	50000	1.0	44	44	1.0

4.7.2 Results analysis

Figure 4.8 shows the variation of tensile stress between the bolt and mortar. We observe under the influence of the expansion force, the ensile stress between the bolt and the mortar increases linearly with time. General empirical data show that the ultimate compressive strength of mortar is around 2MP. As can be seen from the numerical results, 60 years after the bolt started to rust, tensile stress in mortar protective layer due to Expansion Force reached 2MP, and cracking damage begins, thus affects the life of the bolt. When pulling force is simultaneously applied, the tensile stress increases in the mortar protective layer. In the joint action of Expansion Force and Pulling force, the value of tensile stress reaches 2MP after 57 years, followed by crack damage.

Figure 4.9 to 4.16 show per decade the displacement vector of concrete in a horizontal section at an elevation of 3.5m. Figures describe the displacement of the concrete under the influence of Expansion Force, Generally speaking, uniform displacements distribute in the mortar and concrete surrounding the bolt, and the displacement increases in accordance with the time. Displacement in the profile along the radial direction decreases exponentially; it s significant a zone with a radius = 1m.

Figure 4.17 shows the distribution of the axial tensile stress along the bolt under the action of Expansion Force. We observe that under the influence of the rust Expansion Force, the axial stress, is not affected by its position in the bolt. It varies with the Expansion Force, and increases as with time.

Figure 4.18 shows the distribution of the axial tensile stress along the bolt under the joint action of Expansion Force and a pullout of 100 kN. The axial stress decreases exponentially along the length of the bolt, which agrees with the Farmer conclusions. Besides, the numerical results show that bolt stress mainly occurs in the range from 0m to 0.6m along the length, and decays quickly along the depth. This shows that the front of the bolt plays a major role in the reinforcement, the effect of reinforcement is unrelated to the length of bolt, and therefore it is irrational to increase the rod length excessively.

Figures 4.19 to 4.26 show displacement vector under the joint action of Expansion Force and a pullout of 100kN. They describe displacement of concrete under the joint action of Expansion Force and bolt pullout force, diverges from the center to the surrounding. The

displacement peaks occur at the bolt end, the displacement decreases when approaching to the free end.

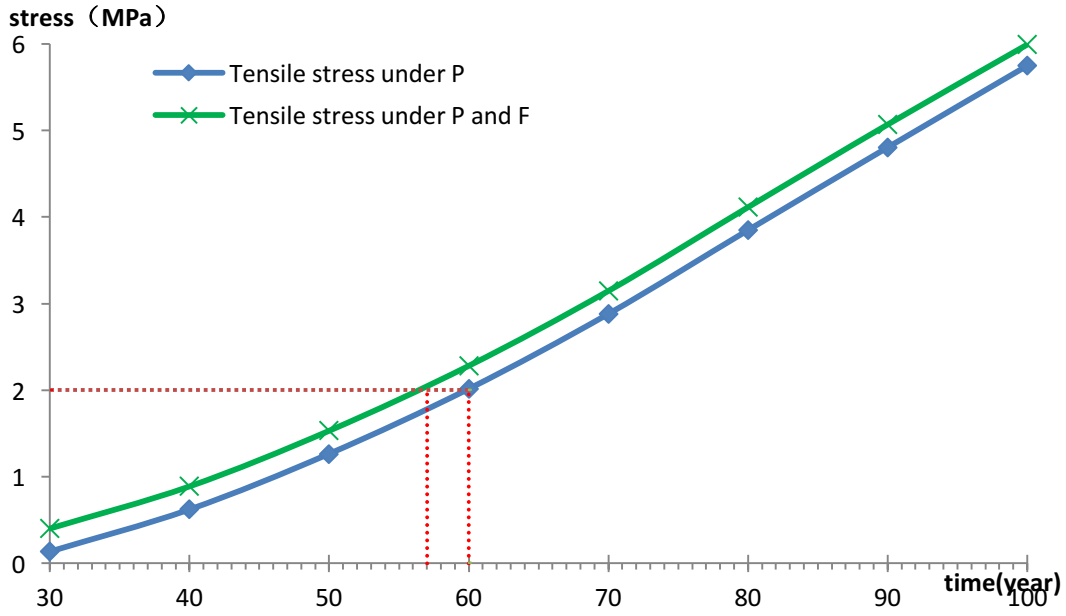

Fig 4.8 The versus time curve of tensile stress between bolt and mortar

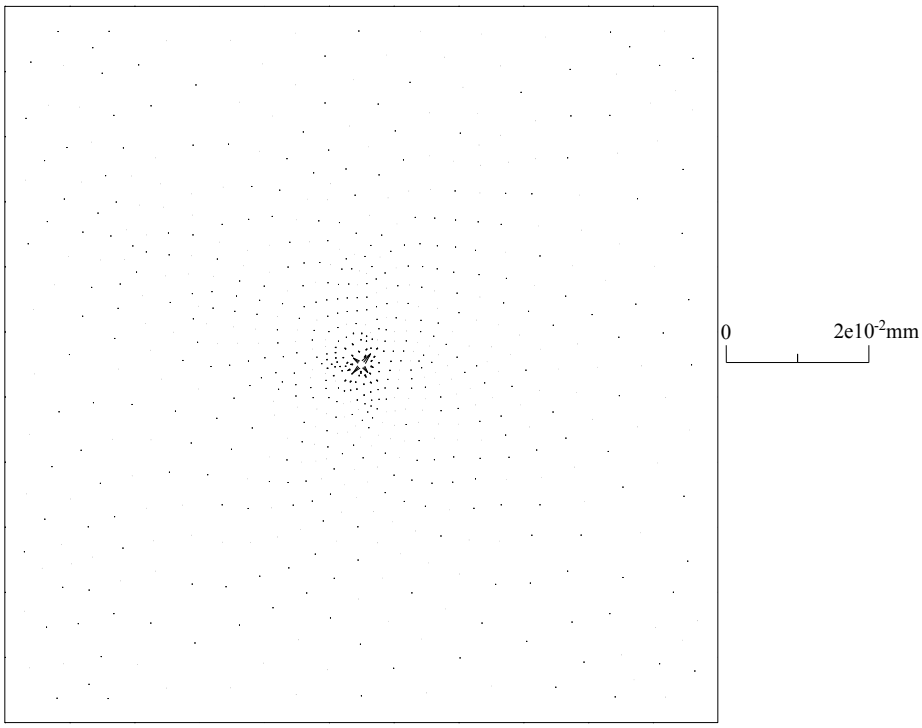

Fig 4.9 Displacement vector at Z = 3.5m horizontal plane when in 30 years

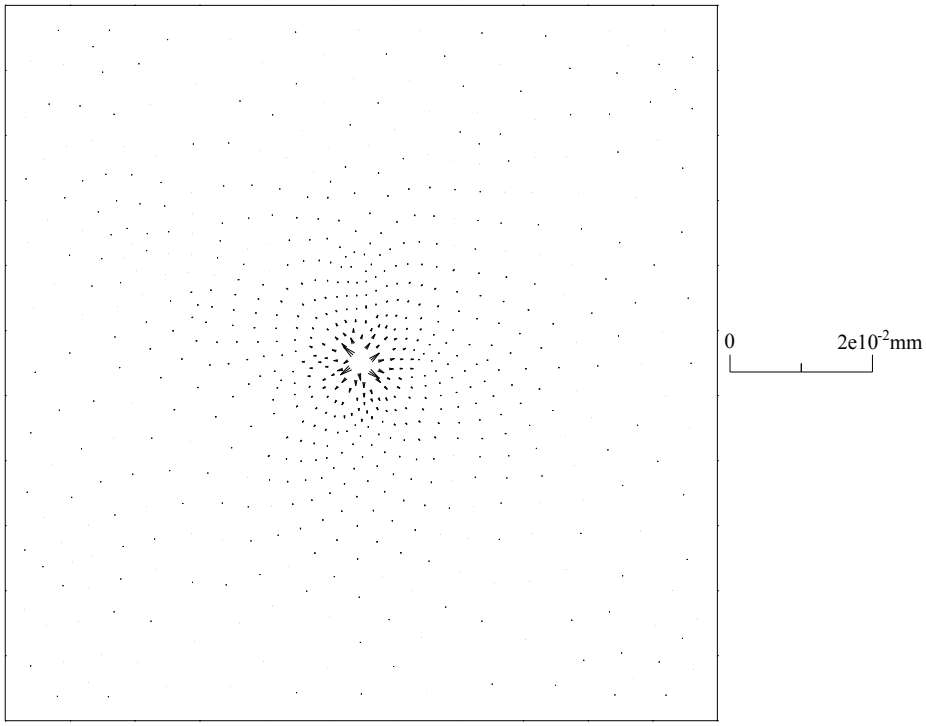

Fig 4.10 Displacement vector at Z = 3.5m horizontal plane when in 40 years

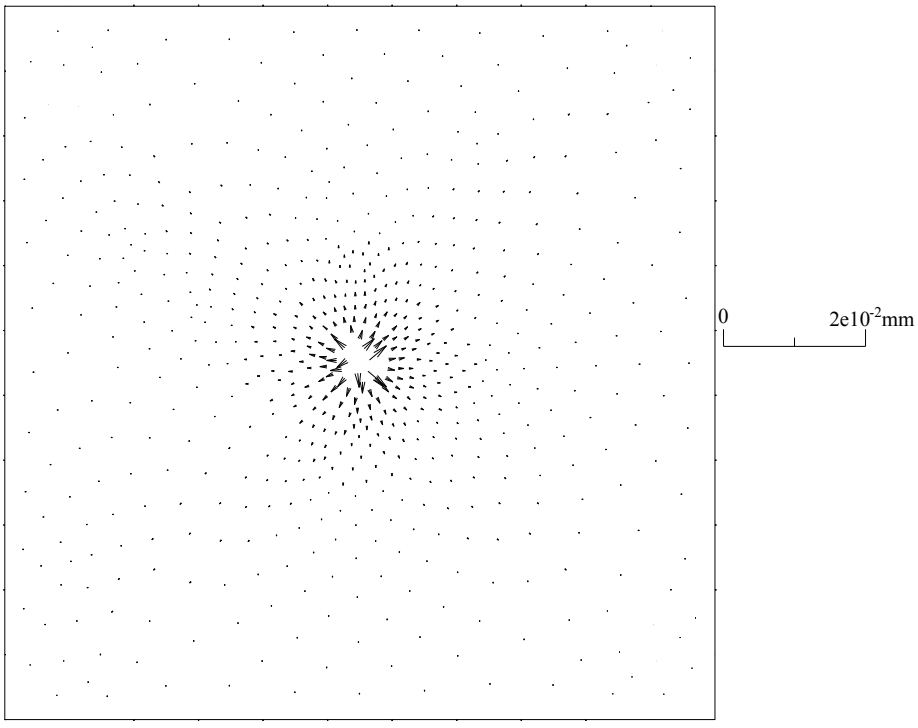

Fig 4.11 Displacement vector at Z = 3.5m horizontal plane when in 50 years

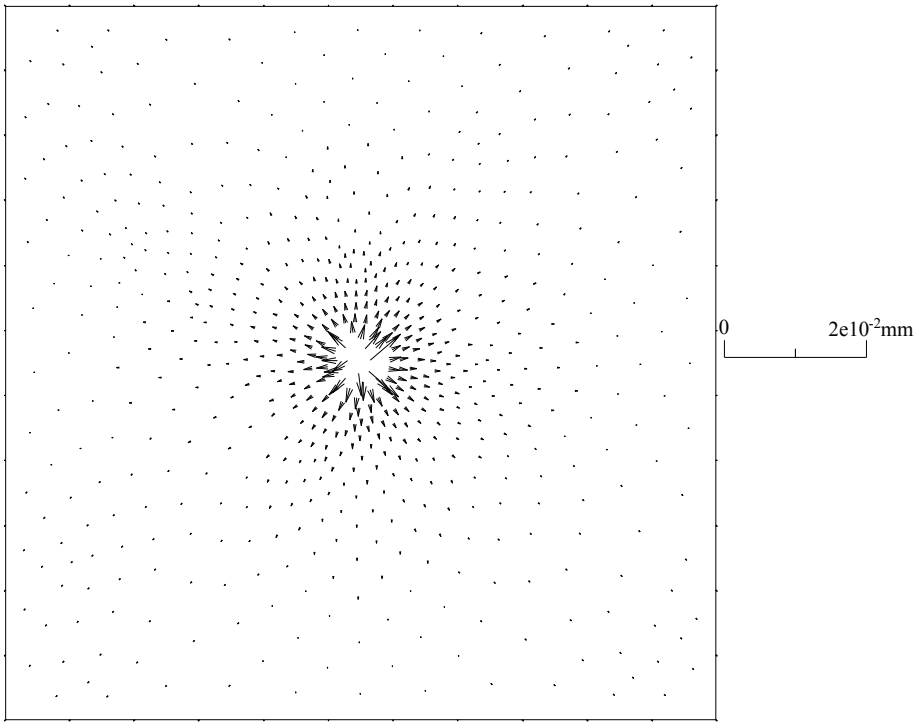

Fig 4.12 Displacement vector at Z = 3.5m horizontal plane when in 60 years

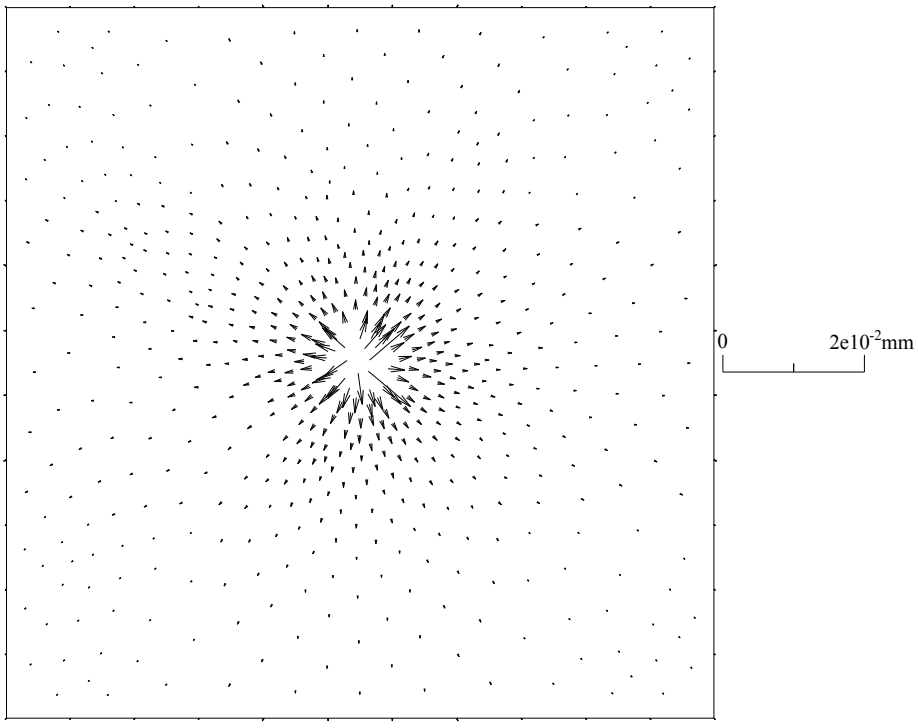

Fig 4.13 Displacement vector at Z = 3.5m horizontal plane when in 70 years

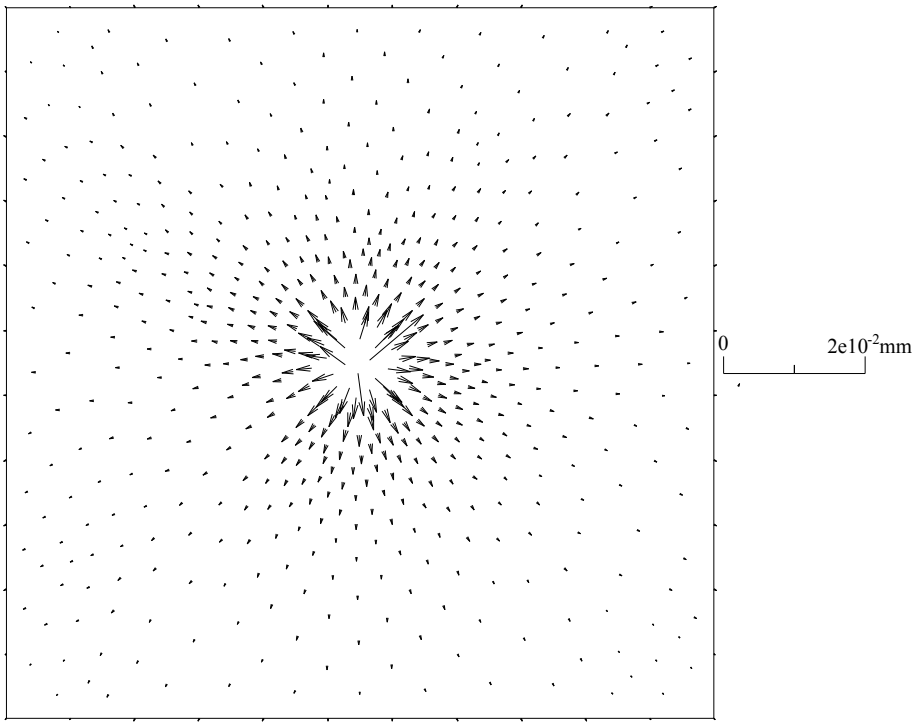

Fig 4.14 Displacement vector at Z = 3.5m horizontal plane when in 80 years

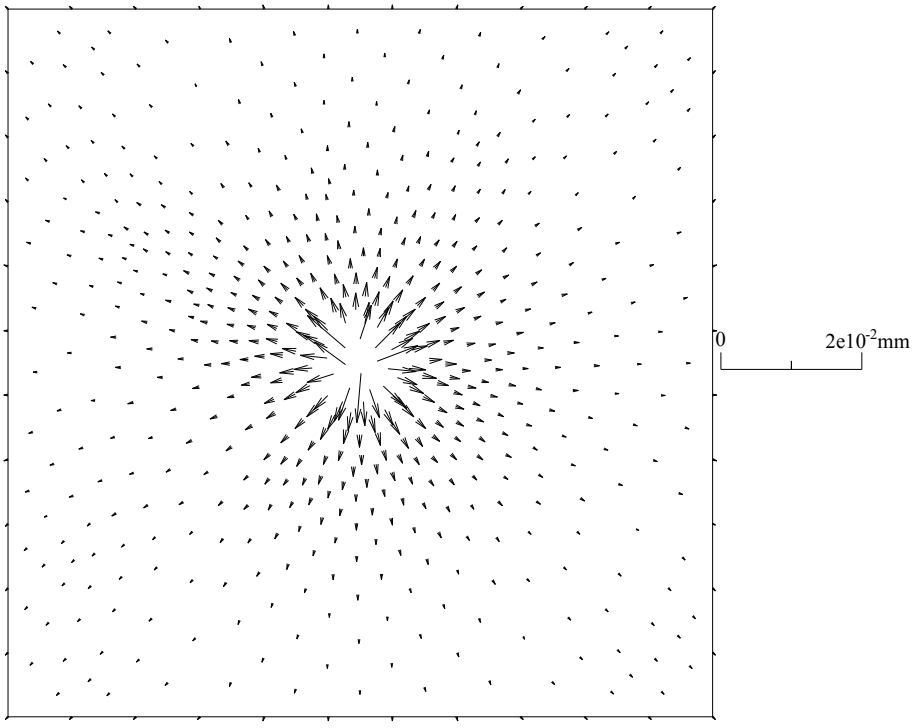

Fig 4.15 Displacement vector at Z = 3.5m horizontal plane when in 90 years

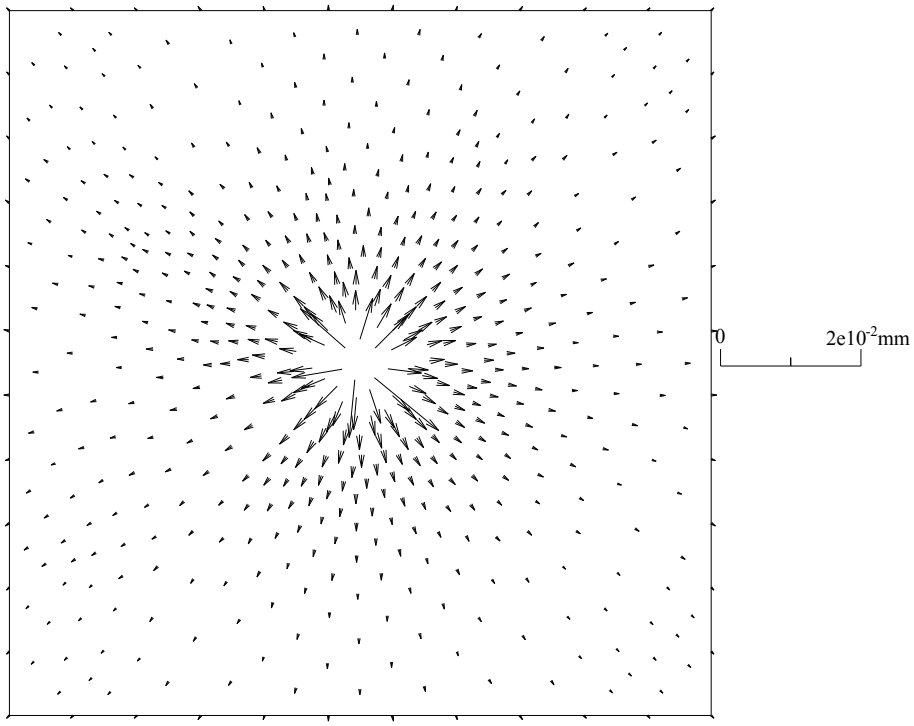

Fig 4.16 Displacement vector at Z = 3.5m horizontal plane when in 100 years

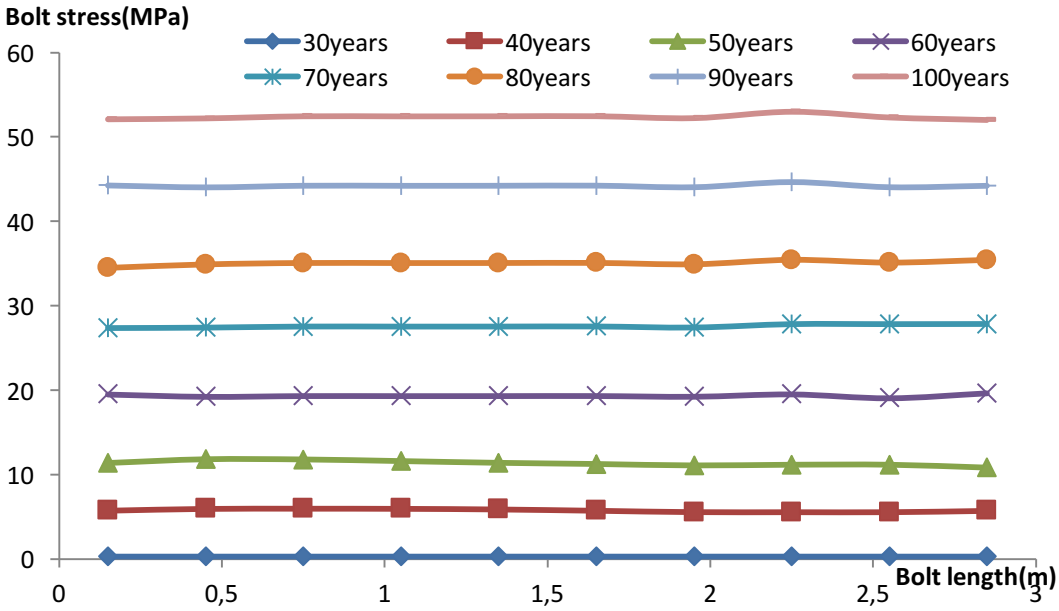

Fig 4.17Bolt axial stress distribution aroused by tension force along the length of the bolt

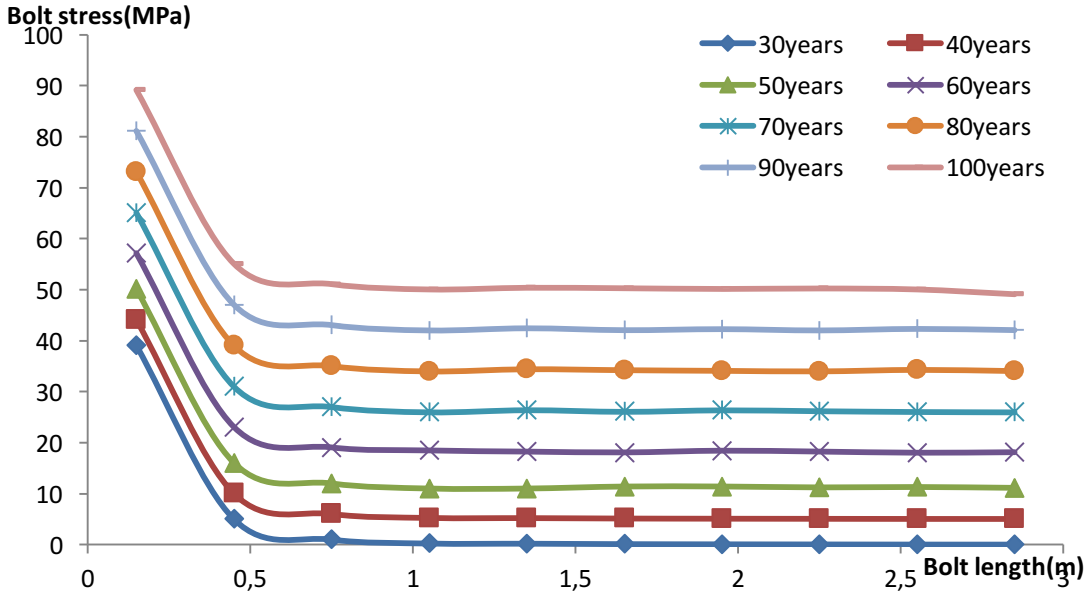

Fig 4.18Bolt axial stress in the tension force and Expansion Force joint action along the length of the bolt distribution

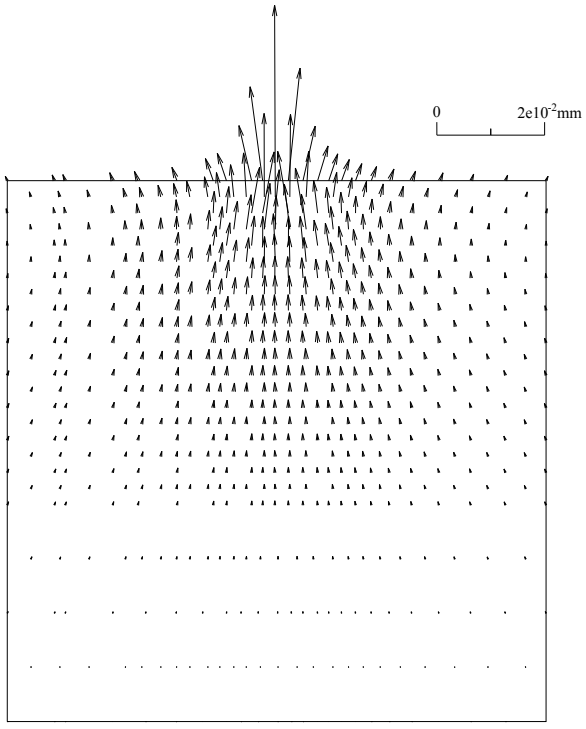

Fig 4.19 Displacement vector at vertical surface when in 30 years

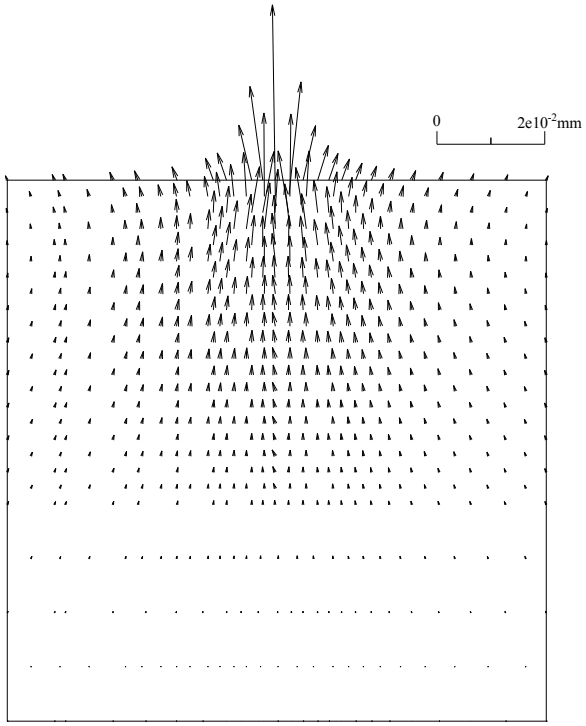

Fig 4.20 Displacement vector at vertical surface when in 40 years

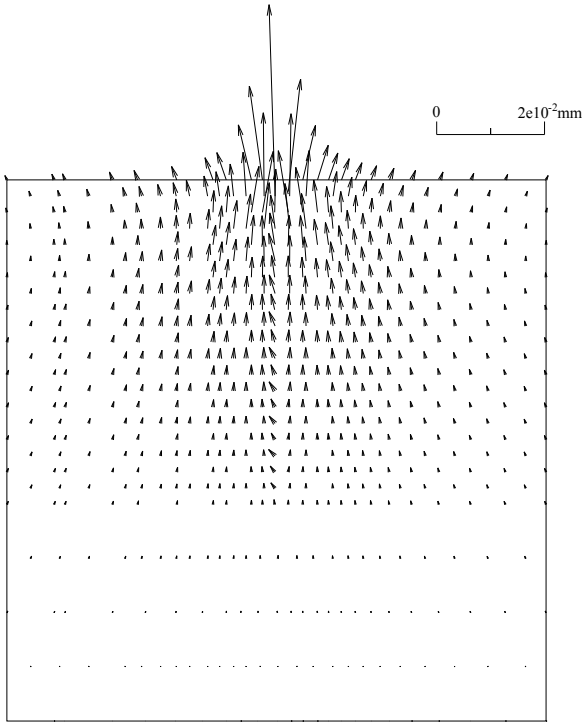

Fig 4.21 Displacement vector at vertical surface when in 50 years

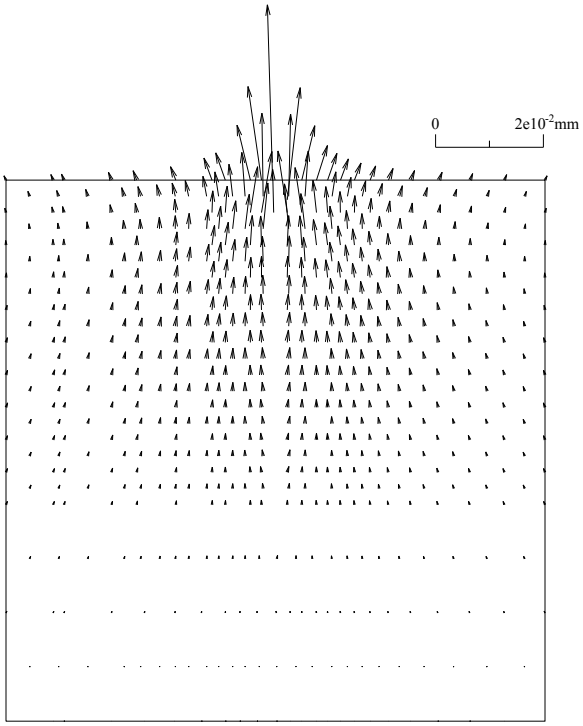

Fig 4.22 Displacement vector at vertical surface when in 60 years

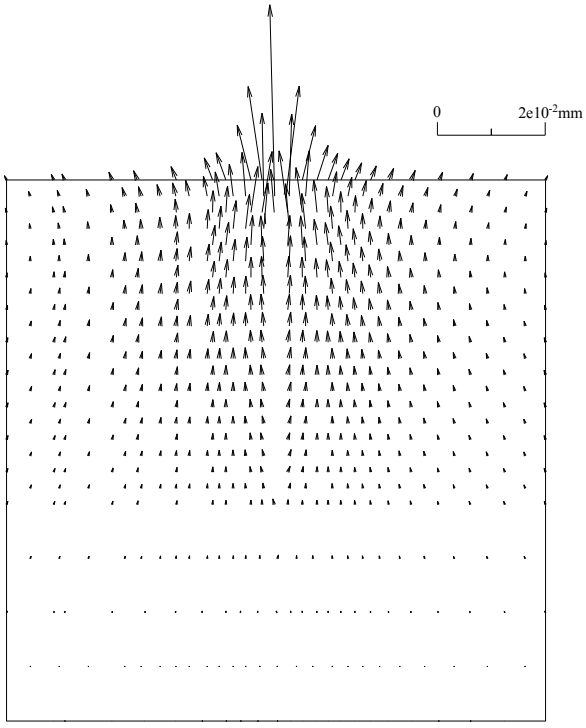

Fig 4.23 Displacement vector at vertical surface when in 70 years

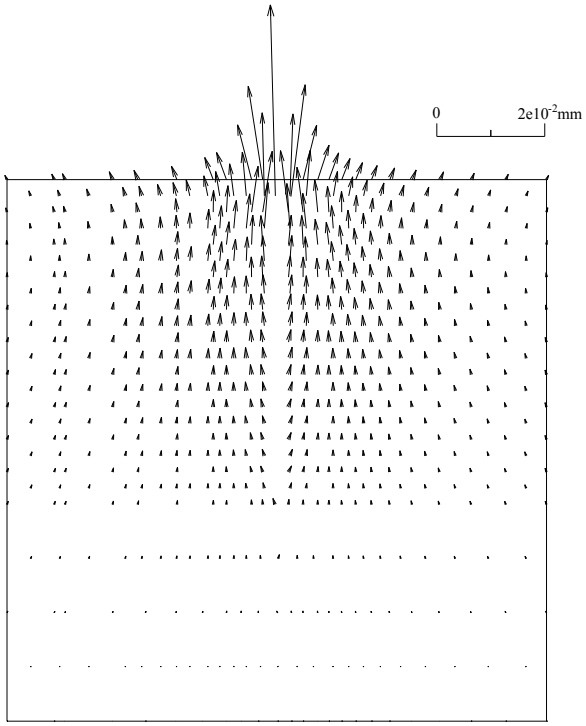

Fig 4.24 Displacement vector at vertical surface when in 80 years

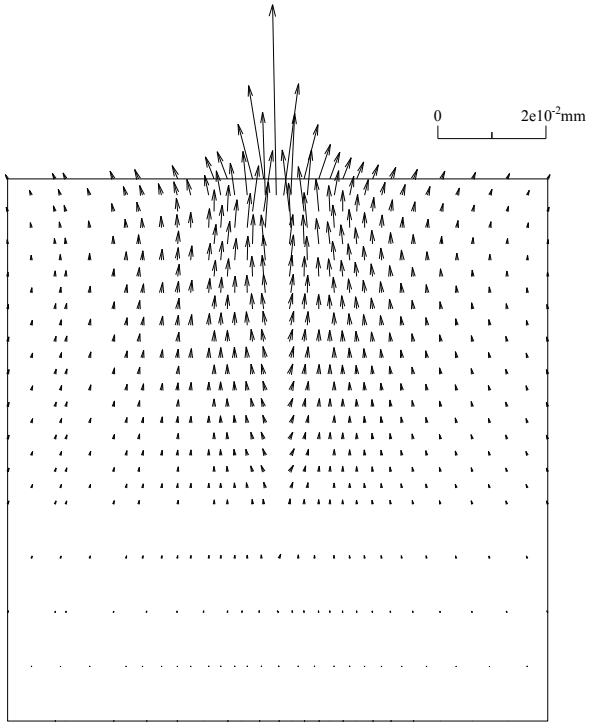

Fig 4.25 Displacement vector at vertical surface when in 90 years

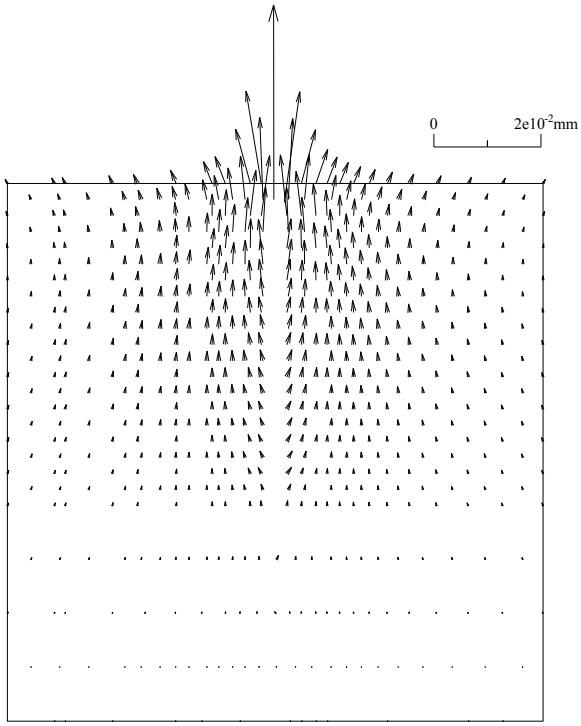

Fig 4.26 Displacement vector at vertical surface when in 100 years

4.8 Conclusions

This chapter presented the application of the convectional finite element method for the analysis of corroded bots. This application required important developments for the integration in an existing finite element software of the blot element, the action of the expansion force and visco-plastic constitutive relations.

The finite element code was then used for the analysis of a rock bloc reinforced by a blot and submitted to corrosion. Numerical results show that:

1. Under the action of the Expansion Force, the axial tensile stress increases linearly along the blot; while the displacement in the concrete increases with time.
2. Under the joint action of Expansion Force and a pullout of 100 kN, the axial stress decreases exponentially along the length of the bolt, while the displacement diverges from the center to the surrounding. The displacement peaks occur at the bolt end, the displacement become decreases when approaching to the free end.

Analysis showed also that the model used for the description of the bolt corrosion requires

further development improves the description of the variation in both time and space of stresses and displacement. This improvement requires experimental results in order to improve our standing and modeling of this complex phenomenon.

References

1. Zienkiewicz O C. The Finite Element Method. 3rd. London: McGraw-Hill, 1977.
2. Owen DRJ, Hinton E. Finite Elements in Plasticity: Theory and Practice. Swansea: Pineridge Press Ltd. 1980.
3. Chen S H and Pande G N. Rheological model and finite element analysis of jointed rock masses reinforced by passive, fully-grouted bolts. International Journal of Rock Mechanics and Mining Sciences & Geomechanics Abstracts. 1994; 31(3):273-277.
4. Spang K and Egger P. Action of fully-grouted bolts in jointed rock and factors of influence. Rock Mechanics and Rock Engineering, 1990, 23(3):201-229.
5. Egger P and Zabuski L. Behaviour of rough bolted joints in direct shear tests. 7th ISRM Conference, Aachen, Germany, 1991, 1285–1288.
6. Egger P and Fernandes H. Nouvelle presse triaxiale - Etude de modèles discontinuos boulonnés. 5th ISRM Conference, Melbourne, Australia, 1983, 171–175.
7. Egger P and Pellet F. Strength and deformation properties of reinforced jointed media under true triaxial conditions. 7th ISRM Conference, Aachen, Germany, 1991, 215-220.
8. E. Hinton, D.R.J Owen. Finite Elements in Plasticity: Theory and Practice, Pineridge Press Ltd., Swansea U.K., 1980.

Chapter 5 Composite element method for bolt corrosion in bolted rock mass

5.1 Composite Element Method

5.1.1 Introduction

In practical engineering, the variety of structures including different materials increases the difficulties for numerical analysis. In concrete structures, different grades of cement can form different media with various layers, joints and steel distribution. In earth and rock-fill dams, we find multiple kinds of earth and stone structures, seepage control measures like drainage holes. In rock slope and foundation project, the structures of rock mass are more complicated for rock properties. Simultaneously, many micro and macro defects, such as cracks, cleavage surfaces, interface, joints, faults, contact zone and shear zone, are formed in the rock mass due to geological processes. Furthermore, the development and utilization of different kinds of bolts, bolt cables, and grouting in rock material add the complexity to rock structure. There are two types of numerical models to study the problems in geotechnical engineering: discrete model and the equivalent model. From the former model, the mechanical behavior of various structures can be tested explicitly, but it is limited in large-scale geotechnical engineering as the requirement of computations with a large number of grids is so high. The latter can be applied to large-scale complex engineering, but it is not ideal in simulating the detailed construction. The two models are used in geotechnical engineering. For example, for small cracks with large area or system bolting bolts, the equivalent method is preferred; for large faults, the discrete method is more adapted.

As the scale and complexity of geotechnical projects increase, researchers will meet the even more complex situation such as multiple faults staggering and cutting, especially the interaction between bolts and joints. In numerical analysis, the mesh generation of complicated structures is quite difficult. Even the mesh can just be generated, but some elements may be poorly shaped which may cause bad impacts on calculation. So, it is very difficult to obtain the mechanical behavior of detailed complex construction; we usually study the mechanical behavior of the whole structure using the equivalent model. Moreover, the construction conditions and the frequent changes in seepage control result in frequent modification of the mesh inducing time loss.

Based on the FEM, the Composite Element Method (CEM) was proposed by Chen et al [1]. It combines the discrete model and the equivalent model. It inherits some advantages of the Numerical Manifold Method (NMM) [2], Block Element Method (BEM) [3] and Finite Element Method (FEM). It treats multi-medium objects as the single media to be discretized. Then, the multi-medium element (e.g. an element with bolt bolts or joints) can be obtained, and these mediums are defined by introducing composite element and sub-element, respectively. The grids can be generated ignoring the substructures (e.g. discontinuities, bolt bolts, drainage holes, etc.). This largely reduces the pre-processor phase.

5.1.2 Development of CEM

The concept of CEM was firstly proposed to simulate the bolts embedded into mortar when analyzing the bolted rock mass [1, 2]. Using the composite element containing the rock, bolt bolts, mortar, contact surface of bolt-mortar and rock-mortar will be modeled separately that one composite element contains three sub-elements: rock, bolts and mortar and contact surface of bolt-mortar and rock-mortar will be treated as the interfaces between connected sub-elements, respectively. The CEM is based on the two basic assumptions: ① three groups of stress are on bolt and mortar section: one group of normal stress along the axis (z direction of local Cartesian coordinates along the bolts axis), and two groups of shear stress vertical to the axis (x and y direction of local Cartesian coordinates); ② three groups of stress are on the interface of bolt-mortar and rock-mortar: one group of normal stress vertical to the contact surface direction (r direction of local cylindrical coordinate along the contact surface), and two groups of shear stress parallel to contact surface direction (ω and z direction of local cylindrical coordinate).

5.2 The basic concepts of CEM

Fig 5.1 shows two types of typical composite elements. In Fig 5.1(a), sub-element No. 2 is enclose by sub-element No. 1, which is viewed as cooling pipes, bolts, drainages holes, and so on, and sub-elements are related with each other through the interface. About this sample, the shape of sub-domain No. 2 is arbitrary, but the shape of sub-domain No. 1 and standard finite element should coincide. So the shape of sub-domain No. 1 must be consistent with the standard FEM for this kind of composite element. In Fig 5.1(b), one composite element is

divided into four sub-elements by discontinuities, such as faults, fractures, cracks and so on, and the cross cuttings state by discontinuities usually appears in this case. The four sub-domains are independent, and the neighbor sub-domains are related with each other through the discontinuities. The shapes of the four sub-elements are arbitrary including concave polygon and polyhedron, but the shape of whole composite must agree with standard FEM.

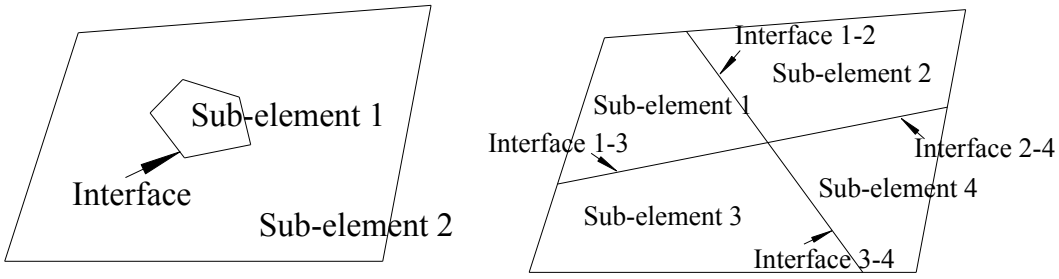

(a) (b)

Fig 5.1 Composite element and its sub-domains

Each of the sub-domains constitutes a sub-element. Generally, if one composite element contains n sub-elements, then the composite element has n set of nodal variables (e.g. displacement for stress-strain analysis, nodal head for seepage analysis, and nodal temperature for heat transfer). The variable values in sub-element interpolated by shape function of conventional FEM and nodal variables of the sub-element. In Fig 5.1, two composite elements contain two and four sub-elements with corresponding two and four sets of nodal variables, respectively. "Stiffness matrix" (structure stiffness matrix for stress-strain analysis, hydraulic conductivity matrix for seepage analysis and heat transfer matrix for thermodynamic analysis) and corresponding right-hand items are established by applying virtual work principle or variational principle to each sub-element. Then the sub-matrix can be assembled into the whole matrix and the governing equations of whole composite element are obtained.

The governing equations of one composite element containing n sub-elements are expressed as

$$\begin{bmatrix} [k]_{1,1} & [k]_{1,2} & \cdots & [k]_{1,n} \\ [k]_{2,1} & [k]_{2,2} & \cdots & [k]_{2,n} \\ \cdots & \cdots & \cdots & \cdots \\ [k]_{n,1} & [k]_{n,2} & \cdots & [k]_{n,n} \end{bmatrix} \begin{Bmatrix} \{\bar{\phi}\}_1 \\ \{\bar{\phi}\}_2 \\ \cdots \\ \{\bar{\phi}\}_n \end{Bmatrix} = \begin{Bmatrix} \{f\}_1 \\ \{f\}_2 \\ \cdots \\ \{f\}_n \end{Bmatrix} \tag{5.1}$$

where the diagonal components of the matrix are composed by the self sub-matrix and the sub-matrix resulted from the related interface:

$$[k]_{i,i} = [k]_{ei,ei} + \sum_{j=1}^{n} A(i,j)[k]_{ei,ej} \tag{5.2}$$

And the non-diagonal components of the matrix only result from the related interface:

$$[k]_{i,j} = -A(i,j)[k]_{ej,ei} \tag{5.3}$$

In which

$$A(i,j) = \begin{cases} 1 & \textit{if } i \textit{ and } j \textit{ are neighbour sub-elements} \\ 0 & \textit{if } i \textit{ and } j \textit{ are not neighbour sub-elements} \end{cases}$$

In Eq.(5.2) and Eq. (5.3), $[k]_{ei,ei}$ is the self sub-matrix of the sub-element i, $[k]_{ei,ej}$ is the relevant part resulted from the interface between the sub-elements i and j, it represents the effect of interface on the sub-elements, and there is a symmetrical relationship, that is $[k]_{ei,ej} = [k]_{ej,ei}$. The "stiffness matrix" of the CEM governing equation is also one symmetrical matrix, because $\{\bar{\phi}\}_i$ and $\{f\}_i$ is the corresponding nodal variables and right side item of sub-elements i, respectively. In all the above expressions, $i, j = 1,2,\cdots,n$, and $i \neq j$.

Take the example of a composite element in Fig. 5.1(b), the formulation of its governing equation is:

$$\begin{bmatrix} [k]_{e1,e1}+[k]_{e1,e2}+[k]_{e1,e3} & -[k]_{e1,e2} & -[k]_{e1,e3} & 0 \\ -[k]_{e2,e1} & [k]_{e2,e2}+[k]_{e2,e1}+[k]_{e2,e4} & 0 & -[k]_{e2,e4} \\ -[k]_{e3,e1} & 0 & [k]_{e3,e3}+[k]_{e3,e1}+[k]_{e3,e4} & -[k]_{e3,e4} \\ 0 & -[k]_{e4,e2} & -[k]_{e4,e3} & [k]_{e4,e4}+[k]_{e4,e2}+[k]_{e4,e3} \end{bmatrix} \cdot \begin{Bmatrix} \{\bar{\phi}\}_1 \\ \{\bar{\phi}\}_2 \\ \{\bar{\phi}\}_3 \\ \{\bar{\phi}\}_4 \end{Bmatrix} = \begin{Bmatrix} \{f\}_1 \\ \{f\}_2 \\ \{f\}_3 \\ \{f\}_4 \end{Bmatrix} \tag{5.4}$$

After the unknown nodal variables $\{\bar{\phi}\}_i \ (i=1,2,\cdots,n)$ have been solved, the values distribution within each sub-element could be calculated by the interpolation formula of Eq. (5.5):

$$\phi_{ei} = [N]\{\bar{\phi}\}_i \quad (i=1,2,\cdots,n) \tag{5.5}$$

in which, [N] is the shape function of FEM that is defined within the whole composite element.

5.3 Principle of the composite element method for rock mass reinforced by grouted rock bolt

5.3.1 Composite element model of grouted rock bolt.

Fig 5.2 shows a finite element, which contains one bolt segment. This element can be defined as a composite element (an embedded one) with five sub-elements: the rock material, the grout material, the bolt material, the rock-grout interface, and the bolt-grout interface, respectively. By adding two sets of virtual nodes in the element, along with the actual nodes, three sets of degrees of freedom will be used to describe the displacement of the rock material, the grout material, the bolt material, respectively. There are no independent degree of freedom for the rock-grout interface and the bolt-grout interface, while their displacement will be obtained by interpolation from the displacement difference between rock-grout material and bolt-grout material, respectively.

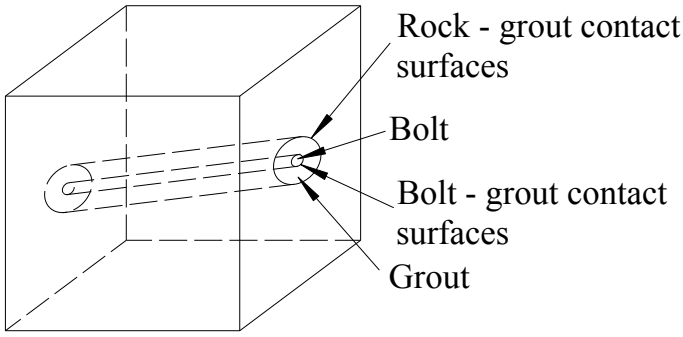

Fig 5.2 Composite element containing five sub-elements

A global coordinate system is defined to formulate the overall governing equations, with the X-axis pointing northward, the Y-axis pointing westward, and the Z-axis being vertical. For each bolt a Cartesian local system is also needed to simplify the computation which is defined as follows (Fig 5.3): the z-axis is along the bolt and upright, the y-axis is perpendicular to the bolt and points in the direction of dip and the x-axis is formed by the right hand rule. On the basis of the local Cartesian coordinate system the local cylindrical coordinate system is defined (Fig 5.4). Let the subscripts r, g, b, rg and bg denote the quantities of the rock material, the grout material, the bolt, the interface between rock and grout, the interface between bolt and grout, respectively; the superscripts c and p are used to denote the quantities in the Cartesian and cylindrical local coordinate system.

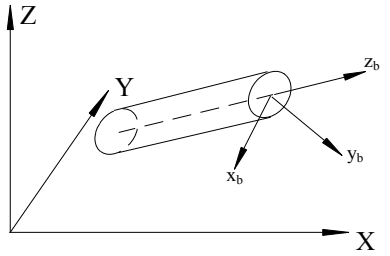

Fig 5.3 Local coordinate system of the bolt (Cartesian)

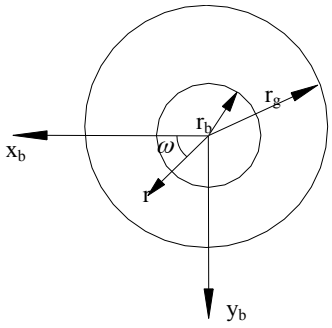

Fig 5.4 Local coordinate system of the bolt (cylindrical)

5.3.2 Assumptions

The basic assumptions are as follows:

(1) At the cross section of the bolt or the grout, there are six stress increments: σ_x、σ_y、σ_z、τ_{xz}、τ_{yz}、τ_{xy}, which are expressed in local coordinate system of the bolt.

(2) At the rock-grout interface and the bolt-grout interface, there are three stress increments: one normal stress perpendicular to the interfaces (r direction) and two shear stresses along the interfaces (ω and z directions).

5.3.3 Transformation between the different coordinate systems

The displacement, strain and stress transformation between the global and the local coordinate systems are defined as follows:

$$\begin{cases} \left\{\Delta u\right\}_b^c = \left[L\right]_c \left\{\Delta u\right\}_b \\ \left\{\Delta \varepsilon\right\}_b^c = \left[T\right]_c \left\{\Delta \varepsilon\right\}_b \\ \left\{\Delta \sigma\right\}_b = \left[T\right]_c^T \left\{\Delta \sigma\right\}_b^c \end{cases} \tag{5.6}$$

The transforming matrix in Eq. (5.6) is:

$$\begin{cases} \left[T\right]_c = \begin{bmatrix} l_1 n_3 + n_1 l_3 & m_1 n_3 + n_1 m_3 & 2 n_1 n_3 \\ l_2 n_3 + l_3 n_2 & m_2 n_3 + m_3 n_2 & 2 n_2 n_3 \\ l_3 n_3 & m_3 n_3 & n_3^2 \end{bmatrix} \end{cases} \tag{5.7}$$

where

$$\begin{cases} \left[L\right]_c = \begin{bmatrix} l_1 & m_1 & n_1 \\ l_2 & m_2 & n_2 \\ l_3 & m_3 & n_3 \end{bmatrix} \end{cases} \tag{5.8}$$

in which φ, θ are the dip direction and dip angle of the bolt segment respectively.

The displacement, strain and stress transformation between the local Cartesian and local cylindrical coordinate systems is defined as follows:

$$\begin{cases} \left\{\Delta u\right\}_b^p = \left[L\right]_p \left\{\Delta u\right\}_b^c \\ \left\{\Delta \varepsilon\right\}_b^p = \left[T\right]_p \left\{\Delta \varepsilon\right\}_b^c \\ \left\{\Delta \sigma\right\}_b^p = \left[T\right]_p^T \left\{\Delta \sigma\right\}_b^p \end{cases} \tag{5.9}$$

The transforming matrix in Eq. (5.9) is:

$$\begin{cases} [T]_p = \begin{bmatrix} l_1 n_3 + n_1 l_3 & m_1 n_3 + n_1 m_3 & 2 n_1 n_3 \\ l_2 n_3 + l_3 n_2 & m_2 n_3 + m_3 n_2 & 2 n_2 n_3 \\ l_3 n_3 & m_3 n_3 & n_3^2 \end{bmatrix} \end{cases} \tag{5.10}$$

where

$$\begin{cases} [L]_p = \begin{bmatrix} l_1 & m_1 & n_1 \\ l_2 & m_2 & n_2 \\ l_3 & m_3 & n_3 \end{bmatrix} \end{cases} \tag{5.11}$$

For the grout material around the bolt the transformations are defined similarly:

$$\begin{cases} \{\Delta u\}_g^c = [L]_c \{\Delta u\}_g \\ \{\Delta \varepsilon\}_g^c = [T]_c \{\Delta \varepsilon\}_g \\ \{\Delta \sigma\}_g = [T]_c^T \{\Delta \sigma\}_g^c \end{cases} \tag{5.12}$$

$$\begin{cases} \{\Delta u\}_g^p = [L]_p \{\Delta u\}_g^c \\ \{\Delta \varepsilon\}_g^p = [T]_p \{\Delta \varepsilon\}_g^c \\ \{\Delta \sigma\}_g^p = [T]_p^T \{\Delta \sigma\}_g^p \end{cases} \tag{5.13}$$

After the stress-strain relation is defined, the governing equation of rock mass reinforced by grouted rock bolt can be obtained and prepared for solving.

5.3.4 The constitutive equations

According to the elasto-viscoplastic potential theory, the constitutive equation for sub-elements could be written as follows:

$$\begin{cases} \{\Delta \sigma\} = [D](\{\Delta \varepsilon\} - \left\{ \dot{\varepsilon}^{vp} \right\} \Delta t) \\ or \\ \{\Delta \varepsilon\} = [S]\{\Delta \sigma\} + \left\{ \dot{\varepsilon}^{vp} \right\} \Delta t \end{cases} \tag{5.14}$$

Δt is the time stepping length, [D] and [S] are the elastic matrix and compliance matrix respectively. The viscoplastic flow rate is:

$$\left\{ \dot{\varepsilon}^{vp} \right\} = \gamma < F > \left\{ \frac{\partial Q}{\partial \{\sigma\}} \right\} \tag{5.15}$$

The constitutive equation for the interface takes the following form:

$$\{\Delta \sigma\}_j = [D](\{\Delta u\}_j - \left\{ \dot{u}^{vp} \right\}_j \Delta t) \tag{5.16}$$

Δt is the time stepping length, [D] is the elastic matrix of interfaces. The viscoplastic flow rate of the interfaces is:

$$\left\{\dot{u}^{vp}\right\}_j = \gamma_j < F > \left\{\frac{\partial Q}{\partial \{\sigma\}}\right\} \tag{5.17}$$

γis the fluidity parameter, F and Q are the yield and potential functions respectively, and the function <F> is defined as:

$$< F >= \begin{cases} F & if\ F \geq 0 \\ 0 & if\ F < 0 \end{cases} \tag{5.18}$$

In the practical engineering application, the fluidity parameter can be obtained by laboratory tests, field tests or feedback analysis. If the fluidity parameter could be confirmed then the histories as well as the steady-state results of the deformation and failure of a structure could be calculated. However, in some cases it is not easy to get the appropriate fluidity parameter or it is thought that only the elasto-plastic solution is of interest. Under such circumstances we can simply assume that the fluidity parameter $\gamma = 1$, in this way the histories are not applicable, but the steady-state results of deformation and failure are identical to the corresponding conventional static elasto-plastic solution [18].

5.3.4.1 The constitutive equation of intact rock

The rock material is taken as an isotropic material whose elastic matrix is:

$$[D]_R = \begin{bmatrix} \lambda+2G & \lambda & \lambda & 0 & 0 & 0 \\ & \lambda+2G & \lambda & 0 & 0 & 0 \\ & & \lambda+2G & 0 & 0 & 0 \\ & & & G & 0 & 0 \\ & SYM & & & G & 0 \\ & & & & & G \end{bmatrix} \tag{5.19}$$

For the yield of the intact rock, both the Mohr-Coulomb and the Drucker-Prager criteria are widely used. In the present study the latter is implemented in a FEM program:

$$\begin{cases} F_R = aI_1 + \sqrt{J_2} - k = 0 \\ a = \sin\varphi_R / \sqrt{3(3+\sin^2\varphi_R)} \\ k = \sqrt{3}c_R\cos\varphi_R / \sqrt{3+\sin^2\varphi_R} \end{cases} \tag{5.20}$$

The associated flow rule is adopted:

$$Q_R = F_R \tag{5.21}$$

In Eq. (5.20) c_R and φ_R are the cohesion and friction angle of the intact rock respectively.

5.3.4.2 The constitutive equation of the bolt

The stranded steel within a bolt segment is also taken as an isotropic material, and its elastic matrix is:

$$[D]_b = \begin{bmatrix} \lambda+2G & \lambda & \lambda & 0 & 0 & 0 \\ & \lambda+2G & \lambda & 0 & 0 & 0 \\ & & \lambda+2G & 0 & 0 & 0 \\ & & & G & 0 & 0 \\ & SYM & & & G & 0 \\ & & & & & G \end{bmatrix} \tag{5.22}$$

The Von Mises criterion is used:

$$\begin{cases} F_b = \sqrt{3J_2} - \sigma \\ \sigma = \sigma_y + (\sigma_u - \sigma_y)\gamma^{-vp} / \gamma_u^{-vp} \end{cases} \tag{5.23}$$

in which, $J_2, \sigma_y, \sigma_u, \gamma^{-vp}$ and γ_u^{-vp} are the yield strength, ultimate strength, ultimate plastic general shear strain, and present plastic general shear strain respectively.

5.3.4.3 The constitutive equation of grout

The grout material is taken as an isotropic material whose elastic matrix is:

$$[D]_g = \begin{bmatrix} \lambda+2G & \lambda & \lambda & 0 & 0 & 0 \\ & \lambda+2G & \lambda & 0 & 0 & 0 \\ & & \lambda+2G & 0 & 0 & 0 \\ & & & G & 0 & 0 \\ & SYM & & & G & 0 \\ & & & & & G \end{bmatrix} \tag{5.24}$$

The Drucker-Prager criterion is used for the yield of grout material:

$$\begin{aligned} F_g &= a\sigma_g + \sqrt{\frac{1}{3}}\sqrt{\sigma_g^2 + 3(\tau_{gzx}^2 + \tau_{gzy}^2)} - k = 0 \\ a &= \sin\varphi_g / \sqrt{3(3+\sin^2\varphi_g)} \\ k &= \sqrt{3}c_g\cos\varphi_g / \sqrt{3+\sin^2\varphi_g} \end{aligned} \tag{5.25}$$

in which c_g and φ_g are cohesion and friction angle of grout material.

The associated flow rule is adopted:

$$Q_g = F_g \tag{5.26}$$

5.3.4.4 The constitutive equation of interfaces

The same relation is used for both the rock-grout interface and the bolt-grout interface [14]. The constitutive equation of the interface is expressed in its local cylindrical coordinate system, and the elastic matrix is:

$$\left[D\right]_j = \begin{bmatrix} k_s & 0 & 0 \\ 0 & k_n & 0 \\ 0 & 0 & k_s \end{bmatrix} \tag{5.27}$$

in which k_n is the normal stiffness and k_s is the tangential stiffness.

A non-associated flow rule of Mohr-Coulomb model is used:

$$\begin{cases} F = \sqrt{\tau_{r\omega}^2 + \tau_{rz}^2} + \sigma_r tg\phi - c \quad if\ \sigma_r \le \sigma_T \\ Q_j = \sqrt{\tau_{r\omega}^2 + \tau_{rz}^2} + \sigma_r tg\varphi + const. \end{cases} \tag{5.28}$$

$$\begin{cases} F = \sigma - \sigma_T \quad if\ \sigma \ge \sigma_T \\ Q = \sqrt{\tau_{r\omega}^2 + \tau_{rz}^2 + \sigma_r^2} + const. \end{cases} \tag{5.29}$$

in which, c, φ, ϕ and σ_T are the cohesion, friction angle, dilatancy angle and tensile strength.

It should be pointed out that the strain increment of the interfaces is denoted as:

$$\left\{\Delta u\right\} = \begin{Bmatrix} \Delta u_\omega \\ \Delta u_r \\ \Delta u_z \end{Bmatrix} \tag{5.30}$$

The corresponding stress increment at the interfaces is:

$$\left\{\Delta \sigma\right\} = \begin{Bmatrix} \Delta \tau_{r\omega} \\ \Delta \sigma \\ \Delta \tau_{rz} \end{Bmatrix} \tag{5.31}$$

5.4 Expansion Force load realization

Unit volume withstand the expansion force is

$$\{p\} = \begin{pmatrix} p_x \\ p_y \\ p_z \end{pmatrix}$$

Under the virtual displacement $\{r^*\}$, the work of the expansion force $\{p\}$ is:

$$\iiint \{r^*\}^T \{p\} dxdydz = (\{\delta^*\}^e)^T \iiint \{N\}^T \{p\} dxdydz$$

It should be equal to the equivalent nodal loads of work:

$$(\{\delta^*\}^e)^T \{p\}_q^e = (\{\delta^*\}^e)^T \iiint \{N\}^T \{p\} dxdydz \tag{5.32}$$

Since the virtual displacement $\{\delta^*\}$ is arbitrary, we obtain the equivalent nodal force:

$$\{p\}_q^e = \iiint \{N\}^T \{p\} dxdydz \tag{5.33}$$

5.5 Implementation of the CEM model for bolt corrosion in bolted rock mass

5.5.1 Pre-process of CEM.

The finite element mesh is first generated without considering discontinuous structures (such as bolt, drainages holes and cooling pipes). Then the information concerning the discontinuous structures is introduced to obtain the mesh with composite element. Topological computation of CEM pre-process procedure generally contains five parts: searching composite elements, recognizing sub-domains, obtaining the topology information of sub-domains and determining material partitions and bolting materials. Its overall objective is to prepare the data information for CEM computation. The main procedure is plotted in Fig.5.5.

Some algorithms in the pre-process concern the research of composite elements, the detection of the relations between points and polygons, recognitions of polyhedrons and determination of material partitions. After this phase, the topological information will be collected and sorted, in particular: elements crossed by bolts or fractures, coordinates of the entry and the exit point in each of these elements, length of bolts or shape of fractures and the information of sub-domains.

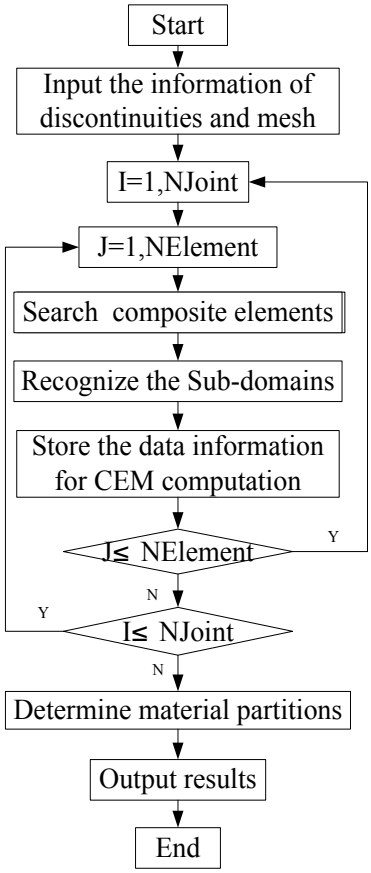

Fig 5.5 Flowchart of the pre-process for CEM

5.5.2 Implementation of the program

The CEM program includes two parts: elements with a single material are treated as the conventional finite element, while elements with multiple materials are treated using the above algorithm. Using the information obtained by pre-processor, a program for modeling the corrosion of bolt in bolted rock mass with CEM can be implemented. Specific attention should be paid to the following:

(1) Numerical integration

When forming the stiffness matrix, different numerical integrations are needed for the sub-elements (rock, bolt, rust, rock-bolt, rust-bolt interface). For the rock mass sub-elements, the Gauss method with equivalent parameter commutation changing expressions of the volume element is used. For the bolt sub-elements and the rock-bolt interface sub-elements, the equivalent parameter commutation is not be used due to their special shapes. The conventional Gauss method is used with the expressions of the volume element and area element under cylindrical local-coordinates.

(2) Assembly of the whole matrix and the whole load vector.

When assembling the whole matrix and the whole load vector of the system, sorting the large amount of degrees of freedom in composite elements requires attention. A unified form of sorting method will benefit the program implementation and the assembly of the whole matrix and the whole load vector. In this work, the sub-elements are sorted and assembled by their types, which imitates the ideas from hierarchical FEM. The degrees of freedom of rock mass sub-elements (i.e., the conventional finite elements) are placed at the beginning, and the corresponding stiffness matrix and load vector will be the first part. Next, degrees of freedom of the bolt sub-elements are placed after rock mass sub-elements, as well as the corresponding stiffness matrix and load vector. The assembling strategy shows its advantage when the bolted designing schemes have changed, that is a few alteration will be needed to the whole matrix and the whole load vector for different bolted designing schemes. At the same time, an organized category will greatly increase the efficiency of program implementation because the program can be checked by blocking.

5.6 Algorithm

The main procedure of the use of the composite element method for modeling pre-stressed bolt cable includes:

(1) Input the information of elements, nodes, material constants, boundary conditions and loading steps of the model.

(2) Input bolt cable parameters, including the amount, material constants, strike, dip angle, coordinates of inner and outer bolt head. Determine which elements are the conventional finite elements, the elements crossed through by inner bolt section or the elements where outer bolt head located in.

(3) Generate stiffness matrix of inner bolt section by CEM and the implicit cable stiffness matrix of outer bolt head by FEM, as well as the load vector of bolt cable.

(4) Assemble the two matrixes, composite element stiffness matrix of pre-stressed bolt cable and the conventional finite element stiffness matrix into the whole matrix. Then assemble the whole load vector in the same way.

(5) Solve the equilibrium equation and calculate elastic strain and elastic strain. Check

whether any of the elements (composite elements or finite elements) has yielded, and then determine to move on to an iterative process for plastic analysis or not.

(6) If no element has yielded or the plastic solution has converged, the calculation is completed. Obtain the final results of stress, strain and displacement.

A more detailed process can be referred to the algorithm flowchart drawn from the above technology roadmap (Fig. 5.6):

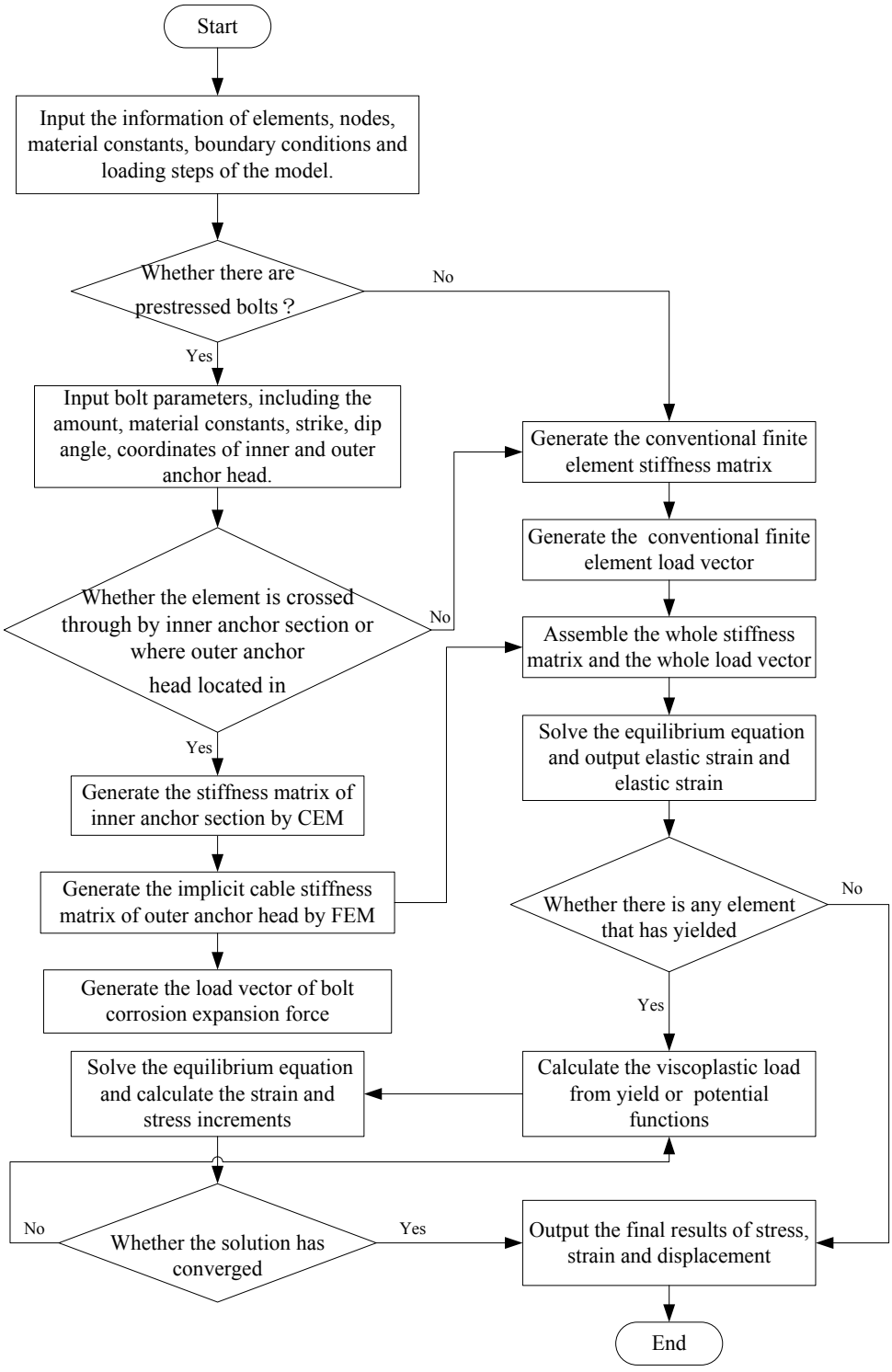

Fig 5.6 Flowchart of the algorithm

5.7 Case study

5.7.1 Model condition

The case concerns a rock mass (5m×5m×5m)reinforced by a 3m hollow bolt (Fig 5.7). With this sample, a pull test is numerically simulated using the CEM and FEM. With the CEM, the sample is meshed with regular elements, and discrete simulation of bolted rock mass is conducted based on the fundamentals of CEM. In the CEM model, elements containing bolt are defined as composite elements, while other rock elements are conventional finite elements. The CEM model includes 416 nodes and 348elements (Fig 5.8).

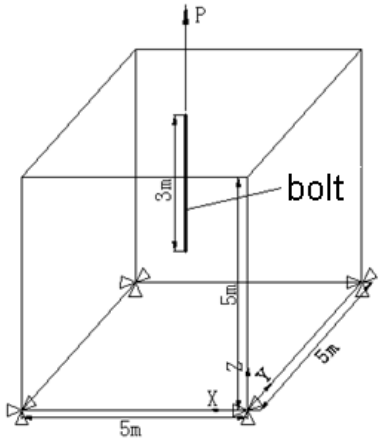

Fig 5.7 Load conditions and boundary conditions of the simulated rock sample

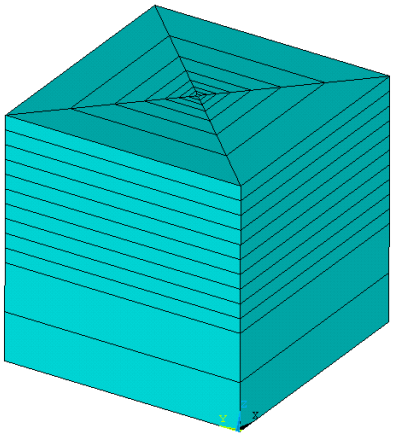

Fig 5.8 The CEM model of the simulated rock sample

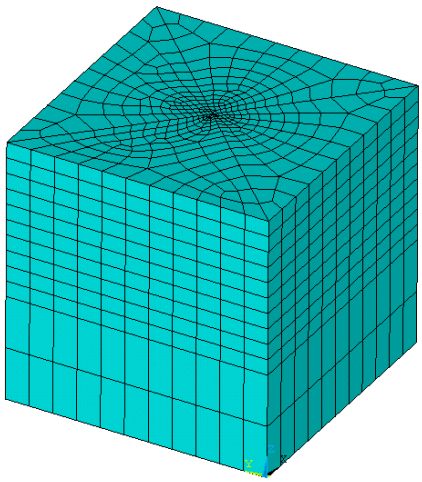

Fig 5.9 The FEM model of the simulated rock sample

Material constants used in the simulation are listed in Table 5.1 and Table 5.2.

Table 5.1 Elastic material constants

material	E[MPa]	ν
steel	200 000	0.30
grout	25 000	0.20

Table 5.2 Material constants of the interfaces

material	Kn [MPa]	Ks [MPa]	C [MPa]	φ [°]	ϕ [°]	σ_T [MPa]
grout-bolt	1000000	50000	1.0	44	44	1.0

5.7.2 Results analysis

Figure 5.10 shows the variation of the tensile stress between the bolt and the mortar as tensile stress between the bolt and the predicted by the composite element method. It shows that under the influence of the expansion force, the mortar increases linearly with time. Empirical data show that the ultimate compressive strength of mortar is around 2MP. Results show that the tensile stress in mortar reaches 2MPa after 49 years. When the pulling force is simultaneously applied the tensile stress increases in mortar protective layer. In the joint action of expansion force and pulling force, the tensile stress reaches 2MP after 46 years, followed by crack damage.

Figure 5.11 to Figure 5.18 show the displacement vector variation in concrete in the horizontal section (z = 3.5m). We observe uniform displacement in the mortar and concrete

surrounding the bolt; the displacement increases with time. Displacement along the radial direction decreases exponentially.

Figure 5.19 shows the distribution of the axial tensile stress along the length of bolt under the action of Expansion Force as predicted by the composite element method. Under the influence of the trust Expansion Force, the axial stress is only dependent on the expansion force, and increases with time.

Figure 5.20 shows the distribution of the axial tensile stress along the bolt under the joint action of expansion force and a pullout force (100 kN) as predicted by the composite element method. We observe that the axial stress decreases exponentially along the bolt. This result well agrees with the conclusions Farmer (1975).

Figures 5.21 to 5.28 show the displacement under the joint action of the expansion force and the pullout force as predicted by the composite element method. We observe the displacement of the concrete diverges from the center to the surrounding. The displacement peaks occur at the bolt end, and decreases when approaching to the free end.

A comparison of the results of the finite element method and the composite element method showed excellent agreement between these methods.

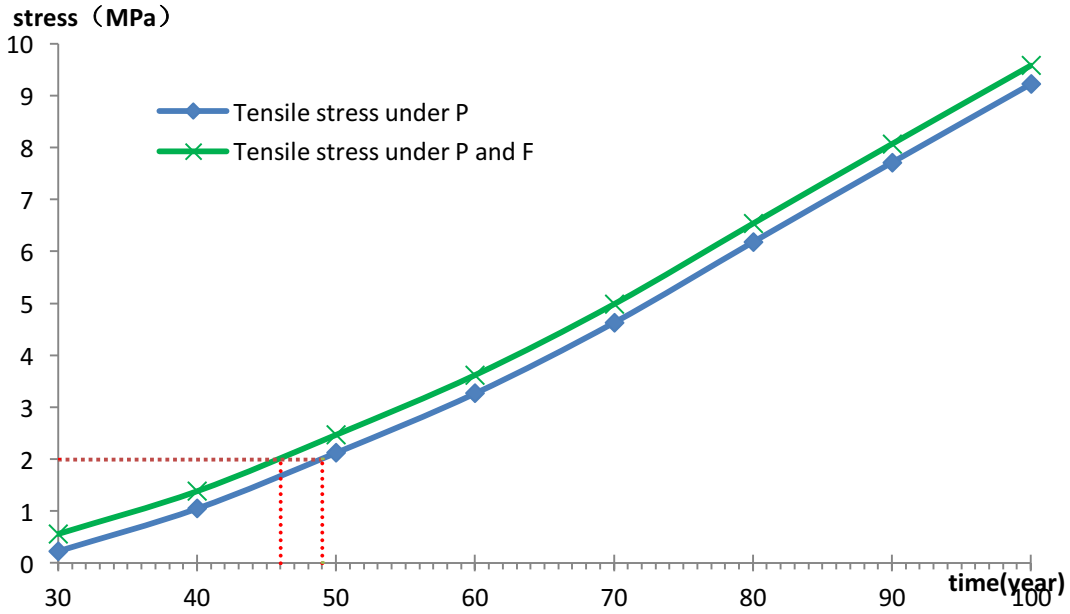

Fig 4.10 The versus time curve of tensile stress between bolt and mortar

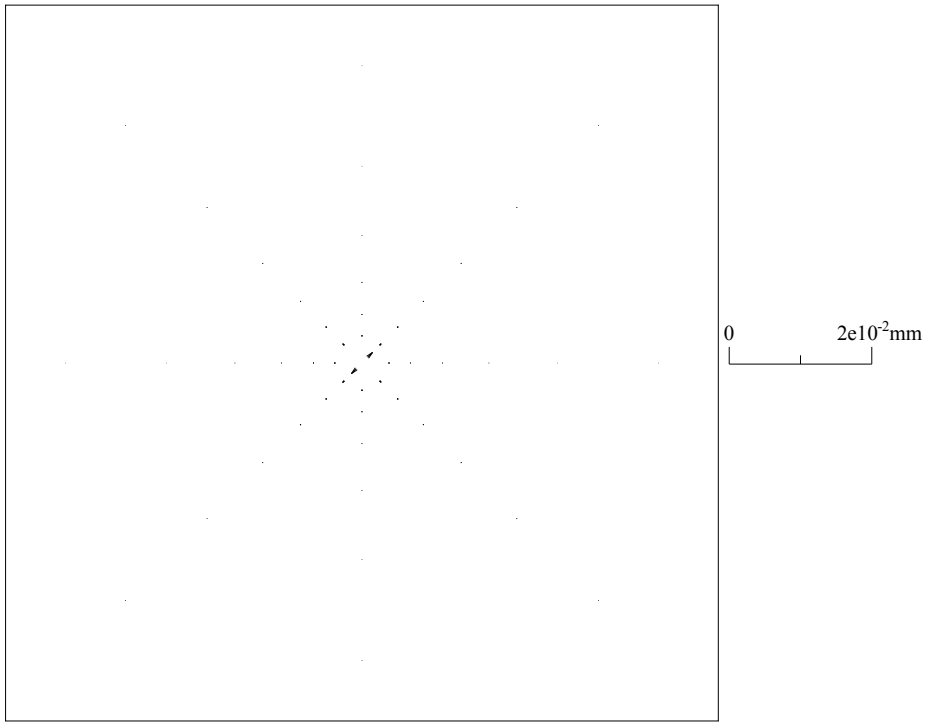

Fig 4.11 Displacement vector at Z = 3.5m horizontal plane when in 30 years

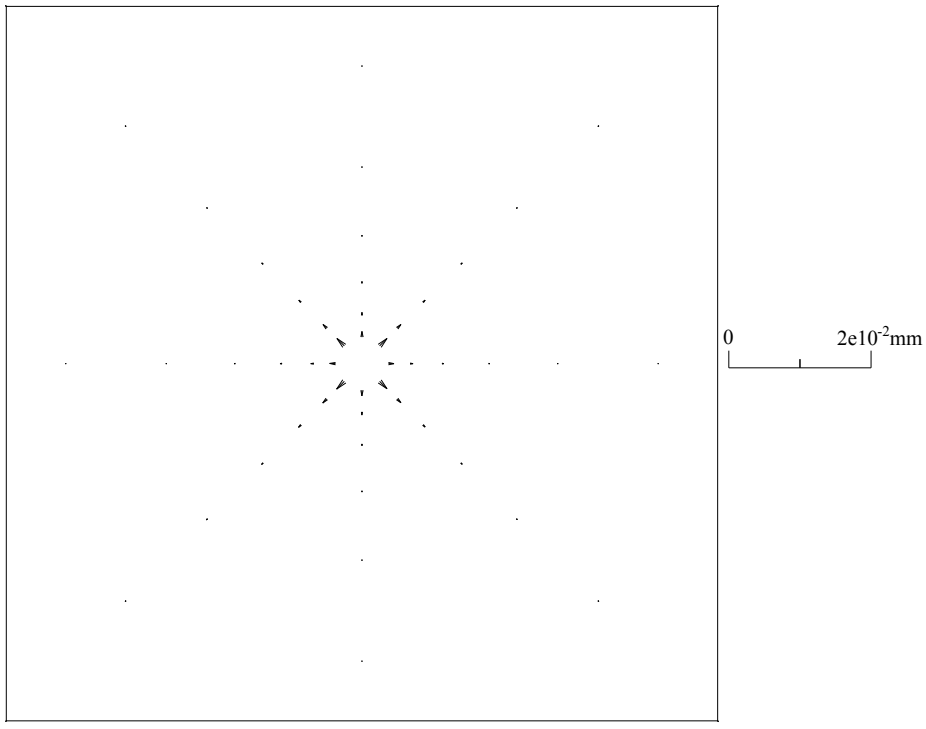

Fig 4.12 Displacement vector at Z = 3.5m horizontal plane when in 40 years

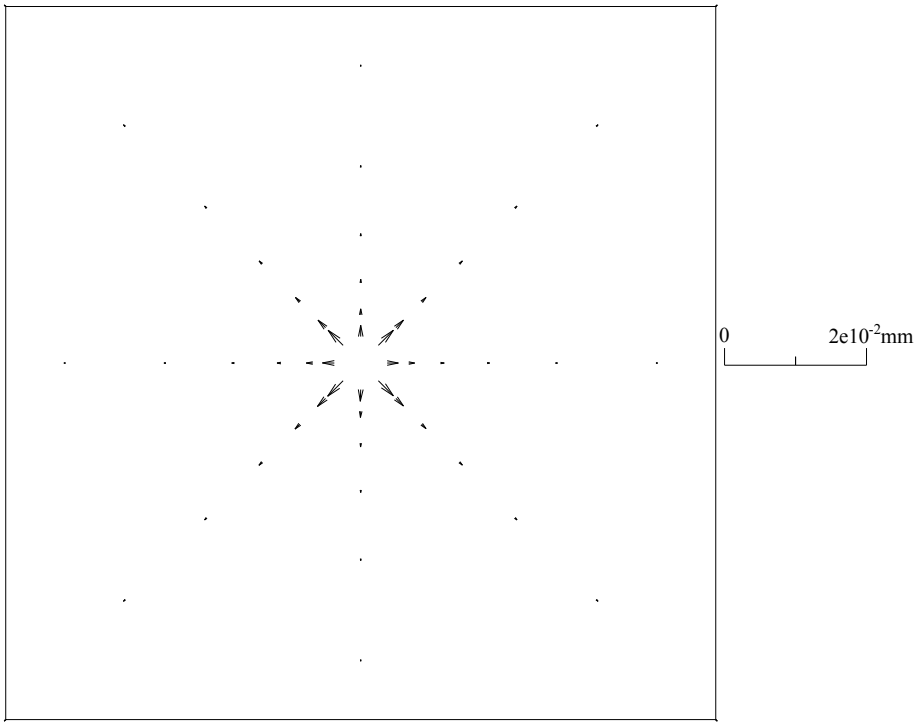

Fig 4.13 Displacement vector at Z = 3.5m horizontal plane when in 50 years

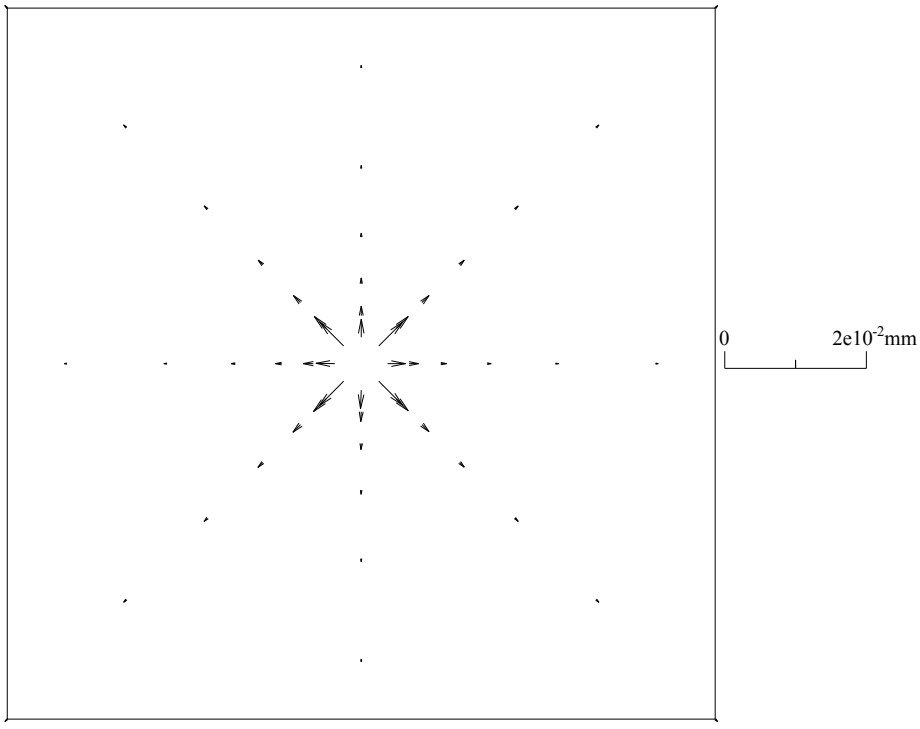

Fig 4.14 Displacement vector at Z = 3.5m horizontal plane when in 60 years

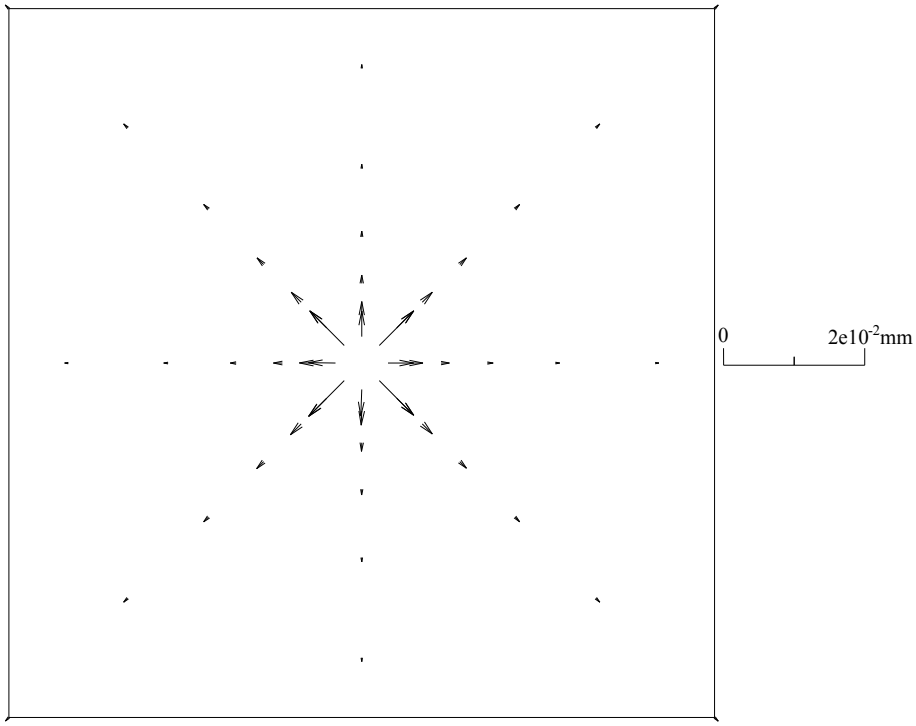

Fig 4.15 Displacement vector at Z = 3.5m horizontal plane when in 70 years

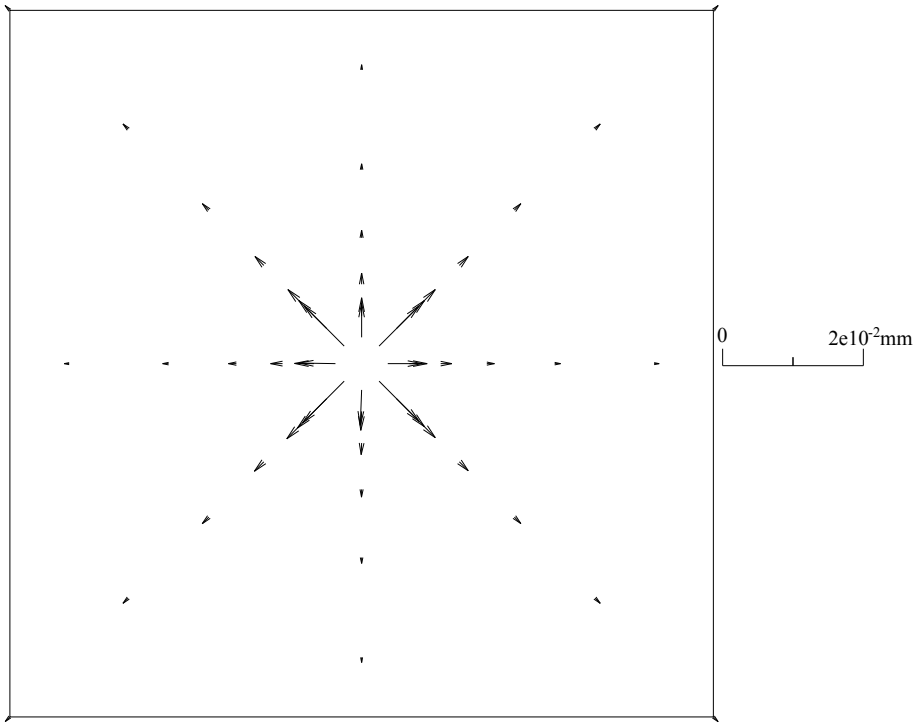

Fig 4.16 Displacement vector at Z = 3.5m horizontal plane when in 80 years

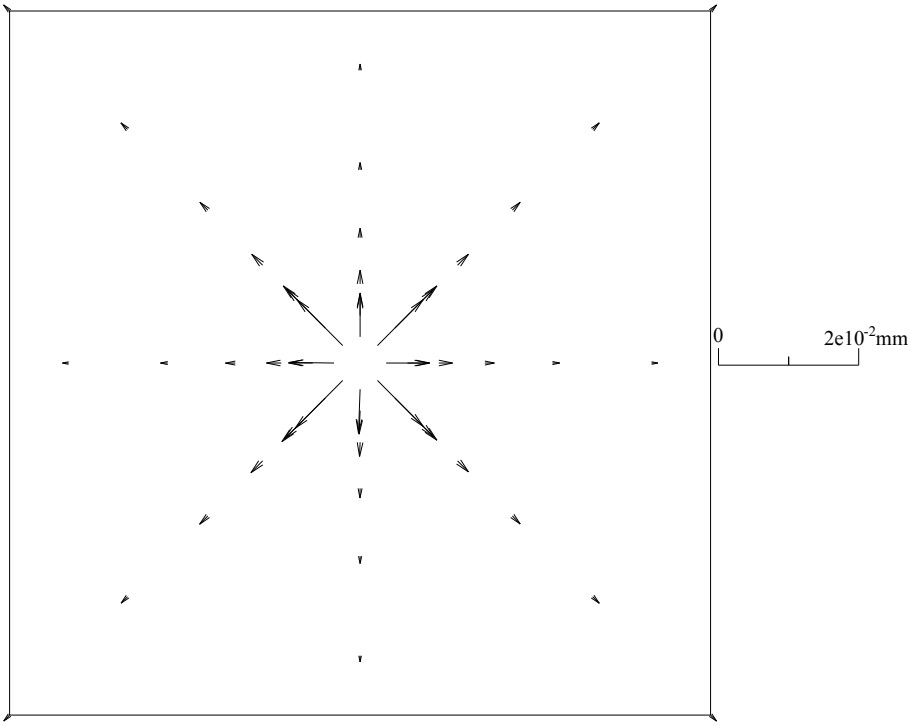

Fig 4.17 Displacement vector at Z = 3.5m horizontal plane when in 90 years

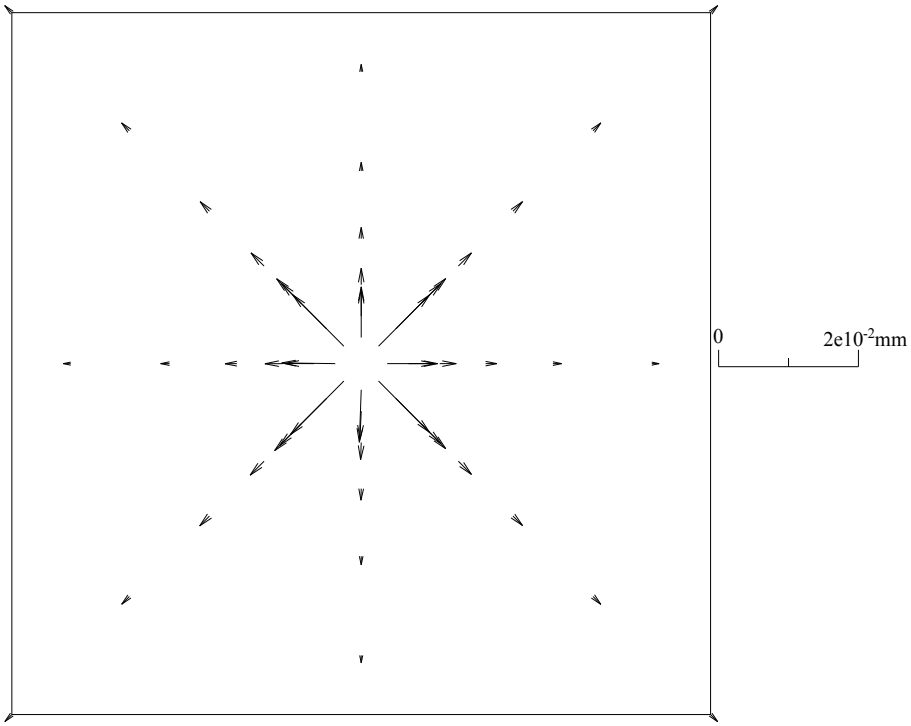

Fig 4.18 Displacement vector at Z = 3.5m horizontal plane when in 100 years

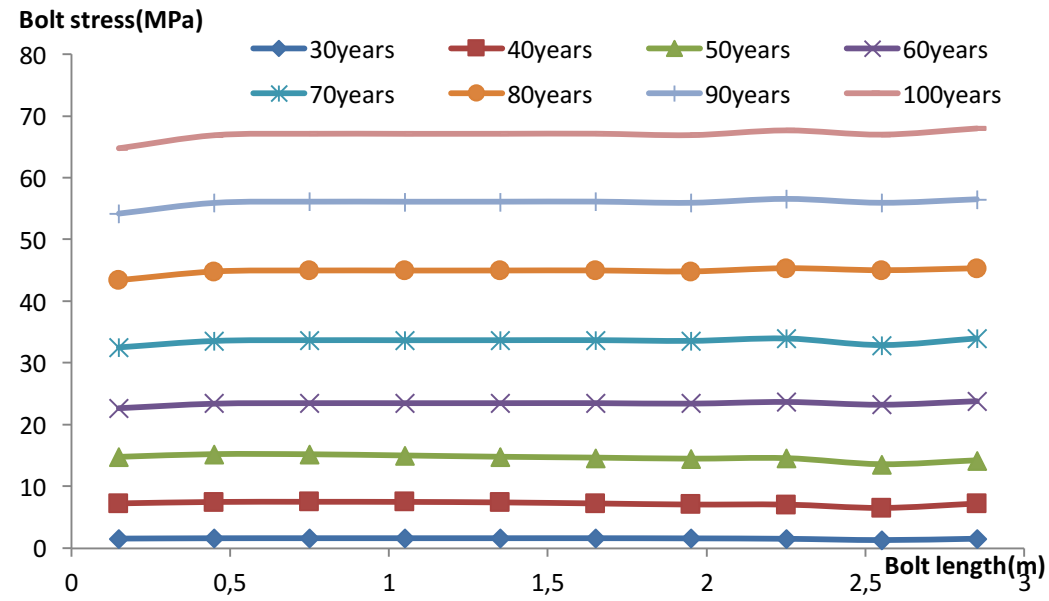

Fig 4.19Bolt axial stress distribution aroused by tension force along the length of the bolt

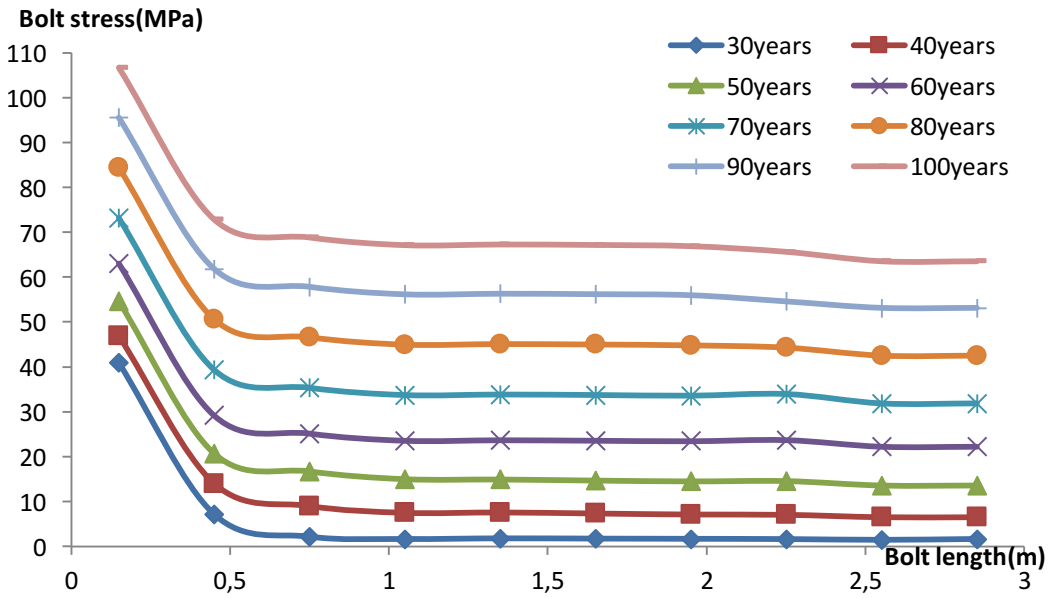

Fig 4.20Bolt axial stress distribution aroused by the tension force and Expansion Force joint action along the length of the bolt

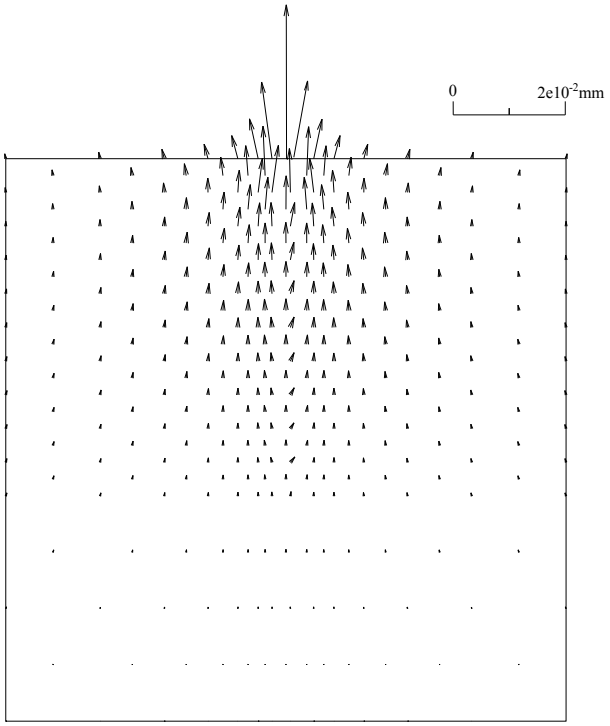

Fig 4.21 Displacement vector at vertical surface when in 30 years

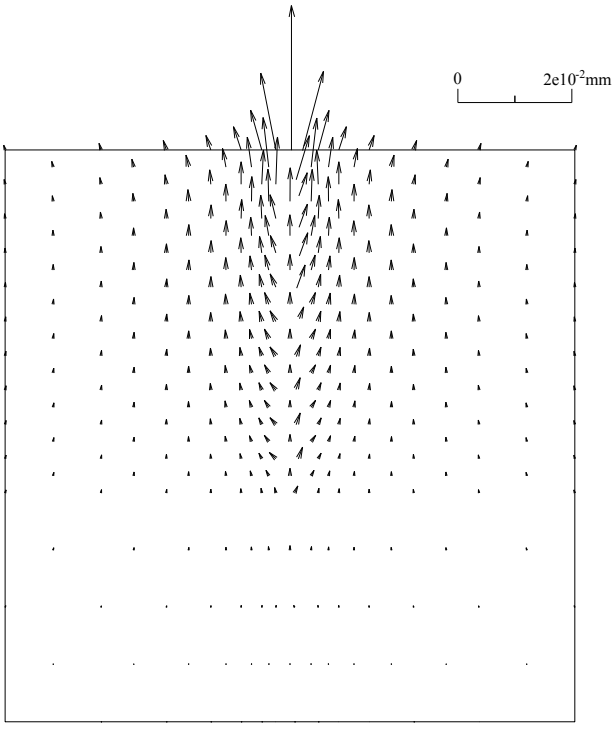

Fig 4.22 Displacement vector at vertical surface when in 40 years

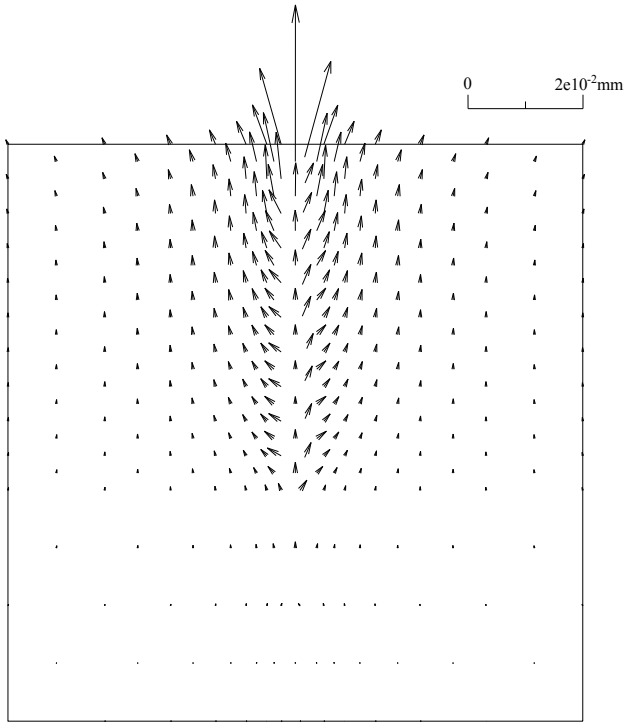

Fig 4.23 Displacement vector at vertical surface when in 50 years

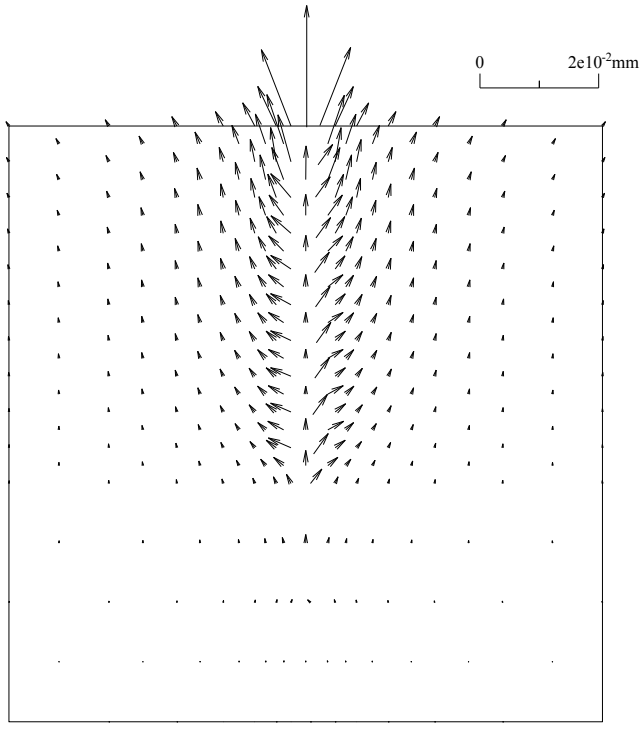

Fig 4.24 Displacement vector at vertical surface when in 60 years

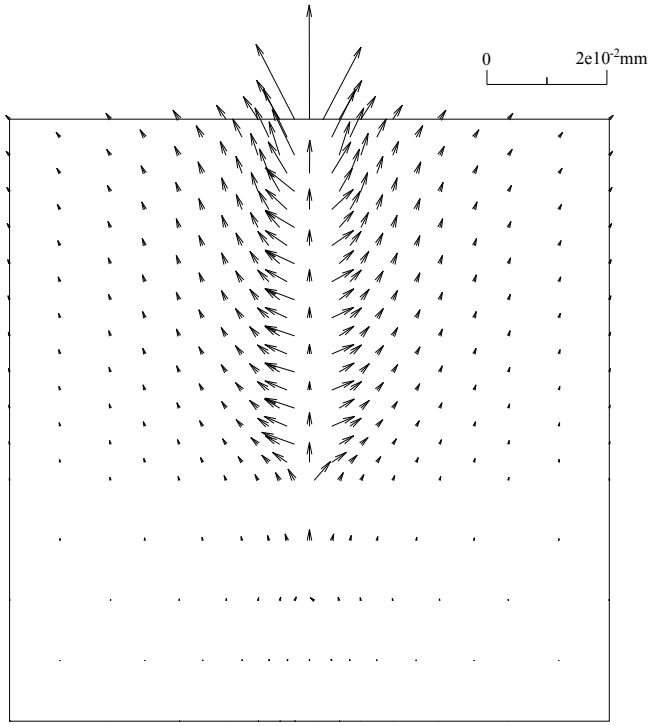

Fig 4.25 Displacement vector at vertical surface when in 70 years

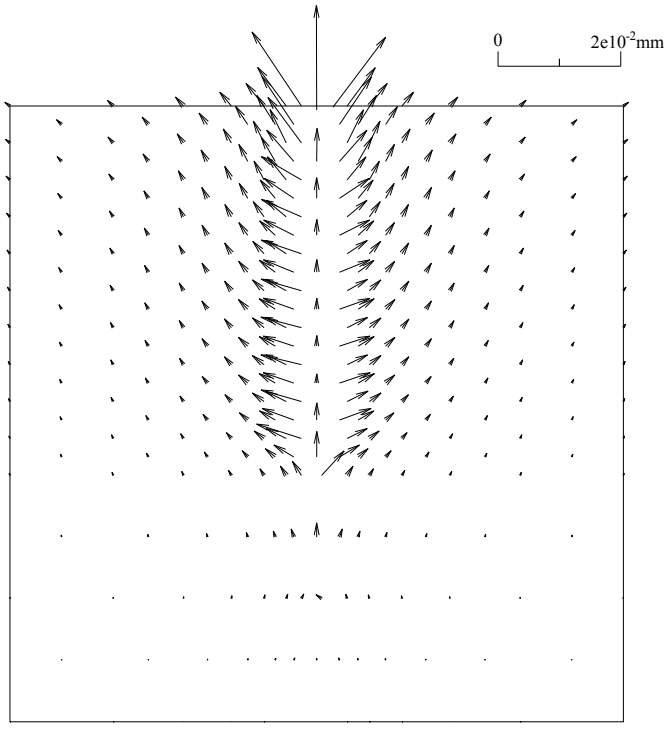

Fig 4.26 Displacement vector at vertical surface when in 80 years

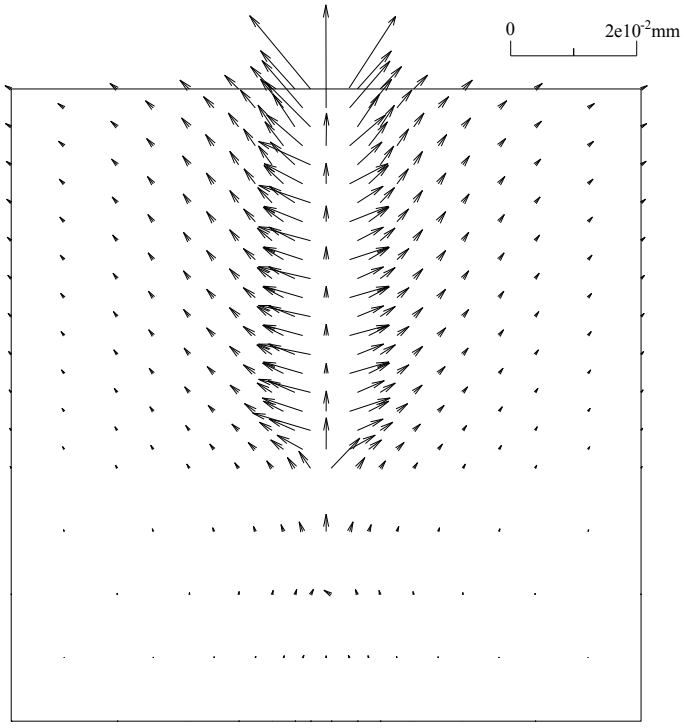

Fig 4.27 Displacement vector at vertical surface when in 90 years

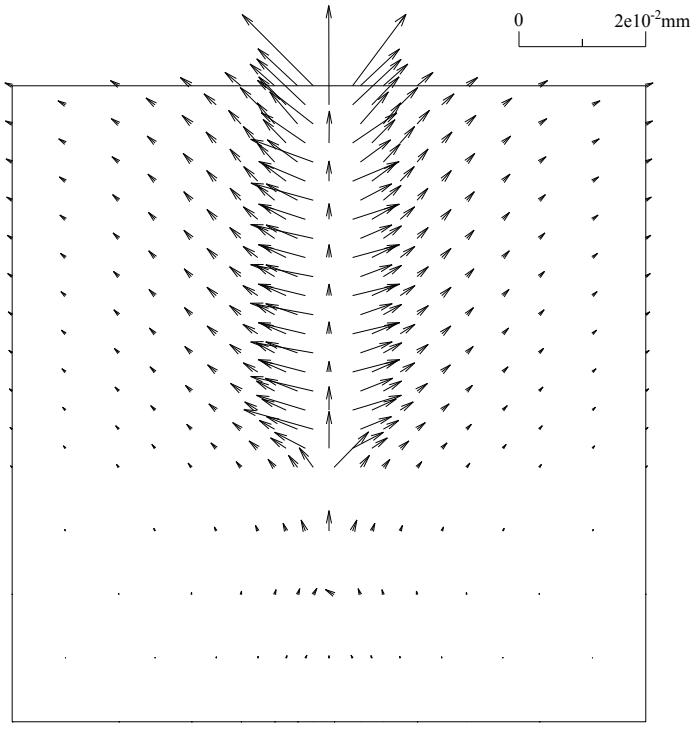

Fig 4.28 Displacement vector at vertical surface when in 100 years

5.8 Conclusions

In this chapter, the composite element method has been presented and extended to deal with corroded bolts. Virtual nodes are added on the node of composite unit to map displacement vector of bolt, mortar and rock sub-units, as well as to interpolate displacement of sub-unit domain. The influence Expansion Force was added. As to the bolt face and mortar joints, the contact surface treatment has been added using the displacement difference of adjacent sub-units between mortar and bolt to interpolate displacement of interface. A detailed description of each component of the bolted jointed rock mass has been presented.

With the composite element method, we do not need to consider bolts, mortar joints and other structural details in the mesh construction. Consequently, the pre-treatment operation is largely simplified.

The Composite element method was compared to the conventional finite element method on a rock bloc reinforced by a bolt and submitted to both pullout force and expansion force due to corrosion. This example confirms the interest of the Composite Element in the pre-processing phase. The results of both methods agree well, which constitutes a good validation of the software developed during this work.

The comments concerning the variation of the stresses and the displacement under the Expansion force and the pullout force are similar to that presented in the previous chapter.

However, the Composite element method for bolted jointed rock mass could be yet improved. Since, it is difficult to describe the deformation mode of jointed rock and bolt accurately with a simple shape functions, we could use advanced methods such as the adaptive technology, H-adaptive theory, and P-type adaptive theory.

References

1. Chen S H, Egger P, Migliazza R, Giani G P. Three dimensional composite element modeling of hollow bolt in rock masses. In Proceedings of the ISRM International Symposium on Rock Engineering for Mountainous Regions–Eurock, 2002, Madeira, PORTUGAL, 25-28 November.
2. Shi G H. Manifold method [A]. In: Proc. of the first Int. Forum on DDA and Simulation of Discontinuous Media[C]. Berkeley, California, USA:1996, 52-204.
3. Chen S H, Shen B K, and Huang M H. Stochastic elastic-viscoplastic analysis for discontinuous rock masses [J]. Int. J. for Num. Meth. In Eng.1994, 37(14):2429-2444
4. Chen S H, Qiang S, Chen S F. Study on the three-dimensional composite element model of bolted rock masses. 2003; 22(1):1-8.
5. Chen S H, He Z G, Egger P. Study of hollow friction bolts in rock by a three dimensional composite element method. Proc., 10th ISRM Congress-ISRM 2003, Johannesburg, South Africa, 203-206.
6. He Z G, Chen S H. Study on bolted rock mass by hierarchical composite element method. Chinese Journal of Rock Mechanics and Engineering. 2006; 25(8):1698-1704.
7. Chen S H, Qing S, Chen S F, Egger P. Composite element model of the fully grouted rock bolt. Rock Mechanics and Rock Engineering. 2004; 37(3):193-212.
8. Chen S H, Qing S. Composite element model for discontinuous rock masses [J]. Int. J. Rock Mech. Min. Sci. & Geomech. Abstr. 2004, 41(7): 865-870.
9. He Z.G, Qiang S, Chen S.H, Egger P. Composite element method for jointed rock masses reinforced by hollow friction bolt. International Journal of Rock Mechanics and Mining Sciences & Geomechanics Abstracts. 2004; 41(3): 551-556.
10. Hu J, Chen S H. Air element method for modeling drainage holes in seepage analysis. Rock and Soil Mechanics. 2003; 24(2):281–287.
11. Chen S H, Xu Q, Hu J. Composite element method for seepage analysis of geo-technical structures with drainage hole array. Journal of Hydrodynamics (Ser. B). 2004; 16(3): 260-266.
12. Chen S H, Shahrour I. Composite element method for the bolted discontinuous rock masses and its application. International Journal of Rock Mechanics & Mining Sciences. 2008; 45(3): 384-396.

13. Chen S H, Qin N, Xu G S, Shahrour I. Hierarchical algorithm of composite element containing drainage holes. Communications in Numerical Methods in Engineering (International Journal for Numerical Methods in Biomedical Engineering). 2010; 26(12):1856–1867.
14. Chen S H, Feng X M. Composite element model for rock mass seepage flow. Journal of Hydrodynamics (Ser. B). 2006; 18(2):219-224.
15. Chen S H, Feng X M, Isam S. Numerical estimation of REV and permeability tensor for fractured rock masses by composite element method. International journal for numerical and analytical methods in geomechanics. 2008; 32(12):1459-1477.
16. Xue L L, Chen S H. Composite element model of seepage-normal stress coupling for rock fractures. Chinese Journal of Rock Mechanics and Engineering. 2007; 26(2):2613-2619.
17. Chen S H, Xue L L, Xu G S, Shahrour I. Composite element method for the seepage analysis of rock masses containing fractures and drainage holes. International Journal of Rock Mechanics & Mining Sciences. 2010; 47(5):762–770.
18. Owen DRJ, Hinton E. Finite Elements in Plasticity: Theory and Practice. Swansea: Pineridge Press Ltd. 1980.

Chapter 6: Applications on the analysis of concrete beam test

6.1 Introduction

At the beginning of this chapter, conventional concrete beam experiments conducted by a Chinese engineer are described. Then the finite element and the composite element programs are used to analyze these experiments. This work aims to check the reliability and performances of numerical algorithms developed in this work through comparison between numerical simulation and physical experiments.

6.2 Test description

Tests were conducted by Chen Jin and Huang Wei [1] in order to develop a good understanding of the mechanical and structural properties of steel fiber reinforced concrete (SFRC).The photograph 6.1 below shows the testing method on concrete beams.

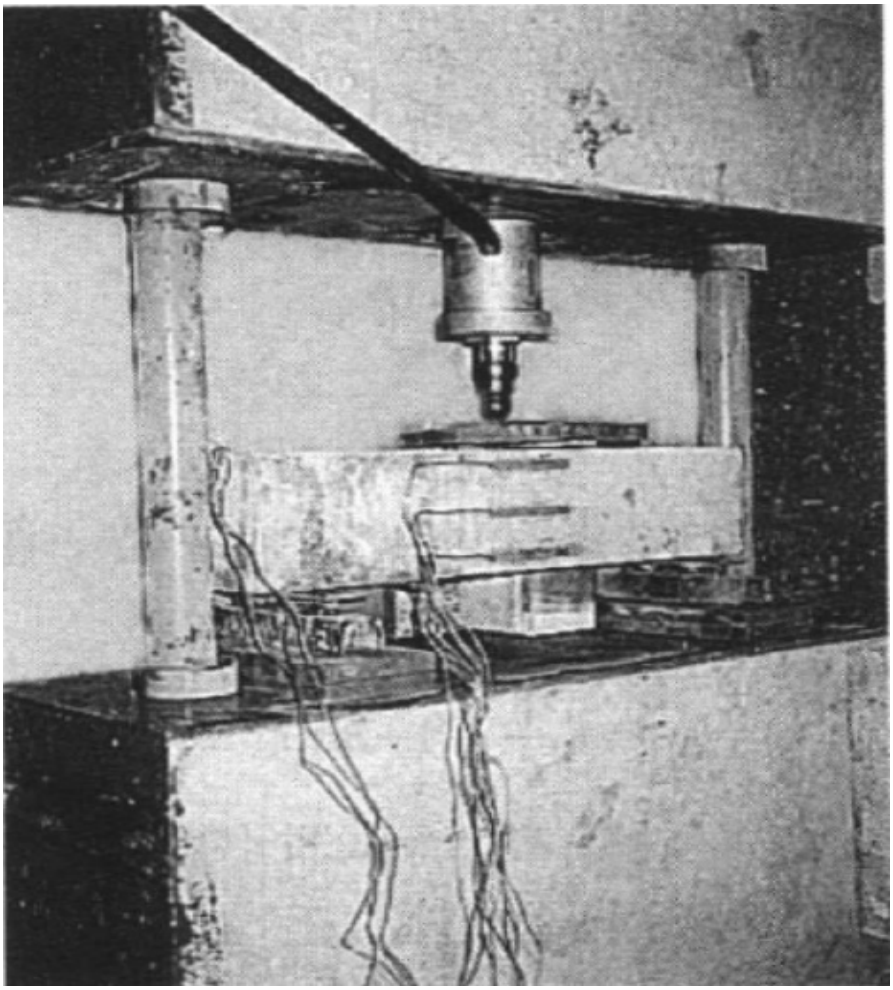

Photograph 6.1

Six concrete beams were prepared with 3 different reinforcement forms: none, single row and double row of steel bars. The beam samples size is: 68cm in length, 10cm in width and 15cm in height. The grade of concrete samples is #250, and the 90d compression strength (cube strength) is 59.5MPa. Screw-threaded steel with 6mm in diameter and elastic modulus of 210GPa are used as the steel bars. The reinforcement forms are shown in figure 6.1.

A jack is used to apply the loads by pressure pump, with 0.2MPa at each step. Strain gauges were attached on the surface of the steel bars and concrete. Measure points are located on the surface of concrete (figure 6.2). The fracture of concrete beams is measured by with numerical microscope.

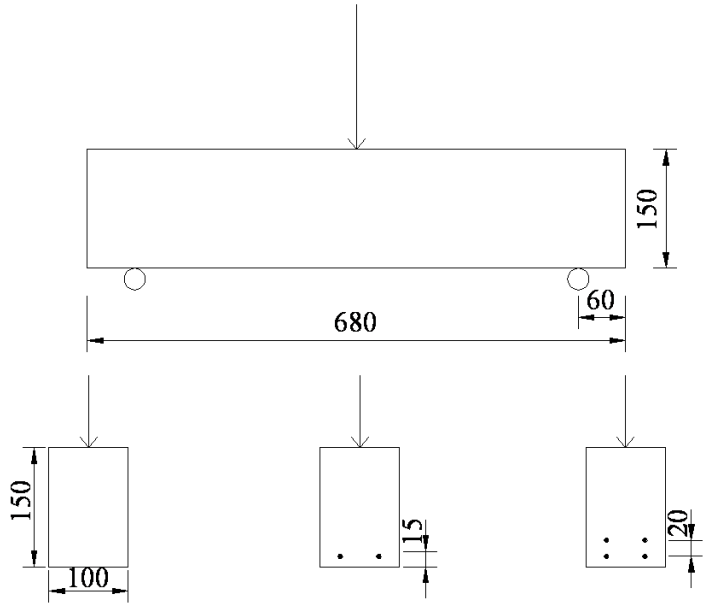

Figure 6.1 Cross sections and reinforcement arrangement of concrete beam (unit: mm).

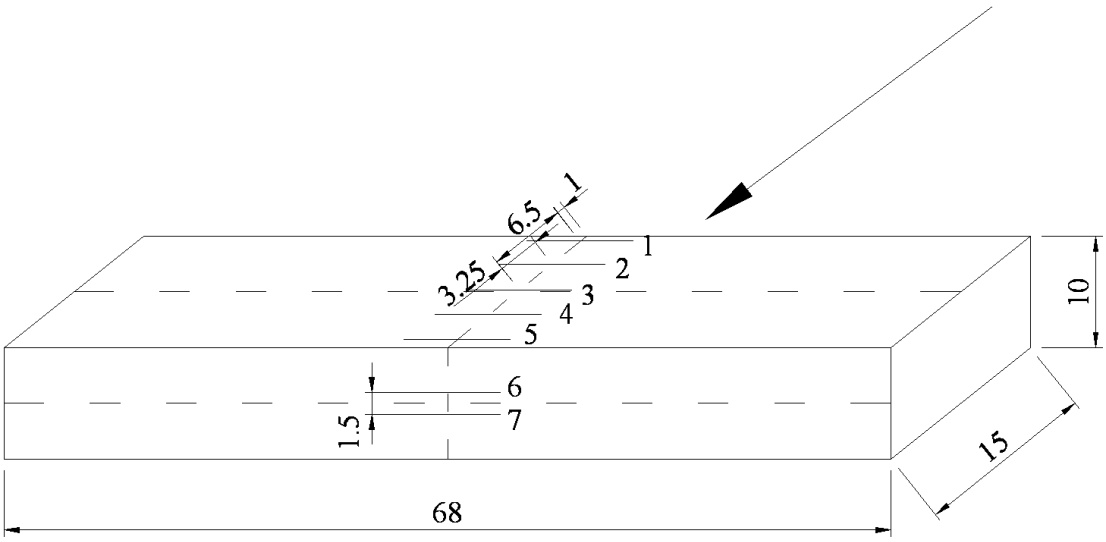

Figure 6.2 Measure point's location on the surface of concrete (unit: cm).

Table 6.1 summarizes the values of the fracturing load for the 6 beams. Beams #1 and #2 are double row reinforced; beams, #3 and #4 are single row reinforced beams, #5 and #6 are non reinforced. From the results, it can be observed that the existence of steel bars significantly increases the bearing capacity of the beam, and the increase in the reinforcement increases the bearing capacity. The fracturing process is plotted in figure 6.3. It shows that the number of fractures and toughness of the beams increase with the increase of steel bars and reinforcement ratios. It is denoted that the data in figure 6.3 corresponds to the load when the crack appears.

Table 6.1 Fracturing load of conventional concrete beams.

Fracturing load	double row reinforced		single row reinforced		none reinforced	
	#1	#2	#3	#4	#5	#6
Initial fracturing load	21	20	20	15	9	11
Ultimate fracturing load	64	45	41	38	9	11

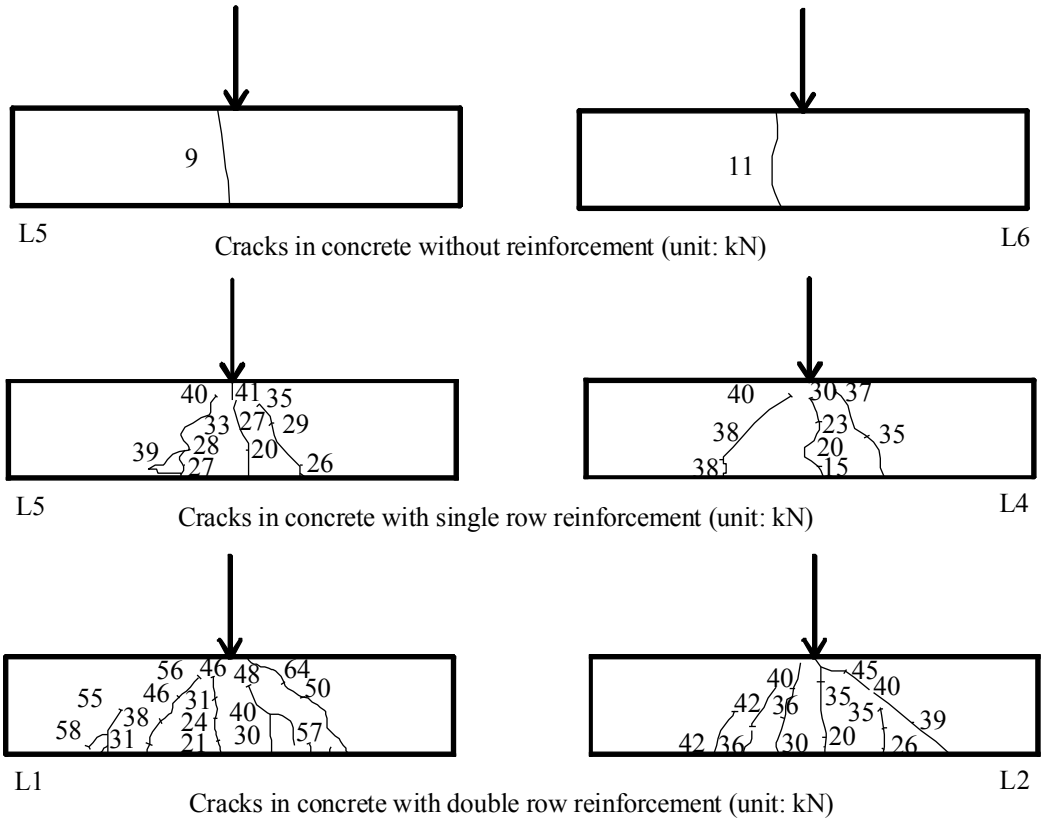

Fig 6.3 The crack routes of beams without fibers

For non-reinforced beam, before the beam breaking, the location of neutral axis has no obvious change. The maximum cracking strain attains 200με when the beam is broken. For the beam with reinforcement, the location of neutral axis moves up when cracks occur. The strain of concrete varies more uniformly. Although the cracks are developing continuously, the obvious softening of concrete strain does not occur until the last.

The stress-strain curves of the middle section of beams are plotted in Fig. 6.4 to 6.6.

For non-reinforced beams (Fig 6.4), although the location of neutral axis does not change, we observe important change in the strain pattern in the lower part of the beam. For the reinforced beam, after the concrete cracking, the strain keeps a nice linear varying. But the neutral axis moves up.

Figure 6.7 shows the variation of the strain at the bottom of the beam. It is observed that the reinforcement by the steel bars significantly increases the bearing capacity of the beam.

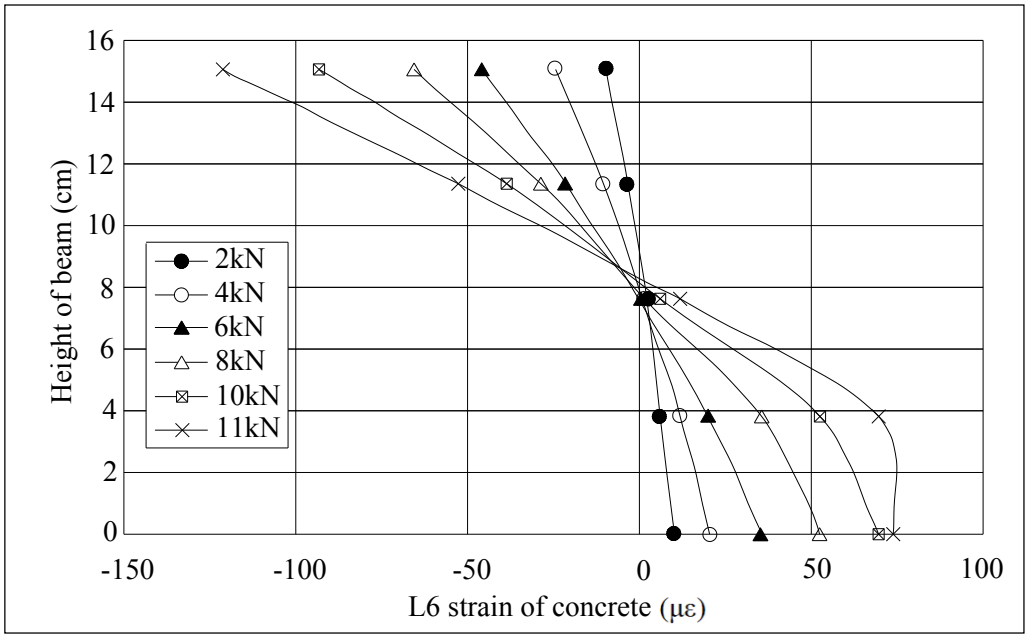

Fig 6.4 The stress-strain curves of the middle section of non-reinforced beam

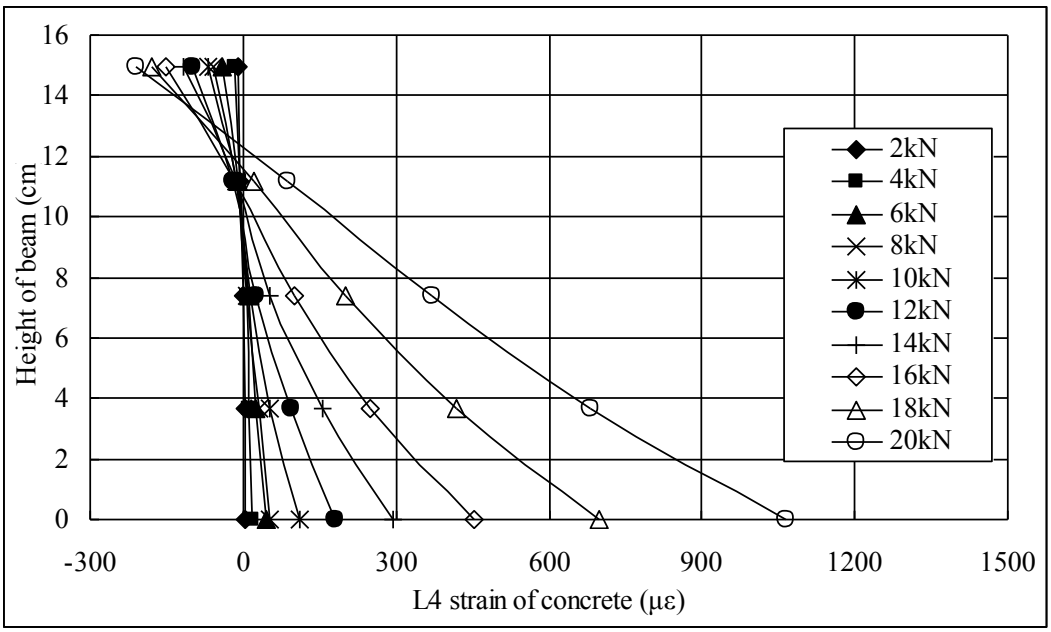

Fig 6.5 The stress-strain curves of the middle section of single row reinforced beam without fibers

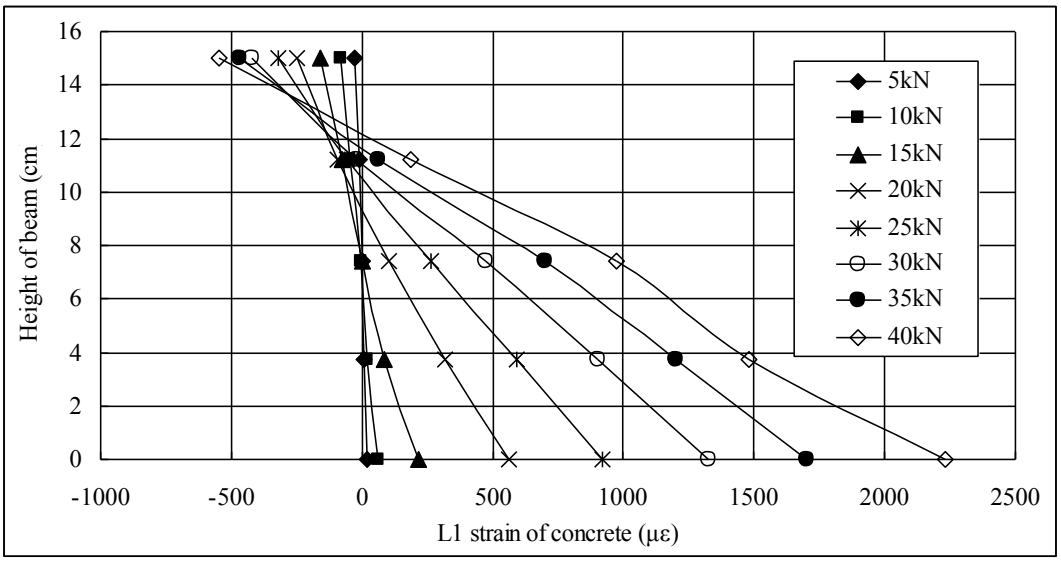

Fig 6.6 The stress-strain curves of the middle section of double row reinforced beam without fibers

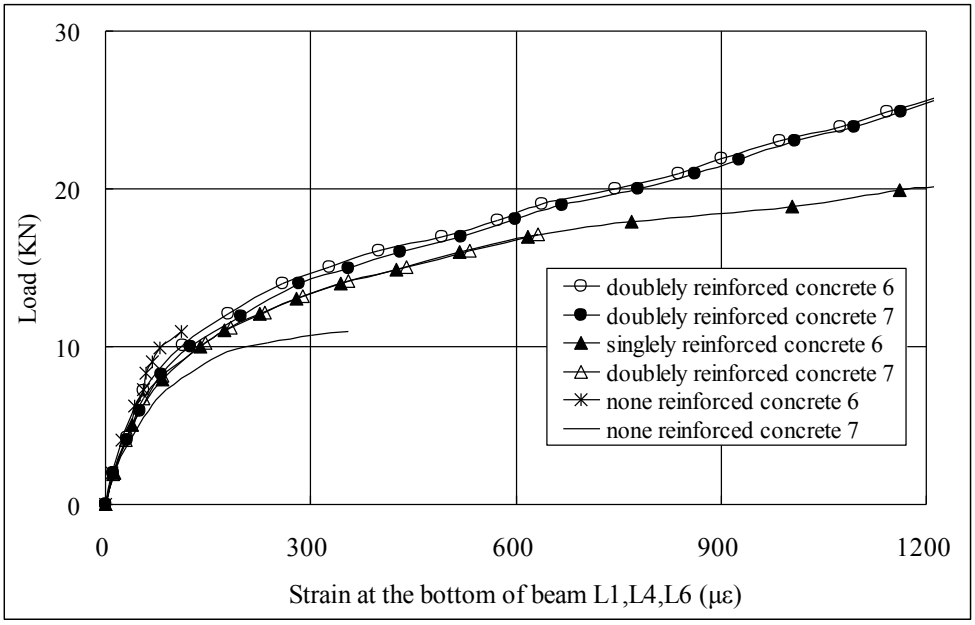

Fig 6.7 Comparison of the strain at the bottom of concrete without steel fibers

6.3 Numerical simulation

Figures 6.8 to 6.10 show a comparison between the experimentations and the finite element method concerning the strain in the middle section of non-reinforced concrete beam under the pressure of 8 kN, 10 kN, 12 kN. We observe a good agreement between these results.

Figures 6.11 to 6.113 show a comparison between the experimentations and the finite element method concerning the strain in the middle section of a reinforced concrete beam under the pressure of 8 kN, 10 kN, 11 kN. We observe also a good agreement between these results.

Figure 6.14 shows the axial force distribution of the bolt located near the middle section as predicted by the finite element method under the pressure of 8 kN, 10 kN, 12 kN. The red dashed line represents the middle section of the beam. As it can be seen from the figure, as the pressure increases, the axial force in the steel increases. This means that with increasing load, the reinforcement shares the more tension.

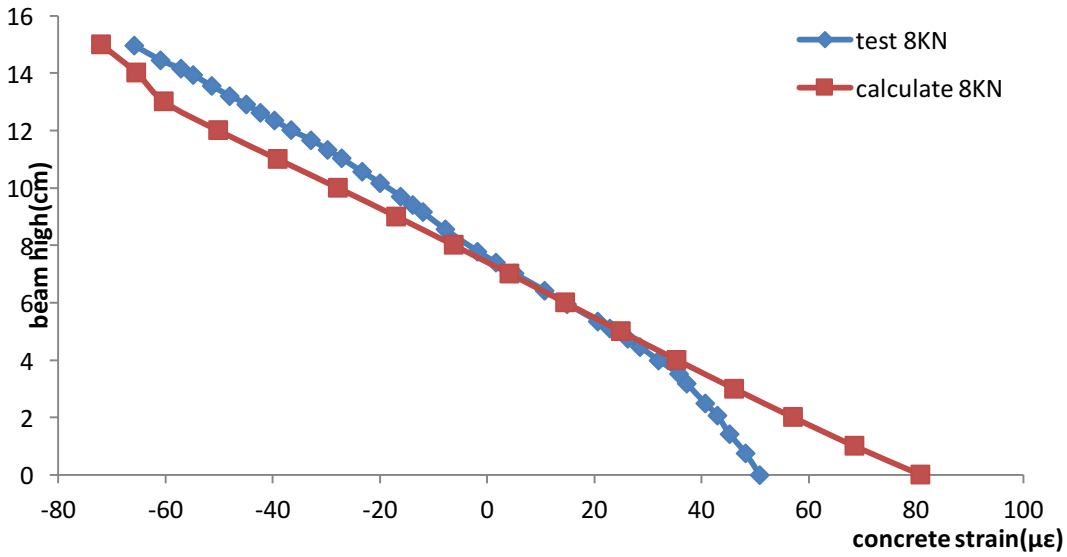

Fig 6.8 Comparison of the stress-strain value of the middle section without reinforced concrete beam in FEM calculates and test under 8KN force

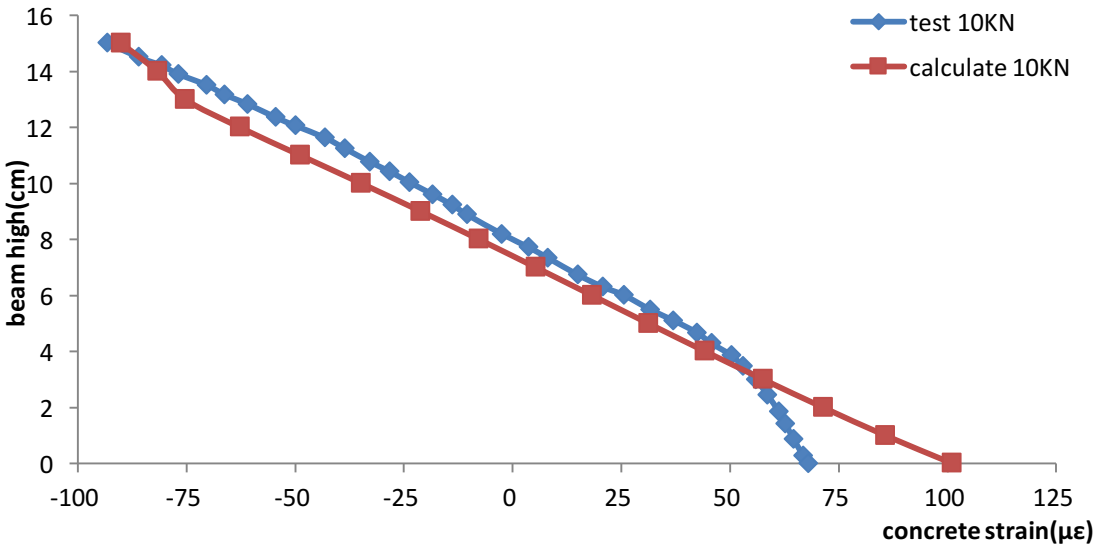

Fig 6.9 Comparison of the stress-strain value of the middle section without reinforced concrete beam in FEM calculates and test under 10KN force

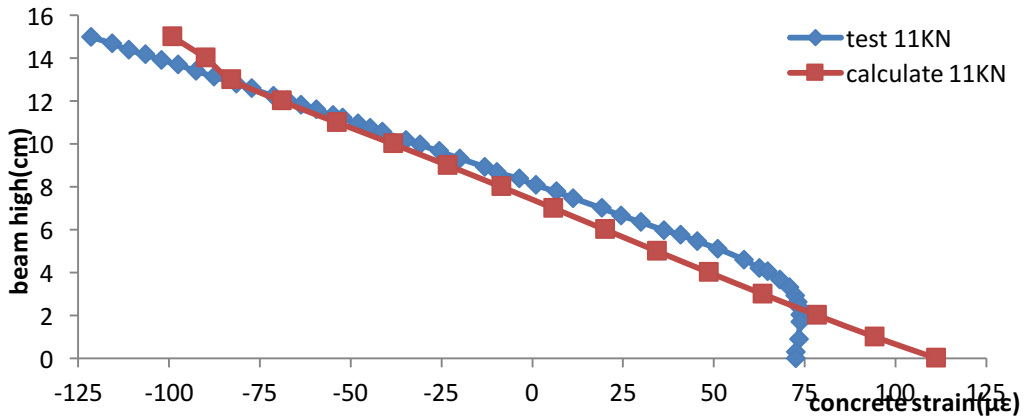

Fig 6.10 Comparison of the stress-strain value of the middle section without reinforced concrete beam in FEM calculates and test under 11KN force

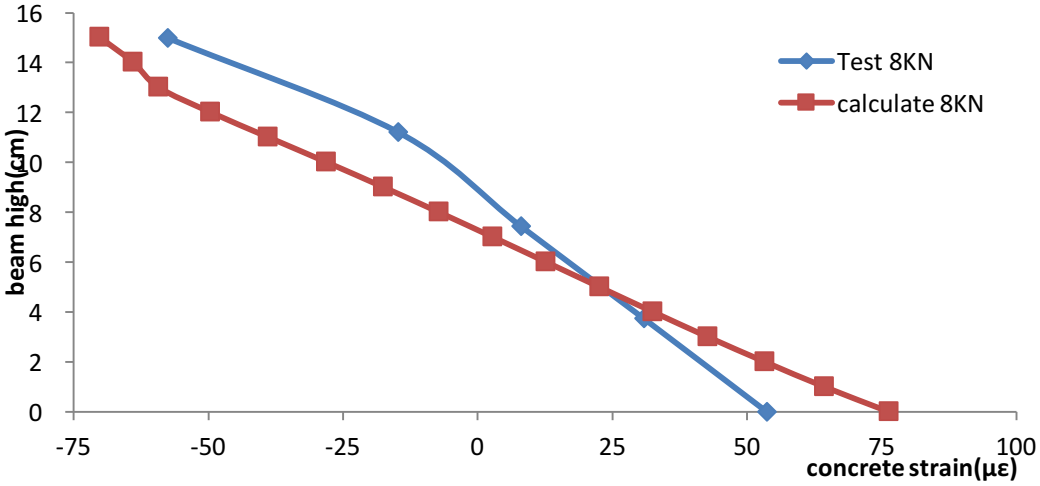

Fig 6.11 Comparison of the stress-strain value of the middle section of single row reinforced concrete beam in FEM calculates and test under 8KN force

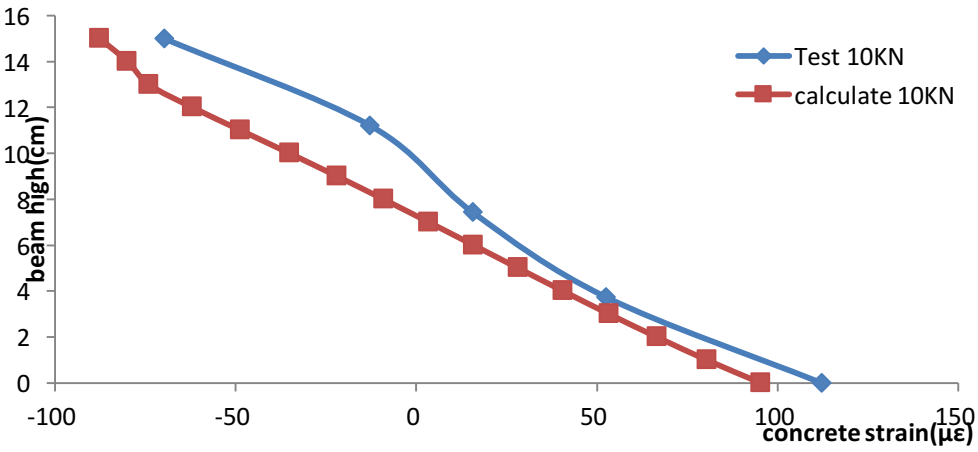

Fig 6.12 Comparison of the stress-strain value of the middle section of single row reinforced concrete beam in FEM calculates and test under 10KN force

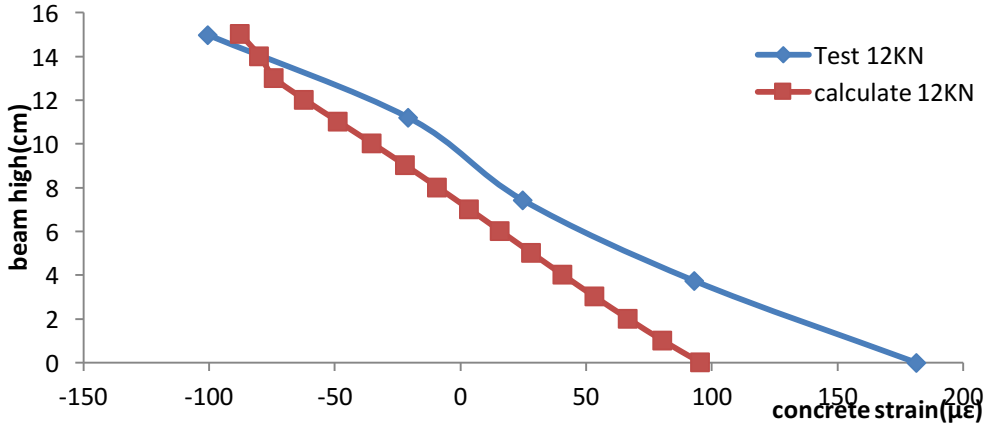

Fig 6.13 Comparison of the stress-strain value of the middle section of single row reinforced concrete beam in FEM calculates and test under 12KN force

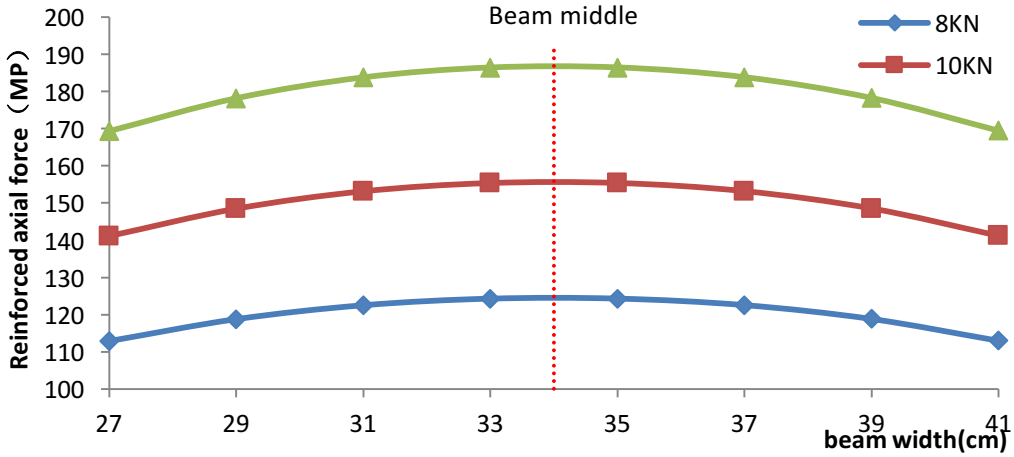

Fig 6.14 The axial force curves of reinforced near the middle section of single row reinforced concrete beam

Figure 6.15 shows the strain profile in the middle section of the beam reinforced with a row of steel bars under the load 8 kN. The same figure shows the strains considering the Expansion Force. We observe the influence of the expansion force near the reinforcement.

Figure 6.16 shows the variation of the strain at the lowermost point in the middle section of the beam with a row of steel reinforcement subjected to a load of 8kN and Expansion Force. As we can see from the figure, the strain increases linearly. This increase is due to the Expansion Force increase.

Figure 6.17 shows the axial force distribution in the steel bar in the middle section of the beam reinforced with a row of steel bars under the joint action of a load of 8kN and the expansion force. As can be seen from the figure, the axial force decreases with time; this decrease results from the influence of the corrosion on the mechanical properties of steel bar.

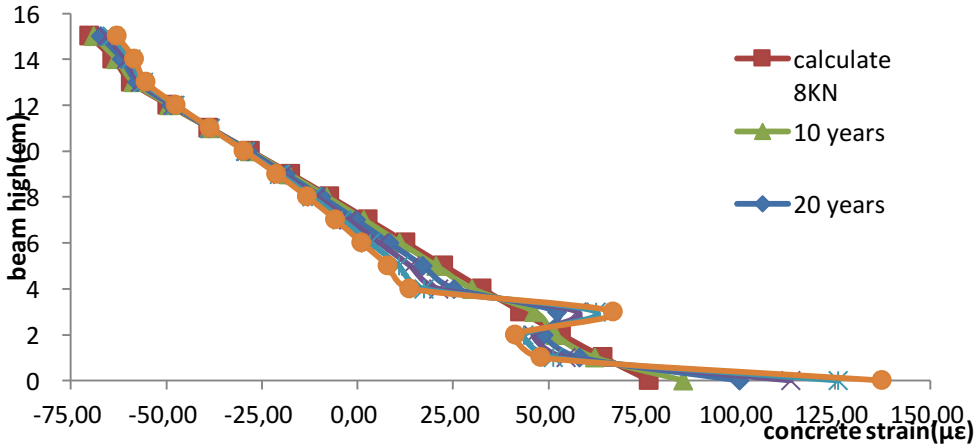

Fig 6.15 Comparison of the stress-strain value of the middle section of single row reinforced concrete beam in FEM calculates under expansion force

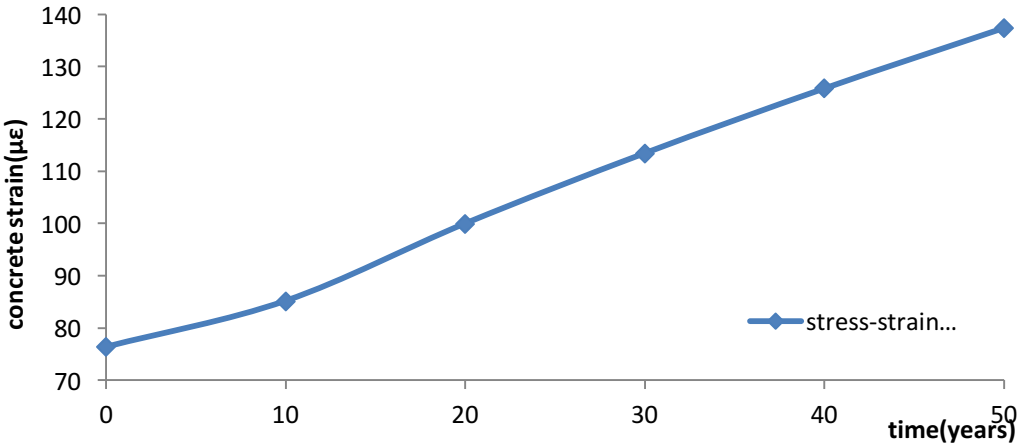

Fig 6.16 The stress-strain value of the bottom of the middle section of single row reinforced concrete beam in FEM calculates under expansion force

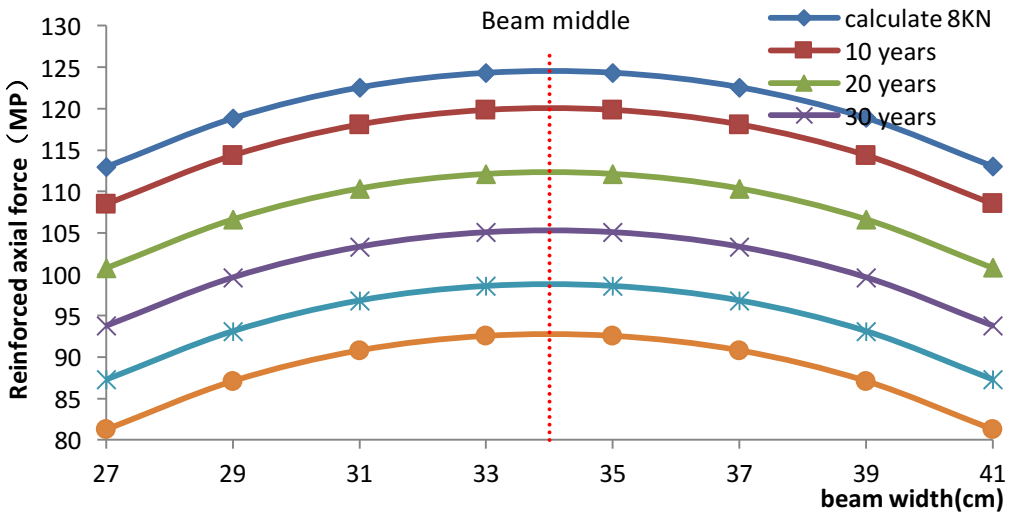

Fig 6.17 The axial force curves of reinforced near the middle section of single row reinforced concrete beam in FEM calculates under expansion force

6.4 Conclusions

This chapter presented comparison between experimental results on concrete beam and the finite element modeling. Experimental tests showed that the reinforcement significantly improves the bearing capacity. The comparison of the finite element method with the experimental tests conducted with beams with different reinforcements gave very good results. This comparison showed the good performances of the finite element program.

The finite element program allowed analyzing the influence of the expansion force on the behavior of the reinforced beam. It showed that the expansion force induces an increase in the strain around the reinforcement and a global decrease in the axial force in the reinforcement.

References

1. Chen Jin, Huang Wei. Experimental and theoretical of hydraulic reinforced concrete structure. Yangtze River Press. January 1, 2005; 52–57.

Chapter 7: Conclusions and Prospects

7.1 Conclusions

This work concerned investigation of the influence of corrosion on the behavior of bolts. This issue is very important in engineering. It concerns the durability and stability of structures reinforced by blots and submitted to corrosion environment. The importance of this issue is confirmed by several structures failure or distress observed around the world.

The performance of the Bolt Bearing Capacity can be seen in horizontal and vertical directions. The horizontal direction concerns the mortar protective layer cracking due to rust expansion; while the vertical direction concerns the degradation between bolt and mortar. These two issues were considered in this work. The work concerned a good understanding of the different phenomena, which take place in the presses of blot corrosion, the development of analytical solution, and the implementation of corrosion bolt model in a finite element program and a Composite Element program.

The mechanisms of corrosion of reinforcing bolt in concrete were summarized; the steel corrosion rate prediction model has been established. In the meantime, theoretical formulas of corroded expansion force changes with time were established and applied to numerical simulation of experiments.

A bolt space rust analytical model has been developed to study the three-dimensional stress field of the bolt under the joint action of pullout force and rust expansion force. The numerical analysis showed that the axial stress in the bolt followed an exponential decay function. In the plane perpendicular to the bolt, the radial stress within the mortar protective layer changes from tensile to compressive stress; tensile stress peaks occur at the radial edge of the mortar. Along the bar, peaks of compressive stress within the mortar occur at the end of the bolt, but in the plane perpendicular to the bolt, hoop stress peaks occur near the edge of the bolt in the mortar. Shear stress between the bolt and mortar follows linear distribution. Most values of shear stress on bolt surface are negative with peaks at the bolt end.

The use of elastic-viscoplastic constitutive relation allows us to describe the evolution of the mechanical process with time. For these reasons, a finite element program for corroded bolt with elastic viscoplastic materials was developed for the first time. Analysis of typical case

showed that the t distribution of axial tensile stress along the bar under the action of Expansion Force increases linearly. Under the influence of Expansion Forces, the displacement in the concrete will increases with time. Under the joint action of Expansion Force and a pull-out force, the axial stress decreases exponentially along the bolt, the displacement diverges from the center to the surrounding. The displacement peaks occur at the bolt end.

The composite element method has been developed to deal with corroded bolts. Virtual nodes were added on the node of composite unit to map displacement vector of the bolt, mortar and rock sub-units, as well as to interpolate displacement of sub-unit domain. The influence Expansion Force was added. As to the bolt face and mortar joints, the contact surface treatment has been added using the displacement difference of adjacent sub-units between mortar and bolt to interpolate displacement of interface. A detailed description of each component of the bolted jointed rock mass has been presented. The Composite element method was compared to the conventional finite element method on a rock bloc reinforced by a bolt and submitted to both pullout force and expansion force due to corrosion. This example confirms the interest of the Composite Element in the pre-processing phase. The results of both methods agree well, which constitutes a good validation of the software developed during this work.

The finite element program was checked on experimental tests conducted on concrete beams. The comparison of the finite element results with the results of tests conducted with beams with different reinforcements gave very good results. This comparison showed the good performances of the finite element program. In addition, the finite element program allowed analyzing the influence of the expansion force on the behavior of the reinforced beam. It showed that the expansion force induces an increase in the strain around the reinforcement and a global decrease in the axial force in the reinforcement.

7.2 Prospects

Structural Durability has become a hot topic in theoretical studies of concrete structure. This work contributed to improve our understanding of this complex issue, but we still need

further development, in particular:

(1) Concrete carbonation, and steel corrosion mechanism constitute the basis of the analysis of durability of reinforced concrete structure. Research enquires large experimental data, t long-term observation.

(2) Steel corrosion is the most important factor in the durability of reinforced concrete structures; consequently establishing a reasonable model for steel corrosion rate is crucial. I believe that, establishing a model for steel corrosion rate based on purely theory or pure experience can not get reasonable results. It is necessary to start with a view of theory, then establish the corrosion rate model, and corrected by measured data.

(3) Three-dimensional analytical model of rusting bolt used in this work can be applied before corrosion of protection layer, when bolting material under the action of force in the elastic stage, under the condition of the bonding is effective along the whole length. Further studied should be conducted on stress distribution in the body of the bolt when cracks occur in the protective layer of mortar and failure occurs in bonding.

(4) Further developments are needed for the application of the composite element method considering the change of corrosion with time. We have difficulties in using a simple shape function to describe jointed rock and bolt deformation mode. We can overcome this problem by using the adaptive technology, the H-adaptive method or the P-type adaptive method.

(5) Numerical methods were used to simulate the bolt-corroded change. At this stage, elastic conditions were considered. The behavior of bolts after cracking of the protective layer was not considered, as well as the change in the crack in the mortar protective layer. To describe the mechanical properties of detailed structure after corrosion, further developments are required.